NONLINEAR EXCITATIONS IN FLOWING COMPLEX PLASMAS

By

SURABHI JAISWAL

(PHYS06201204001)

Institute for Plasma Research, Gandhinagar

A thesis submitted to the

Board of Studies in Physical Sciences

In partial fulfillment of requirements

for the Degree of

DOCTOR OF PHILOSOPHY

of

HOMI BHABHA NATIONAL INSTITUTE

December, 2016

Homi Bhabha National Institute

Recommendations of the Viva Voce Committee

As members of the Viva Voce Committee, we certify that we have read the dissertation prepared by **Surabhi Jaiswal** entitled "**Nonlinear excitations in flowing complex plasmas**" and recommend that it may be accepted as fulfilling the thesis requirement for the award of Degree of Doctor of Philosophy.

PKaw

Chairman - Prof. P.K. Kaw **Date:** 02-02-2017

Pintu Bandyopadhyay

Guide / Convener - Dr. Pintu Bandyopadhyay **Date:** 02-02-2017

Co-guide - Prof. Abhijit Sen **Date:** 02-02-2017

Examiner - Prof. H. Bailung **Date:** 02-02-2017

Member 1- Prof. Prabal Chattopadhyay **Date:** 02-02-2017

Devendra Sharma

Member 2- Dr. Devendra Sharma **Date:** 02-02-2017

Final approval and acceptance of this thesis is contingent upon the candidate's submission of the final copies of the thesis to HBNI.

We hereby certify that we have read this thesis prepared under our direction and recommend that it may be accepted as fulfilling the thesis requirement.

Date: **2nd February 2017**

Place: Gandhinagar

Pintu Bandyopadhyay

Prof. Abhijit Sen
Co-guide

Dr. Pintu Bandyopadhyay
Guide

STATEMENT BY AUTHOR

This dissertation has been submitted in partial fulfillment of requirements for an advanced degree at Homi Bhabha National Institute (HBNI) and is deposited in the Library to be made available to borrowers under rules of the HBNI.

Brief quotations from this dissertation are allowable without special permission, provided that accurate acknowledgement of source is made. Requests for permission for extended quotation from or reproduction of this manuscript in whole or in part may be granted by the Competent Authority of HBNI when in his or her judgement the proposed use of the material is in the interests of scholarship. In all other instances, however, permission must be obtained from the author.

Surabhi

Surabhi Jaiswal

DECLARATION

I, hereby declare that the investigation presented in the thesis has been carried out by me. The work is original and has not been submitted earlier as a whole or in part for a degree / diploma at this or any other Institution / University.

Surabhi

Surabhi Jaiswal

List of Publications arising from the Thesis

Journal

1. *"Flowing dusty plasma experiments: generation of flow and measurement techniques"*, S. Jaiswal, P. Bandyopadhyay and A.Sen, Plasma Sources Science and technology, **2016**, 25, 065021.

2. *"Experimental investigation of flow induced dust acoustic shock waves in a complex plasma"*, S. Jaiswal, P. Bandyopadhyay and A. Sen, Physics of Plasmas, **2016**, 23, 083701.

3. *"Experimental observation of precursor solitons in a flowing complex plasma"*,S. Jaiswal, P. Bandyopadhyay and A.Sen, Physical Review E, **2016**, 93, 041201(R).

4. *"Dusty Plasma Experimental (DPEx) device for complex plasma experiments with flow"*, S. Jaiswal, P. Bandyopadhyay and A.Sen, Review of Scientific Instruments, **2015**, 86, 113503.

5. *"Theoretical study of head-on collision of dust acoustic solitary waves in a strongly coupled complex plasma"*, S. Jaiswal, P. Bandyopadhyay and A.Sen, Physics of Plasmas, **2014**, 21, 053701.

6. *"Vortex shedding in flow past an obstacle"*, S. Jaiswal, P. Bandyopadhyay and A.Sen, (*Under Preparation*), **2016**

Other

1. *"Scientists observe plasma waves that could help prevent space debris collisions*, Physics Central: Physics buzz blog, **2016**

Surabhi

Surabhi Jaiswal

Dedicated to

My family

ACKNOWLEDGEMENTS

It gives me great pleasure to convey my sincere thanks to all those who supported and guided me to make this thesis possible. At the very outset, I convey my hearty gratitude to my thesis supervisor Dr. Pintu Bandyopadhyay for his invaluable guidance, support, and discussions during the entire period of PhD work. His diligent, friendly and spirited support and guidance through this long journey has been the source of inspiration for me. His experimental skills, enthusiasm and active participation in experiments made the journey much easier. I am also thankful to him for providing incredible independence in deciding the experiments and excellent support in lab set up, writing codes and papers. Sir, I am very thankful to you for everything you did to make my PhD a success.

I also gratefully acknowledge my thesis co-supervisor Prof. Abhijit Sen who has a significant contribution to this thesis through the motivating ideas and fruitful suggestions he provided to me throughout the tenure. He helped me in deciding the experimental problem, giving talks and seminars and writing proposals. Besides the discussion about the PhD project, he taught me various concept of plasma physics. All of these enriched my growth from a student to a researcher.

I am obliged to Prof. P. K. Kaw, Prof. Prabal Chattopadhyay and Dr. Devendra Sharma for consenting to be my Doctoral Committee members. I really enjoyed the valuable discussions during academic reviews. In every discussion, I got enriched with some novel Ideas. It was privilege to have them in the committee.

I would like to thank Prof. R. Ganesh, Prof. S. Mukherjee, Prof. Sudip, Dr. A Chattopadhyay, Dr. M Kundu, Dr. V. P. Anitha, Dr. Santanu Karkari, Dr. G. Ravi, Dr. Ramasubramanian and staff at FCIPT for their endurance while teaching us during the first year course work. Prof. P.K. Kaw and Prof. D. Bora, Prof. Sudip, Prof. P.K Chattopadhyay, Dr. Joydeep and Prof. S. Mukherjee, Dr. Mainak Bandyopadhyay have been of continuous support and advice in Academic affairs.

I would like to thank Prof. P. K. Chattopadhyay for providing the fund and space to pursue my experiments. I am also very thankful to Prof. A. Sen and Dr. Joydeep Ghosh for funding me during my visit to Taiwan and Germany.

The library staff, computer centre staff and administrative staff of IPR have always remained cooperative. I convey my thanks to Mrs. Sutapa Ranjan, Mr. Shailendra Trivedi, Mr. Arvind Singh, Mr. Hemant Joshi, Mr. Gaurav Garg, Mr. Prashant Kumar, Mr. Govind Lokhande, Mr. Saroj Das, Mr. Shravan Kumar, Ms. Smita Parmar, Mrs. Shilpa Khandker, Mr. Souraban, Mr. H.K. Sharma, Mr. H.C.

Khanduri, Mr. Hitesh Mehta, Mr. Dinesh Nair, Mr. H. Chamunde, Mr. Silel Shah, Ms. Shirin Bhesania for their help and advice on numerous occasions. I convey my thank to workshop and stores staff for their support during my entire PhD tenure. I thank to Kaila Bhai, Kanu Bhai, Bhat Bhai for their immense support for conducing the experiments. I would like to thank Mrs. Minsha shah for her invaluable help in designing and developing the necessary electronic circuits for my experiments.

I thank to my seniors Dr. Sanjay Mishra, Dr. Sushil, Dr. Sanat, Dr. Vikram Sagar, Dr. Aditya, Dr. Soumen Ghosh, Dr. Sita Sunder, Dr. Sayak Bose, Dr. Manjeet kaur, Dr. Deepak sangwan, Dr. T. Shekhar Goud for their help whenever I needed.

I would like to convey my sincere gratitude to Dr. G Vedaprakash for his valuable support during construction phase of my experiments and for teaching me electrical circuits and mechanical software. I acknowledge Mr. Rupak mukherjee and Dr. G Vedaprakash for thorough proofreading of my thesis and valuable comments and criticism. I thank to my batchmates Arghya, Bhumika, Umesh, Patel, Devraj, Sonu, Narayan, Ratan, Modhu for providing me their support during this long journey. I thank to my juniors Prabhakar, Pallawi, Meenakshi, Sandeep, Sagar, Deepak, Harshita, Atul, Shivam, Rupak, Avaneesh and other IPR colleagues for providing me friendly atmosphere in IPR. A special thanks to Arghya, Veda and Satyendra for being too supportive and listening me with all their patience during entire course of PhD life.

I am extremely thankful to my family for their incredible support and motivation which encourages me to reach my goal.

Contents

Synopsis

Plasma flows are an important topic of research due to their prevalence in many natural situations, as an area of fundamental studies and for their potential engineering applications. Some well-known occurrences of plasma flows in nature are the spectacular plasma jets emitted along the axis of rotation of compact objects [1] and the streaming solar wind released from the upper atmosphere of the sun and the helio-sheath region [2] that continuously impinges on the earth and other planetary bodies. Plasma flows also occur in laboratory situations such as in tokamak devices where their presence has important implications for the stability of the plasma discharge and the concomitant impact on energy transport [3–5]. Research on flowing plasmas has also been inspired and has benefited from various investigations in hydrodynamics since in many parametric regimes a plasma behaves much like a charged fluid and analogies drawn from hydrodynamics help provide insights into the linear and nonlinear behaviour of plasmas. As an example, the various phenomena associated with fluid flowing past an obstacle [6] (or an obstacle moving in stationary fluid) that has been widely studied in fluid dynamics for its applications in oceanography, atmospheric dynamics and a variety of engineering applications, often have corresponding analogous phenomena when a plasma flows over a charged obstacle (or a charged particle moves through a plasma). A common occurrence is that of wake patterns generated behind an object travelling in a fluid that is also seen in plasmas when a charged particle travels through it. When the speed of the travelling object becomes supersonic the boundaries of the wake are defined by a shock structure and the resultant trailing structures are called Mach cones. Mach cones have been observed both in neutral fluids as well as in plasmas. However under certain conditions a supersonically travelling object in a fluid also shows interesting nonlinear excitations in the fore-wake region i.e. in the region upstream of the moving object. These take the form of periodic emissions of coherent structures like solitons or shocks and have been both experimentally observed and theoretically studied in hydrodynamics [7–10]. In principle such excitations should also happen in a plasma and one should be able to excite precursor solitons or shocks by moving a charged object rapidly in a plasma or having a plasma flow supersonically over a charged obstacle. Surprisingly this topic has not received much attention in the plasma physics community and the problem of precursor excitations in a flowing plasma has remained an open and relatively unexplored area of research. The primary motivation of my work has been to investigate this open problem and experimentally explore the possibility of observing such a phenomenon in plasmas in a controlled laboratory situation. The nature and conditions governing the existence of such nonlinear structures in plasmas, besides being of fundamental scientific importance, can also help provide insights into nonlinear events happening in many real life situations.

To carry out such experimental investigations I have chosen to work with a dusty plasma medium that consists of micron or submicron sized particles immersed in an electron-ion plasma. A dusty plasma offers several advantages from an experimental point of view. The highly charged and low temperature dust particles constitute a strongly coupled system that is closer to a being a fluid system than a normal plasma. The dust particles being of macroscopic size can be easily visualized and their movements recorded videographically. The corresponding sound speed in a dusty plasma, namely the dust acoustic speed, is also extremely low and therefore easily detectable and measurable using visual techniques. The low phase velocity of the dust acoustic wave also makes it easier to achieve a supersonic flow in the dust component.

For performing the experiments a versatile table-top dusty plasma experimental (DPEx) device [11] has been built up in IPR, which consists of a Π-shaped Pyrex glass tube that has an experimental area of 8 cm inner diameter and 65 cm length in the horizontal section and two service portions of 30 cm length and of same diameter that form the vertical sections. The basic geometry and design philosophy of this device has been inspired by the PK-4 space experimental device [12] however, there are significant differences and enhancements in factors like the dimensions of the system, the electrode geometry and arrangement, as well as the plasma generation mechanism. In DPEx, a dusty plasma is formed in the horizontal portion whereas the service part is utilized for pumping, gas inlets, electrodes connections, and for venting the system. These experimental arrangements provide a good access for optical diagnostics. A rotary pump is used for evacuation of the vacuum vessel and a mass flow controller interfaced with a computer is used to inject neutral gas into the chamber in a regulated manner and to manipulate the dust cloud by changing the gas flow. A stainless steel circular disc of 3 cm diameter is used as an anode and a stainless steel long tray placed inside the experimental part of the vessel is used as a cathode. The two edges of the cathode are bent to provide a radial confinement to the dust particles as well as to mount different obstacles over it. A couple of stainless steel strips placed over the cathode tray provides the axial confinement to the particles. To introduce monodispersive dust particles into the device a dust dispenser is mounted on the experimental part of the vessel. The dispenser is connected to a trigger circuit which is interfaced with the computer so that a controlled amount of dust can be introduced into the device by tuning the trigger signal. In the case of a dusty plasma formed from polydispersive kaolin (hydrated aluminium silicate) particles, the particles are simply sprinkled uniformly on the cathode plate before closing the device.

A DC glow discharge plasma is produced between the electrodes by applying a high voltage DC in the background of a neutral gas (Ar). The plasma parameters such as density, temperature, plasma/floating potential are first measured in the absence of dust particles by using Langmuir and emissive probes. The electron temperature varies from 2 eV to 5 eV, whereas plasma density is found to be of the order of $10^{15}/\mathrm{m}^3$ for a range of discharge voltages between 250 and 350 V and a working pressure between 0.1 and 0.2 mbar. The plasma density increases and temperature decreases with the increase of neutral pressure and discharge voltage. This suggests that the sheath thickness over the cathode decreases with the increase of discharge voltage and background pressure. The plasma/floating potential increases with the increase of the discharge voltage and decreases with the increase of neutral gas pressure although the change is not significant.

A dusty plasma is created by introducing micron sized dust particles that get charged by collecting ions and electrons and are levitated in the sheath region above the cathode. The vertical component of the cathode sheath electric field provides the necessary electrostatic force to the particle to levitate them against the gravitational force. The radial and axial sheath electric field due to the bent edges of the cathode and the strips are responsible for the radial and axial confinement of the dust particles against their mutual Coulomb repulsive force. The equilibrium dust cloud is formed by adjusting the pumping speed and gas flow rate. A set of optical instruments such as combination of laser and line generator is used to illuminate the axial length of the experimental chamber to view the complete dust cloud, and a couple of CCD cameras of high and low speed and of high /low resolution are used to capture the dynamics of the dust cloud as well as the single dust particles from top and side of the setup. Parameters like the pair co-relation function, intergrain distance, density, thermal velocity of the particles, and temperature are estimated from the consecutive frames of the images by using particle tracking data with the help of an IDL based (super) Particle Identification and Tracking (sPIT) code.

After a detailed characterization of plasma and dusty plasma I have next explored and established different techniques of flow generation in our device [13] and tested a variety of tools to measure the flow velocity of the flowing fluid and particles and measured the Epstein drag coefficient [14] etc. to properly decipher the underlying physical mechanism responsible for the flow induced excitations of linear/nonlinear waves. Among the techniques to induce flow in the dust component, apart from the single gas method I have also used a dual injection scheme by employing an additional gas feeding port on the right service part of the vacuum vessel. In the single gas injection technique, initially the equilibrium cloud is formed by maintaining the pumping speed and gas flow rate through just one port. A flow is then generated by reducing the gas flow rate in steps of 2.75 ml_s/min. from the equilibrium value. After initiating the flow of dust particles, the gas feed rate is set back to its original value within a second to regain the equilibrium condition. In this case the particle velocity can be raised upto 20-25 cm/sec. In this method the equilibrium state is disturbed momentarily. In the dual gas injection method, the initial equilibrium dust cloud is again formed by maintaining the pumping speed and gas flow rate through a single port but the flow is generated by injecting additional gas through the second port. In this case we can maintain a constant gas pressure while performing the experiments. In a third technique, the equilibrium dust cloud is formed in between the confining potential strips placed at the right edge of the cathode and a potential hill formed over a biased wire that is placed in between the two confining strips. The wire can be kept either at a floating or a ground potential. Initially the wire is kept grounded and dust cloud is trapped in between the strips and the wire and then a flow is induced by switching the wire to the floating potential (i.e. by reducing the potential hill over the wire). By this method the one could achieve only modest values of induced flow velocities.

The flow velocity is then estimated by three different techniques, namely, by a super Particle Identification (sPIT) code [15], a Particle Image Velocimetry (PIV) analysis [16] and the excitation of Dust Acoustic Waves (DAWs). In the sPIT code, the particle trajectory can be tracked in consecutive frames and particle coordinates can be easily obtained. This code works efficiently as long as the particles are distinguishable. For relatively higher particle densities and for higher flow velocities, the sPIT code fails to measure the velocity accurately. Thus for relatively higher density, the PIV tool has been used. However, this technique also gives good results when the individual particles are detectable otherwise the measurement of high velocity by this technique become difficult. Both these methods, namely the sPIT and PIV techniques, fail to measure the velocity of highly dense dust fluids, where the particles are indistinguishable. Thus to measure the flow velocity of highly dense dust fluid, a novel technique based on the excitation of dust acoustic wave (DAW) has been employed. In this technique, a low amplitude DAW is initially excited in the absence of flow by applying a sinusoidal voltage to a mesh and its phase velocity is measured. Then, in the presence of flow a similar low amplitude DAW is excited in the direction opposite to the direction of flow. The measured velocity of the DAW is lower in this case due to the equilibrium flow of the dust and the difference of this velocity from the original phase velocity is a measure of the flow velocity. The dust flow in our device is seen to initially depend on the position, time, discharge parameters and the gas flow rate. However the dust particles that are initially accelerated achieve a terminal velocity after travelling a certain distance. This is due to the drag force mostly caused by the background neutrals. Additionally, the flow velocity reduces with the increase of pressure due to frequent dust neutral collisions and the flow velocity increases with the increase of flow rate difference.

After establishing the various means of generating and measuring dust flows in the device I have next carried out experiments on wave excitations in the dust medium- in particular an investigation of the phenomenon of precursor solitons [17–19]. The experiment has been performed at a discharge voltage of 340-350 V with the working pressure of P=0.09 mbar with kaolin particles (with a size dispersion ranging from 4 to 6 μm) as a dust component. For flow generation the third technique discussed above has been used, namely, a potential hill created by a wire mounted on the cathode has been used to induce dust flow by a sudden change in the hill height. The flow velocity has been controlled by changing the hill height. I have found that whenever the mass flow over the electrostatic potential hill was supersonic nonlinear solitary dust acoustic waves (DAWs) were excited. In the frame where the fluid is stationary and the hill is moving the solitons are found to propagate ahead of it in the upstream direction as precursors while wake structures consisting of linear DAWs are seen to propagate in the downstream region. The solitary structures are seen only for supersonic flows and up to an upper limit of flow. For flows that are slow compared to the DAW phase speed and hence subsonic, only wakes are excited in the downstream direction. I have also made a detailed characterization of these nonlinear structures by plotting the variation of the parameter consisting of the product of the soliton amplitude and the square of its width with the Mach number and found it to be nearly constant - a property characteristic of KdV solitons. I have also found that the the time interval between generation of two such solitons (T_s) varies inversely with the 3/2 power of the amplitude i.e. $T_s \propto A^{-3/2}$ - which is in agreement with theoretical results obtained from a solution of a forced KdV equation for precursor solitons [19].

In the second physics problem, I have performed an experiment on flow induced large amplitude dispersive dust-acoustic shock waves (DASW) in a complex plasma [20]. Shock waves which are a class of nonlinear structures in the form of propagating discontinuous disturbances are characterized by sharp jumps in velocity, pressure, temperature, and density across a narrow front. In a plasma medium, they can be excited when a large amplitude mode propagates in the presence of strong dissipation such as due to collisions with neutrals, viscosity, or Landau damping [21]. Usually, when an object moves through a stationary fluid with highly supersonic speed then shock waves get excited. They can also be excited when a supersonically flowing fluid encounters a charged stationary object. While a number of experimental results have been reported on shock formation by applying an external pulse [22–26] only a few results have been reported on shock excitations in a flowing complex plasma for different experimental situations [27–29]. In particular, there are no reports on the excitation of flow induced dispersive dust acoustic shocks and variation of their propagation characteristics as a function of the perturbation strengths and flow velocities. I have performed a detailed experiment on dust flow driven excitation and changes in the propagation characteristics of dispersive shock waves by flowing the dust fluid over a stationary object with very high velocity (high Mach number of M>2). To perform the experiment, a copper wire has been placed over the cathode and the potential of the wire varied by connecting it to a variable resistance ranging from 10 kΩ to 10 MΩ. The experiment has been carried out in a dc glow discharge plasma with kaolin particles as the dust component in a background of Ar gas. The equilibrium dust cloud has been formed at a discharge voltage of V_d=360-370 V and the neutral pressure of P=0.11-0.12 mbar at a discharge current of $I_p \sim 4$ mA. The dust cloud equilibrium has been maintained by adjusting the pumping speed and gas flow rate. A sudden change of gas flow rate has then been used to trigger the onset of high velocity dust acoustic shocks whose dynamics has been captured by fast video pictures of the evolving structures. The physical characteristics of these shocks have been delineated through a parametric scan of their dynamical properties over a range of flow speeds and potential hill heights. It has been found that a threshold in the difference of gas flow rate exists below which the DASWs do not get triggered. Similarly, there is also a threshold in the height of the potential hill above which shock waves get triggered. Also the shocks are not excited whenever the wire is kept on a floating potential as the particles then did not feel the presence of the wire (the surface potential of the dust is always close to the floating potential). The observed evolution of the shock waves and their propagation characteristics are found to compare well with model numerical results based on a modified Korteweg-de-Vries-Burgers type equation [30]. The effect of dust-neutral collision has also been considered in accounting for the underlying dissipation mechanism [29].

In summary, a versatile experimental setup has been developed to carry out detailed investigations of different nonlinear waves and structures in a flowing complex plasma. Different techniques of subsonic to supersonic dust flow generation and methods of measuring their velocities have been investigated and compared for their efficacies. The principal physics investigation carried out has been the exploration of fore-wake excitations due to the interaction of a supersonic dusty plasma flow with a charged obstacle. My experimental findings have established for the first time the existence of precursor solitons in a plasma medium-a phenomenon hitherto observed only in hydrodynamic experiments. My experimental studies have also considered the excitation of dispersive shock waves and observed their occurrence when the flow velocity exceeds a Mach number of 2. The propagation characteristics of such shocks have been studied as a function of the flow velocity and other experimental parameters. I have also compared my experimental observations with model theoretical results and found them to be in good agreement.

The thesis is organized as follows. In the **first chapter**, I provide an introduction to dusty plasmas and a literature survey of past work that has been carried out in flowing dusty plasmas. In the **Chap. 2**, I have described in detail the experimental set-up and associated instrumentation for my flowing plasma experiments. **Chap. 3** contains results on the characterization of the Ar plasma (that provides the background for creation of the dusty plasma) and estimation of the plasma parameters for a range of discharge parameters. The chapter also provides a detailed characterization of the dusty plasma in terms of the measured and/or inferred values of the inter-particle distance, the dust density, the dust temperature, and other characteristics of the dust cloud. Various flow generation techniques, methods for measurement of the fluid flow velocity with different tools and the calculation of the drag coefficient are described in **Chap. 4**. In **Chap. 5**, the experimental observation of precursor soliton and their characteristic are described. **Chap. 6** is devoted to the experimental observation of flow induced dispersive dust acoustic shocks in a dusty plasma along with the theoretical explanation based on the model KdV burgers equation. In the last chapter, i.e. in **Chap. 7**, we provide some concluding remarks and a discussion about possible future extensions of the work reported in this thesis.

Bibliography

[1] E. T. Meyer, M. Georganopoulos, W. B. Sparks, E. Perlman, R. P. van der Marel, J. Anderson, S. T. Sohn, J. Biretta, C. Norman, and M. Chiaberge, Nature, **521**, 495-497 (2015).

[2] J. D. Richardson, E. C. Stone, J. C. Kasper, J. W. Belcher, and R. B. Decker, Geophys. Res. Lett., **36**, L10102 (2009).

[3] J. Seol, K. C. Shaing, and A. Y. Aydemir, Phys. Plasmas, **23**, 42501 (2016).

[4] Z. Lin, T. S. Hahm, W. W. Lee, W. M. Tang, and R. B. White, Science (80), **281**, 1835-1837 (1998).

[5] L. Guazzotto, R. Betti, J. Manickam, and S. Kaye, Phys. Plasmas, **11**, 604 (2004).

[6] V. Strouhal, Ann. Phys. Und Chemie, Neue Folge, **5**, 216-251 (1878).

[7] T. R. Akylas, J. Fluid Mech., **141**, 455 (1984).

[8] R. C. Ertekin, W. C. Webster, and J. V. Wehausen, J. Fluid Mech., **169**, 275 (1986).

[9] N. F. Smyth, Pure Appl. Geophys. PAGEOPH, **133**, 619-633 (1990).

[10] D. Zhang and A. Chwang, Generation of solitary waves by forward- and backward-step bottom forcing (2001).

[11] S. Jaiswal, P. Bandyopadhyay, and A. Sen, Rev. Sci. Instrum., **86**, 113503 (2015).

[12] A. Usachev, A. Zobnin, O. Petrov, V. Fortov, M. Thoma, M. Kretschmer, S. Ratynskaia, R. Quinn, H. Hoefner, and G. Morfill, Czech. J. Phys., **54**, 1-10 (2004).

[13] S. Jaiswal, P. Bandyopadhyay, and A. Sen, **25**, 065021 (2016).

[14] P. S. Epstein, Phys. Rev., **23**, 710-733, (1924).

[15] Y. Feng, J. Goree, and B. Liu, Rev. Sci. Instrum., **78**, 53704 (2007).

[16] W. Thielicke and E. J. Stamhuis, J. Open Res. Softw., **2**, 1 (2014).

[17] S. Jaiswal, P. Bandyopadhyay, and A. Sen, Phys. Rev. E, **93**, 41201 (2016).

[18] T. Y.-T. Wu, J. Fluid Mech., **184**, 75 (1987).

[19] A. Sen, S. Tiwari, S. Mishra, and P. Kaw, Adv. Sp. Res., **56**, 429-435 (2015).

[20] S. Jaiswal, P. Bandyopadhyay, and A. Sen, Phys. Plasmas, **23**, 83701 (2016).

[21] H. K. Andersen, N. D' Angelo, P. Michelsen, and P. Nielsen, Phys. Fluids, **11**, 606 (1968).

[22] A. Usachev, A. Zobnin, O. Petrov, V. Fortov, M. H. Thoma, H. Höfner, and M. Fink et al., New J. Phys., **16**, 53028 (2014).

[23] Q.-Z. Luo, N. D' Angelo, and R. L. Merlino, Phys. Plasmas, **6**, 3455 (1999).

[24] Y. Nakamura, Phys. Plasmas, **9**, 440 (2002).

[25] S. I. Popel, A. A. Gisko, A. P. Golub', T. V. Losseva, R. Bingham, Phys. Plasmas, **7**, 2410 (2000).

[26] V. E. Fortov, O. F. Petrov, V. I. Molotkov, M. Y. Poustylnik, V. M. Torchinsky, V. N. Naumkin, and A. G. Khrapak, Phys. Rev. E, **71**, 36413 (2005).

[27] D. Samsonov, G. Morfill, H. Thomas, T. Hagl, H. Rothermel, V. Fortov, A. Lipaev, V. Molotkov, A. Nefedov, O. Petrov, A. Ivanov, and S. Krikalev, Phys. Rev. E, **67**, 36404 (2003).

[28] Y. Saitou, Y. Nakamura, T. Kamimura, and O. Ishihara, Phys. Rev. Lett., **108**, 65004 (2012).

[29] J. Heinrich, S.-H. Kim, and R. L. Merlino, Phys. Rev. Lett., **103**, 115002 (2009).

[30] P. K. Shukla and A. A. Mamun, IEEE Trans. Plasma Sci., **29**, 221-225 (2001).

List of Figures

List of Tables

List of Symbols

Symbol	Description	Unit
e	Charge of electron	C
ϵ_0	Permitivity of free space	Fm^{-1}
k_B	Boltzmann constant	Jk^{-1}
E	Sheath electric field	Vm^{-1}
m$_s$	Mass of sth species	kg
ρ	Density of dust particle	m^{-3}
T$_s$	temperature of sth species	eV
n$_s$	density of sth species	m^{-3}
I_j	jth species current	A
λ_{De}	electron Debye length	mm
λ_{Di}	Ion Debye length	μm
λ_D	Dust Debye length	μm
ω_{ps}	Frequency of sth species	s^{-1}
V_{Ts}	Thermal velocity of sth species	ms^{-1}
U	Surface potential	V
C	Capacitance of spherical dust particle	F
Q_d	Dust charge	C
Z_d	Dust charge number	–
r_d	Radius of dust particle	μm
d	Intergrain distance	μm
σ_s^n	Scattering cross section of sth species with neutral molecule	m^2
g	Acceleration due to gravity	ms^{-2}
P	Neutral gas pressure	mbar
Γ	Coulomb coupling parameter	–
Γ_c	Critical value of Γ	–

d_e	Inter electrode distance	m
U_{dc}	Breakdown voltage	V
I_d	Discharge current	A
V_d	Discharge voltage	V
I	Probe current	A
V_p	Plasma potential	V
V_f	Floating potential	V
A_{probe}	Effective probe area	m^2
ϵ_e	Energy of the electron	eV
I_{is}	Ion saturation current	A
f(ϵ_e)	Electron energy distribution function	–
v_{ph}	Phase velocity	mms^{-1}
C_d	Dust acoustic phase velocity	mms^{-1}
ω_{pd}	Dust plasma frequency	$rads^{-1}$
ν_{dn}	Dust neutral collision frequency	s^{-1}
λ_{dn}	Dust neutral collision mean free path	mm
μ_d	Coefficient of compressibility	–
γ_{Eps}	Epstein constant	–
M	Mach number	–

Chapter 1

Introduction

1.1 Introduction and Motivation

In late twenties, a great deal of interest developed in the field of plasma when Tonks and Langmuir first described the inner region of a glowing ionized gas which was produced by means of an electric field in a tube and termed it as 'plasma' [1]. Plasma is an electrically neutral medium of unbound positive and negative particles at the macroscopic level (i.e. the negative and positive charges nearly balance each other at the macroscopic level hence overall charge of a plasma is approximately zero) [2] - so called fourth state of matter. It is likely that 99% of the visible matter in our universe is in the state of plasma [3]. As an example, the Sun is about 100% plasma, as are all stars, ejecting continuous flux of hot plasma in the form of solar wind [4]. Plasma makes up nearly 100% of the interplanetary, interstellar and intergalactic medium. The Earth's ionosphere, fire, fluorescent and neon lights contain plasma. In space plasmas, the micron or submicron sized particles (dust particulates) are ubiquitous, constituting the solid matter in the universe. These grains are charged due to inelastic collision with surrounding plasma components and hence act as a third charged species of the plasma [5]. Thus, a plasma with highly charged dust, electrons, ions with background neutrals is denominated as "dusty plasma".

Dusty plasmas are omnipresent in different parts of our solar system [6] and have various technological [7, 8] as well as laboratory plasma applications where dust can be either grown inside the plasma or intentionally added to the system. Astronomical evidence of dusty plasmas is found in the dark bands of nebulae where the dust absorbs the light from the nebula [9]. They are also observed in other astrophysical situations like in the rings of Saturn (shown in Fig. 1.1) [10], in cometary tails (Fig. 1.2) [11] and in interstellar clouds (particles of size 0.5 μm for ices, 0.25 μm for silicates, 0.1 μm for graphite . . .) [12], Earth's magnetosphere, Zodiacal lights [13] *etc.*.

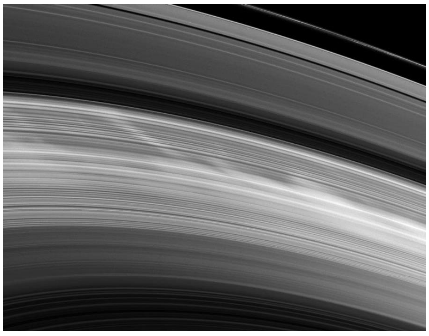

Figure 1.1: Spokes appear on Saturn's Rings recorded by the Cassini spacecraft. (Credit: Cassini Imaging Team, ISS, JPL, ESA, NASA)

Figure 1.2: Dust tail of a comet which is more curved than blue ion tail. (Credit: Robert Jones (SAO student))

The dust particles present in space get charged and have been found to determine many properties of interstellar media, stars and planet formation regions, properties of planetary rings [14, 15], the shock formation during star explosion (shock breakout) and during the interaction of solar wind with the earth magnetic fields [16]. In technological processing plasmas, dust particles grow from molecules in reactive gases to nanometre sized particles [7, 17]. The removal of such plasma-grown particles is an essential issue in computer chip manufacturing. In contrast, materials with novel properties, such as solar cells with much improved efficiency, can be manufactured from thin films with incorporated dust particles [8]. Another instance of natural dust formation in laboratory plasmas is in fusion reactors, where the dust forms from the energetic plasma particles colliding with the chamber walls and the heat exchangers of the reactor [18, 19]. Presence of such dust grains can have a significant adverse effect on the performance of fusion plasmas by enhancing power loss due to radiation and dilution of fuel [20]. There are also more concomitant applications of dusty plasma such as sterilization of wounds with the help of atmosphere-pressure plasmas. Due to all these scientific and technological implications, the understanding of physical properties and utilization of dusty plasma is important and current topic of research in the field of plasma science.

Dusty Plasma also enriched with several physical properties similar to the other complex fluid and colloidal suspensions. Thus, sometimes dusty plasma is also called as complex plasma or colloidal plasma [21]. The unique feature of dust component in plasma is that they are bigger in size and highly massive than the electron and ion species. Moreover, it has been observed in laboratory experiment that the dust particles acquire high negative charges of hundreds or thousands (typically 10^3e to 10^5e) [22, 23] of elementary charges due to the inflow of electrons and ions (the electron thermal velocity is larger, hence it collects more electron than ion). The dust charge often fluctuate with time due to time variation of plasma parameter and becomes another dynamical variable that discriminate the dusty plasma from a conventional two component plasma. Furthermore, due to heavy mass, their charge to mass ratio is small which supports collective phenomena of slow time scales and larger length scales [5]. The high charge state enables the dust component in the plasma to exist in a strong coupling regime, wherein the interparticle potential energy exceeds the thermal kinetic energy of the dust species. When the ratio of the Coulomb energy to the dust thermal energy (defined as coupling parameter Γ) crosses a critical value, the particles can arrange in an ordered crystal-like structure, so-called Coulomb crystal [24, 25]. Such crystals are observed in various lattice configurations and can be transformed into fluid and gaseous phase by increasing the dust temperature or decreasing neutral pressure. These characteristics directly relate the dusty plasma medium with other areas of physics, e.g. condensed matter, complex fluids systems *etc.* [26, 27]. Furthermore, an additional advantage of dusty plasma is associated with the diagnostic tool. The macroscopic size of the dust species and slow time scale phenomenon facilitate to capture its collective dynamics by using low power laser and normal CCD camera. The individual particle tracking and estimation of position and velocity is feasible by analysing the still images recorded by the camera. Therefore at a fundamental level, dusty plasma offers an excellent medium for understanding the physics associated with the kinetic effect occurring at particle levels and for exploring collective excitations in the gaseous, liquid and solid state manifestations [24, 28].

The complex plasma in their liquid state have bulk properties similar to water (e.g. viscosity) and the similarity parameters such as Reynolds and Mach number of these systems are comparable to those of water. This suggest that the dusty plasma can provide a unique tool to model classical fluids and various phenomena associated with fluid (e.g. shear flows, development of “wake” exhibiting stable vortex flows and, instabilities) has been widely studied in the last couple of decades [29, 30].

Fluid flow past an obstacle (or obstacle moving in a stationary fluid) is one of the important topic of research that has been widely explored in fluid dynamics for its application in oceanography, atmospheric dynamics, and variety of engineering applications, often have corresponding analogous phenomenon when a plasma flows through a charged obstacle (or a charged particle moves through a plasma). Some interesting examples are kinetic investigations of boundaries, instabilities and the transition to turbulence *etc.*, which are regarded as outstanding problems in hydrodynamics [31]. Another very common example is that of wake pattern generated behind an object travelling in a fluid that is also seen in plasmas [32–35] when a charged particle travels through it. When the speed of the travelling object becomes supersonic, the boundaries of the wake are defined by a shock structure and the resultant trailing structures are called Mach cones. Mach cones have been observed both in neutral fluids as well as in plasmas [36–38]. However under certain conditions a supersonically travelling object in a fluid also shows interesting nonlinear excitations in the fore-wake region i.e. in the region upstream of the moving object. These take the form of periodic emissions of coherent structures like solitons or shocks and have been both experimentally observed and theoretically studied in hydrodynamics [39–42]. In principle such excitations should also happen in a plasma and one should be able to excite precursor solitons or shocks by moving a charged object rapidly in a plasma or having a plasma flow supersonically over a charged obstacle. The existence of such nonlinear wave patterns in plasma has been predicted by Sen *et al.* [43] using a theoretical model based on forced Korteweg-de Vries (fKdV) equation but experimental feasibilities are still unexplored. To excite these structures, a precise control over the dust flow and size of the obstacle is needed. Motivated by such a consideration this thesis is devoted to laboratory investigation and theoretical studies related to flow induced excitation of nonlinear waves and structures in dusty plasma. To do so we have carried out controlled experiments to explore various techniques of flow generation and measurement of flow velocities at the single particle level and fluid level, propagation characteristic of shock wave and, the precursor soliton excitation (a forewake phenomenon associated with transcritical flows) in flowing dusty plasma. These studies are very impactful as they relate the phenomenon occuring at satellite and planetary interactions [44, 45].

Rest of this chapter is organized in the following way: in the next section (Sec. 1.2) we have introduced some basic concept and parameter definitions needed to describe complex plasmas. In the later section (Sec. 1.3), a brief review of some of the past work on waves and instabilities in such a medium is provided. Sec. 1.4 provides an outline of the thesis.

1.2 Basics of Complex Plasma

The laboratory experiments of complex plasma are usually performed in weakly ionized plasma in which the degree of ionization is very small ($\ll 1$) and the high energy particles are mostly composed of electrons while the energy of ions are of the order of energy of gas molecules which are usually as room temperature. Hence, these plasmas are also known as low temperature plasmas. The characteristic features of conventional plasma can be described by the characteristic screening length and response time scale of the plasma particles to the applied electric field. Similarly, dusty plasma is also characterized by certain parameters and associated length and time scales.

In this section, we will briefly describe the basic parameters of a dusty plasma such as its characteristic lengths and frequencies, quasineutrality condition, dust charging and surface potential, basic forces acting on the dust particles and magnitudes of the Coulomb coupling parameter and phase transition to establish necessary background for the analysis of the experimental results and their physical interpretation that are given in subsequent chapters.

1.2.1 Characteristic Lengths

There are three different scale lengths for combined dust and plasma mixture, namely the plasma Debye length (λ_D), dust radius (r_d) and, average inter-grain distance d, that decide the role of charged dust grains in plasma. In a situation $r_d \ll \lambda_D < d$, the dust particles get shielded by opposite charge species hence treated as isolated screened grains. In this case, the dust particles do not participate in the collective dynamics of a plasma and correspond to "Dust in Plasma", whereas for $r_d \ll \lambda_D > d$, dust grains act as massive charged particles similar to multiply charged negative or positive ions and show a collective behaviour. This corresponds to "a dusty plasma".

a) Debye length

One of the underlying characteristic of plasma is screening out of the electrostatic potential of the individual charged particle introduced into the plasma. In the case of a dusty plasma, along with the electrons and ions, the charged dust particles also take part in the shielding of external electric potential. A measure of the plasma shielding is called the Debye length λ_D and is defined for a dusty plasma as [5],

$$\lambda_D = \frac{\lambda_{De}\lambda_{Di}}{\sqrt{\lambda_{De}^2 + \lambda_{Di}^2}}. \tag{1.1}$$

Where, $\lambda_{De(i)} = (k_B T_{e(i)}/4\pi n_{e(i)} e^2)^{1/2}$ is the electron (ion) Debye length. For a dusty plasma with negatively charged dust grains $n_e << n_i$ and $T_e \geq T_i$, *i.e.* $\lambda_{De} >> \lambda_{Di}$. Consequently, we have $\lambda_D \approx \lambda_{Di}$. This shows that the shielding distance in a complex plasma formed due to negatively charged dust grains is mainly determined by the temperature and density of the ions.

b) Dust radius

Grain size is another important characteristic length in a dusty plasma that describes its various features. The dust particle size plays a key role in deciding the amount of positive or negative charge resides on the dust surface and hence determining the dust surface potential. The particle radius also decides the collision cross-section between various species present in the plasma and the magnitude of various forces acting on the dust particles such as gravity, electrostatic forces, drag forces *etc.*.

c) Inter-grain spacing

Dusty plasma consists of electrons, ions and extremely massive charged dust grains in a background of neutral gas. The dust radius is much smaller than the plasma

Debye length λ_D but the inter-particle spacing can be larger or smaller than the λ_D. The inter-grain spacing mainly decides whether the dust particles participate in the collective dynamics or not depending upon its relation with the dust Debye length.

1.2.2 Characteristic Frequencies

a) Frequency of oscillation

In a plasma medium, the non-compensated charge density exists only upto the Debye radius whereas at a distance much greater than the Debye radius the plasma becomes quasi-neutral. Likewise, the dusty plasma also maintains the macroscopic space charge neutrality. The small disturbance in the position of plasma particles result in building up of an internal space charge field that gives rise to collective particle motions which tends to restore the space charge neutrality. The inertia of particle leads to collective particle oscillation around their mean position. The frequency of these collective oscillations is known as plasma frequency (ω_p). The plasma frequency associated with the plasma species 's' is defined as:

$$\omega_{ps} = \left(\frac{4\pi n_{s0} Q_s^2}{m_s} \right)^{1/2}. \tag{1.2}$$

Since the frequency of such oscillations depends on mass, charge and number density of plasma particles, it is different for the electrons, ions and dust particles.

b) Collision frequency

The other important characteristic frequency is linked with the collision of plasma particles with stationary neutrals. In a weakly ionized plasma, there are a significant number of neutral particles. Thus, the plasma particles (electrons, ions and dust grains) can undergo frequent collisions with neutrals. These collisions can be characterized by respective collision frequencies ν_{sn}. The collision frequency of the plasma particles 's' with the neutrals can be written as;

$$\nu_{sn} = n_n \sigma_s^n V_{Ts}. \tag{1.3}$$

Where n_n is the neutral number density, σ_s^n is the scattering cross section and $V_{Ts} = \sqrt{\frac{k_B T_s}{m_s}}$ is the thermal speed of the species 's'. The collision of plasma particles with the neutrals leads the damping of the collective particle oscillations. This will happen only when the collision frequency ν_{sn} is smaller than the plasma frequency ω_p i.e.

$$\nu_{en}, \nu_{in}, \nu_{dn} < \omega_p. \tag{1.4}$$

1.2.3 Grain charging and Dust Surface Potential

The dust particles introduced into the plasma get charged negatively or positively through various fundamental charging processes. The important elementary charging processes are, (a) interaction of dust grains with gaseous plasma particles, (b) photo-ionization due to incident UV radiation and (c) secondary electron emission (due to interaction of dust grains with energetic electrons and ions). Other charging mechanism can also occur (e.g. thermionic emission, field emission, impact ionization *etc.*), but they are significant in some special circumstances. In low temperature laboratory plasma, the charging of dust grains mainly occur due to collection of plasma particles flowing onto their surface. As the electron thermal speed is much higher than the ion thermal speed, the electrons will reach the dust surface earlier than the ions. This results in the attachment of a large number of electrons on the dust surface and hence the particles will be negatively charged. Therefore, the ions are accelerated towards the dust grains and electrons are repelled by the dust grains until the currents are equalized, $I_i = I_e$. The dust charges reaches to its final value at this point. The grain charge can fluctuate around the final value due to random nature of charging process. The magnitude of charge fluctuation Z_1 in a typical gas discharge complex plasma is given by [46] $\langle Z_1 \rangle \sim 0.5\sqrt{Z_d}$, where Z_d is the equilibrium charge. The dust grain charge Q_d is determined by

$$\frac{dQ_d}{dt} = \sum_j I_j \tag{1.5}$$

where j represents the plasma species (electrons and ions) and I_j is the current associated with the species j. At equilibrium, the net current flowing onto the dust grain surface becomes zero, i.e. $\sum_j I_{j0} = 0$, where I_{j0} is the equilibrium current. Assuming electrons and ions obey Maxwellian distribution, an expression for their charging current can be given by [47]

$$I_e = -en_e\sqrt{\frac{k_BT_e}{2\pi m_e}}exp\left(\frac{eU}{k_BT_e}\right)\pi r_d^2, \tag{1.6}$$

$$I_i = en_i\sqrt{\frac{k_BT_i}{2\pi m_i}}\left(1 - \frac{eU}{k_BT_i}\right)\pi r_d^2. \tag{1.7}$$

In Eq. 1.6, the exponential factor is due to the repulsion of electrons by negatively charged dust grains, whereas the factor $(1 - eU/k_BT_i)$ in Eq. 1.7 is due to the orbital motion effects. The ion current to the grain is usually approximated by the 'Orbital Motion Limit' (OML) model for a spherical probe. The OML theory is applicable as long as the particle radius is small compared to the Debye length, $r_d << \lambda_D$. In the case of streaming ions, the temperature (T_i) in Eq. 1.7 has to be replaced by its kinetic energy. Using Eq. 1.6 and Eq. 1.7 in $I_e + I_i = 0$, we get

$$\sqrt{\frac{m_i}{m_e}}\left(1 + \frac{4\pi\epsilon_0}{e}P\frac{eU}{k_BT}\right)exp\left(\frac{eU}{k_BT}\right) + \frac{eU}{k_BT} - 1 = 0. \tag{1.8}$$

Where we have assumed that the electrons and ions to have the same temperature denoted by T. An approximate expression (for $n_e \approx n_i$ and $T_e \neq T_i$) for surface potential can be derived from Eq. (1.8) which is given as [48]

$$U = 0.73\frac{k_B T_e}{e}\ ln\ (m_e T_e/m_i T_i)^{1/2}. \tag{1.9}$$

The dust grain charge Q_d can be estimated by using the relation:

$$Q_d = CU. \tag{1.10}$$

Where U is the surface potential of the dust particles and C is the capacitance of dust grains of radius r. For an isolated, conducting spherical grain, the capacitance is given by $C = 4\pi\epsilon_0 r_d(1+r_d/\lambda_D) \approx 4\pi\epsilon_0 r_d$ (where, r_d/λ_D comes from the screening effect and reduces to the vacuum value for $r_d << \lambda_D$).

1.2.4 Quasi-neutrality Condition

In the absence of any external perturbation the dusty plasma is macroscopically neutral (i.e. the net resulting electric charge is zero). The charge neutrality condition for a dusty plasma can be written as [5]

$$Q_i n_{i0} = e n_{e0} - Q_d n_{d0}. \tag{1.11}$$

where, n_{i0}, n_{e0} and n_{d0} are the unperturbed ion, electron and dust number density and $Q_i = Z_i e$ the ion charge whereas $Q_d = Z_d e$ is the dust particle charge (Z_d is the number of elementary charge residing on the surface of dust grains). In a laboratory dusty plasma, the dust grains are mostly negatively charged by collecting more electrons than ions as described in Sec. 1.2.3. Hence the expression for quasi-neutrality condition becomes

$$n_{i0} = n_{e0} + Z_d n_{d0}. \tag{1.12}$$

Typically, a dust grain acquires thousands to several hundred thousand of electrons onto its surface, hence the electron density gets significantly depleted. Consequently, the quasineutrality condition in a more simplified form could be $n_{i0} \approx Z_d n_{d0}$.

1.2.5 Coulomb Coupling Parameter and Phase Transition

A very important feature of dusty plasma is that they could be found in solid, liquid and gaseous state under suitable conditions. Highly charged dust grains which interact with each other via a strong electrostatic potential are characterized by Coulomb coupling parameter Γ (a measure of coupling of plasma species). The Coulomb coupling parameter (defined as the ratio of dust potential energy to the dust thermal energy) is represented by

$$\Gamma = \frac{Z_d^2 e^2}{d k_B T_d} exp\left(-\frac{d}{\lambda_D}\right). \tag{1.13}$$

Where d is the inter-particle distance, related to the particle density n_{d0} by $d = \left(\frac{3}{4\pi n_{d0}}\right)^{1/3}$ and the factor $exp\left(-\frac{d}{\lambda_D}\right)$ takes into account the screening of the dust charge by the plasma over a distance of the Debye length λ_D.

A dusty plasma is found in a crystalline state when $\Gamma \gg 170$, a strongly coupled fluid regime when $1 << \Gamma << 170$ and gaseous state when the coupling between particle is extremely weak, $\Gamma << 1$ [24, 25, 28]. The coupling parameter Γ decreases if the dust temperature increases. Hence, by increasing the temperature it is possible to see the phase transition of dust crystal. Thus, dusty plasma provide an excellent medium for the study of phase transition.

1.2.6 Forces on Dust Particles

The dynamics of dust grains in a plasma is governed by various forces that act simultaneously when particle gets charged. The important fundamental forces acting on the particles such as electrostatic force, gravitational force, drag forces, thermophoretic force *etc.* are briefly introduced in the following. A schematic of these forces is shown in Fig. 1.3.

a) Electromagnetic force

The electromagnetic force ($\vec{F}_{EL}$) acting on a dust particle is equal to the sum of electrostatic force ($\vec{F}_E$) and Lorentz force ($\vec{F}_L$) and is given by [49],

$$\vec{F}_{EL} = \vec{F}_E + \vec{F}_L = Q_d\left(\vec{E} + \vec{v}_d \times \vec{B}\right). \tag{1.14}$$

Where $\vec{B}$ and $\vec{v}_d$ are the magnetic field and the dust velocity, respectively.

b) Gravitational force

In ground based laboratory experiments, one of the strongest force acting on the microparticles is gravitational force ($\vec{F}_g$) in downward direction. It can be expressed as [49]

$$\vec{F}_g = m\vec{g} = \frac{4}{3}\pi r_d^3 \rho \vec{g}, \tag{1.15}$$

Where m_d is the mass of dust particle and g is the acceleration due to gravity. The gravitational force on the dust grain of radius r_d varies as $F_g \propto r_d^3$.

c) Drag force

The time rate of momentum transfer from the dust grains to the plasma particles or plasma particles to the dust grains is defined as drag force. It arises mainly due to collision of ions and neutrals to the dust. Hence, there are two types of drag forces exist in a dusty plasma which are discussed below:

i) Ion drag force

The ion drag force exerted on the dust particles originate by three different ways: a) collection of ions by their direct impact on the dust grains, referred as collection drag force ($\vec{F}_{di}^{coll}$), b) Coulomb interactions between ions and microparticles results Coulomb drag force ($\vec{F}_{di}^{coul}$), c) the distortion of the shape of Debye sphere around the dust microparticles due to ion fluid flow causes the ion flow drag force ($\vec{F}_{di}^{flow}$). So the total drag force is given by [49],

$$\vec{F}_{di} = \vec{F}_{di}^{coll} + \vec{F}_{di}^{coul} + \vec{F}_{di}^{flow}. \tag{1.16}$$

The contribution of ion flow is usually small in the sheath region thus $\vec{F}_{di}^{flow}$ can be neglected. The other two forces can be expressed as [49]

$$\vec{F}^{coll,coul} = n_i m_i \sigma^{coll,coul} V_{it} v_i. \tag{1.17}$$

where, $V_{it} = (v_i^2 + 8k_B T_i/\pi m_i)^{1/2}$ and σ^{coll} is the collection cross section which can be expressed in terms of floating potential and the ion energy. That is

$$\sigma^{coll} = \pi b_c^2 = \pi r_d^2 \left(1 - \frac{2eU}{m_i v_i^2}\right). \tag{1.18}$$

The expression for Coulomb cross section can be derived from the classical Coulomb theory;

$$\sigma^{coul} = 4\pi b_{\pi/2}^2 \Gamma_c = 2\pi b_{\pi/2}^2 ln \left(\frac{b_{\pi/2}^2 + \lambda_{De}^2}{b_{\pi/2}^2 + b_c^2}\right). \tag{1.19}$$

In the Eq. 1.19, $b_{\pi/2}$ represents the impact parameter which results in a deflection of the particle by $\pi/2$ and the term $\Gamma_c = \frac{1}{2} ln \left(\frac{b_{\pi/2}^2+\lambda_{De}^2}{b_{\pi/2}^2+b_c^2}\right)$ denotes the Coulomb logarithm. Now, the total ion drag force can be written as:

$$\vec{F}_{di} = n_i m_i \pi \left(b_c^2 + 4b_{\pi/2}^2 \Gamma_c\right) V_{it} v_i. \tag{1.20}$$

This equation (Eq. 1.20) is known as Barnes' formula [50].

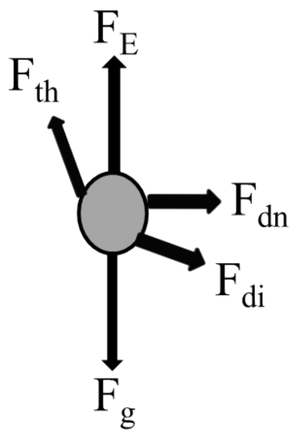

Figure 1.3: Different type of forces acting on a spherical dust particle

ii) Neutral drag force

The charged dust particles moving relative to background neutrals are subjected to neutral drag force which can be defined as the rate of momentum exchange between the dust particles and neutrals during their collision. There are two regimes which can be considered to estimate neutral drag force. One is hydrodynamic regime where the Knudsen number (ratio of neutral mean free path to the microparticle radius) is much smaller than unity (i.e. $K_n \ll 1$) and another one is the kinetic regime where Knudsen number is much larger than unity (i.e. $K_n \gg 1$). In the hydrodyamic or high prssure regime where $K_n \ll 1$, the neutral drag force can be estimated from Stokes' law. In this case, it is found that the drag force is proportional to the relative speed (u_{dn}) between the dust and the neutral particles and the radius (r_d) of the microsphere. For kinetic regime, where the neutral mean free path is much greater than the microparticle radius, the Epstein formula can be used, provided that the relative speed $\mid v_d - v_n \mid$ should be very small in comparison with the mean thermal velocity of the gas atom [51]. The expression for Epstein neutral drag force is

$$\vec{F}_{dn} = -m_d \nu_{dn} \vec{u}_{dn}. \tag{1.21}$$

where, $\vec{u}_{dn}$ is the velocity of the dust particle relative to that of the neutral gas atoms and ν_{dn} is the damping rate coefficient which can be defined as:

$$\nu_{dn} = \frac{4}{3}\gamma_{Eps}\pi r_d^2 m_n n_n V_{Tn}/m_d \tag{1.22}$$

In the Eq. 1.22, n_n representing the number density of gas atom , $V_{Tn}\left(=\sqrt{8k_B T_n/m_n\pi}\right)$ is the neutral thermal speed. The mass of the neutral atom and dust are denoted by and m_n and and m_d respectively. γ_{Eps} is known as Epstein drag coefficient with values between 1.0 for specular reflection and 1.44 for diffuse reflection.

d) Thermophoretic force

If a temperature gradient is maintained in the gas, the momentum transfer during the collision between the gas molecules and dust grains is larger on the hot side of the dust particle. Therefore there will be a net momentum transfer from the gas to the dust grains. The resulting force is referred as the thermophoretic force. It is proportional to the temperature gradient and is directed from higher gas temperature to lower temperature region. The thermophoretic force can be expressed as [49],

$$\vec{F}_{th} = -\frac{32}{15}\frac{r_d^2}{V_{Tn}}\left[1+\frac{5\pi}{32}(1-\alpha)\right]\kappa\nabla T_n. \tag{1.23}$$

Where κ is the translational thermal conductivity and T_n is the temperature of the gas. A feasible approximation for the accommodation coefficient (α) is $\alpha \approx 1$ for the dust surface temperature less that 500K.

Typical magnitude of various forces (discussed in Sec. 1.2.6) acting on a micron sized dust particle is given in the table 1.1. It is clear from the table that the gravitational force and the electrostatic force are comparable in magnitude and compete with each other for a particle of radius $1\mu m$.

Type of force	Magnitude (Newton)
Gravitational force (F_g)	$10^{-13} r_d^3$
Electrostatic force (F_E)	$10^{-13} r_d$
Neutral drag force (F_{dn})	$10^{-14} r_d^2$
Ion drag force (F_{di})	$10^{-14} r_d^2$
Thermophoretic Force (F_{th})	$10^{-14} r_d^2$

Table 1.1: Different types of forces acting on a micron sized dust particle, where r_d is in μm.

1.3 An Overview of Earlier Works

In this section we provide an overview of previous studies that have been made to understand the dusty plasma medium. Dust particles, when added into the conventional electron-ion plasma, collect more electrons than ions and get negatively charged. The highly charged dusts freeze into the crystal in a strongly coupled regime and can be transformed into the fluid depending upon the parameters such as dust temperature and neutral pressure. The comparison of liquid plasmas with other fluids assures that they can provide a unique tool to model classical fluids. Thus, most of the phenomena occurs in the water and other fluids viz. nanofluids and colloid suspension can be modelled in dusty plasma medium. The presence of highly charged dust particles in astrophysical scenario, which govern many properties and features in Saturn's rings (such as mysterious dark spoke formation, Bow waves, wake formation) as well as interstellar molecular clouds (such as shock formation during the star explosion) *etc.*, motivated the various theoretical and experimental studies from a long time. Some of the structures observed in Saturn's rings have connection with the dust acoustic wave (DAW) which was first described theoretically by Rao *et al.* in 1990 [52]. DAW is a compressive wave like a sound wave in an air. After the Rao's discovery, the dusty plasma research has boosted up and the DAWs have been studied by different groups. Other linear modes which exist in dusty plasma such as dust ion-acoustic (DIA) waves [53], dust lattice (DL) waves [54], dust Coulomb waves [55] *etc.* have been studied widely. The linear theories are valid upto a small amplitude wave limit but sometimes the unstable mode attains a larger amplitude and nonlinear effect comes into play. The nonlinearities contribute to localization of the wave, and leads to nonlinear structures such as solitons, shocks, vortices and many more [26, 56]. The nonlinear form of the waves and structures such as DIA solitary waves [56], the DA solitary waves [57], the DL solitary waves [58], Dust acoustic shock waves (DASW) [57], Dust ion-acoustic shock waves (DIASW) [56], have also been extensively studied both theoretically and experimentally. The ion acoustic shock waves in collision-dominated double electron temperature plasma have been introduced by Shukla *et al.* in 1976 [59]. In a dusty plasma medium, the properties of dust ion acoustic shocks and holes have been examined by Shukla *et al.* [60] assuming that a dusty plasma contains immobile charged dust grains, warm electrons and ions. In an article by Popel *et al.* [61], the presence of dust charge fluctuations have been identified as important dissipation sources contributing to the formation of shock waves. The formation of shock waves in a strongly coupled dusty plasma have been reported by Shukla *et al.* [62]. They have used the generalized hydrodynamic (GHD) equation to derive the KdV-Burger's equation and the possible stationary solutions of the KdV-Burger's equation are represented in terms of monotonic/oscillatory shock profiles. According to them, the shear and bulk viscosity play an important role in the formation of monotonic and oscillatory dust acoustic shock waves. The concept of shock wave in weakly coupled dusty plasma medium is stated by Eliasson *et al.* [63]. The other nonlinear structure of interest is solitary wave which is also studied extensively in last decade. This is a coherent structure which maintains its shape while propagating for a larger distance. In addition, it can even propagate after the mutual collision without losing their identity because of exact balance between the nonlinear wave steepening and dispersion induced broadening. The concept of solitary wave in dusty plasma has been first given by Rao *et al.* [52]. They have explained soliton propagation by using KdV equation which is obtained by integrating the fluid equations along with the

Poisson's equation in weakly nonlinear regime. After that, a number of theoretical studies on the propagation and collision of two solitary wave have been carried out by different researchers [57, 64–70].

Experimentally, first observation of DAWs and DIAWs have been made by Barken *et al.* [71]. Since then many experimental studies on DAWs in weakly and strongly coupled dusty plasma medium have been reported by several authors [72–75]. The experiments on transverse shear wave in strongly coupled dusty plasma have been performed by Nonumura *et al.* [76] and Pramanik *et al.* [77]. The existence of transverse shear wave and turn over effect in DAWs for the strongly coupled dusty plasma has verified the earlier prediction using Generalized Hydrodynamic (GHD) description given by Kaw and Sen [78]. The Dust Ion Acoustic (DIA) solitons and DIA shocks have been observed experimentally by Nakamura [79, 80]. The DA shock wave under microgravity condition has been first observed by samsonov *et al.* [81] on board of the International Space Station ISS. Further the shock melting in 2D plasma crystal has also been observed by Samsonov *et al.* [82]. The dissipative longitudinal solitary wave has been first reported by Samsonov *et al.* [83] and later the low frequency DA solitary wave has been investigated by Bandyopadhyay *et al.* [84] where they have compared their experimental observation with the analytic solution of a model Korteveg-de Vries equation. Further, various forces, that act on the dust grains and may govern their dynamics, in the plasma have also been extensively studied [85–91]. The thermophoretic force on the dust grains has been utilized to counteract gravity and lifting up (suspending) the dust particles by Rothermel *et al.* [85]. The effect of radiation force on the dynamics of dust grains has been studied by Liu *et al.* [86]. The different drag forces such as ion drag force and neutral drag force have been reported by many groups worldwide [87–91].

Shukla *et al.* [92, 93] have provided a comprehensive review article having main focus on collective processes and forces acting on dust grains in dusty plasma. Most of the basic principles of dusty plasma has covered in the monograph by Shukla and

Mamun [5].

The strongly coupled dusty plasmas either in the form of lattice [24, 25] or strongly coupled fluid [29, 94] have been substantially utilized by many authors to understand the physics behind the generation of Mach cones, shear flows, linear/nonlinear waves and different hydrodynamic instabilities *etc.* [30, 36, 38, 81, 94]. These studies are important as they mock up the various astrophysical phenomena and having fundamental importance too. A great deal of research has also been inspired and has benefited from various investigations in hydrodynamics such as shear flow, layer formation in stratified shear flow, shear flow induced instability, different waves and instabilities *etc.* The laboratory experiment on laser excited Mach cones has been observed by Melzer *et al.* [36] when, a focused beam was swept at a supersonic speed through the crystal in a controlled and repeatable manner. Samsonov *et al.* [37] have studied V-shaped shocks which produced spontaneously by a supersonic particle moving below the main two-dimensional particle layer. Mach cones composed of shear waves have been observed experimentally by Nosenko *et al.* [38] in a two-dimensional screened Coulomb crystal. They have been excited by applying a force from the radiation pressure of a moving laser beam. Morfill *et al.* [29] have performed first experiment on dust fluid flow (at particle level) around an obstacle under microgravity condition in the background of rf discharge. In that experiment, a void, formed due to effect of thermophoretic force, has been treated as an obstacle for the flow. They have observed stable laminar shear flow around the obstacle, the development of "wake" exhibiting stable vortex flow and an unstable mixing layer between the flow and the wake. Soon after, Nosenko *et al.* [30] have experimentally measured the shear viscosity of a two-dimensional liquid-state dusty plasma where two counter propagating Ar^+ laser beams have been used to push the particles, causing shear-induced melting of the monolayer and a shear flow in a planar Couette configuration. The similar configuration has also been used by Nosenko *et al.* [95] to study the nonlinear mixing and harmonic generation of compressional waves in 2D

Yukawa lattice. They have excited two sinusoidal waves with different frequencies in the lattice by pushing the particles with modulated Ar^+ laser beams and above an excitation-power threshold due to frictional damping, a nonlinear interaction of phonons have been observed. In 2006, Ratynskaia *et al.* [96] have experimentally observed the viscoelastic vortical fluid motion in a strongly coupled particle system within a narrow range of neutral pressure. The large scale vortex flows coexistent with partial preservation of the global hexagonal lattice structure. Steinberg *et al.* [97] have theoretically studied the shear instability that can be triggered in compressible fluid where the viscosity depends on density. This has happened when the flow has been two- or three-dimensional and the shear rate has exceeded the threshold value, which depends on the viscosity scaling exponent ϵ. It has been showed that the instability is only possible for $\epsilon > \frac{4}{3}$. Ashwin *et al.* [98, 99] have performed a molecular dynamics simulation to study the Kelvin Helmholtz instability for the first time in 2-D strongly coupled Yukawa liquid. The instability has been observed when a subsonic shear profile has superposed on an equilibrated Yukawa liquid. Vortex-roll has also been observed for nonlinear regime. Later on, they have performed the similar exercise with GH model and have found a qualitative agreement in the growth rate in the range of coupling parameter $1 < \Gamma < 100$ for these two approaches. After the Ashwin's report, K-H instability and shear flow instability has been theoretically studied in weakly coupled and strongly coupled dusty plasma by Tiwari *et al.* [100] and Banerjee *et al.* [101]. The Rayleigh-Taylor instability has also been studied theoretically by several authors [102–104]. Experimentally, it has been studied by Heidemann *et al.* [94] and Pacha *et al.* [105] in a highly dissipative cloud of complex plasma, .

In recent years, different waves and interesting structures, induced by flowing the dust fluid via manipulative geometries (obstacle), or by controlling or manipulating the microsphere by the neutral gas, has been observed in laboratory by several authors. In this domain, Mitic *et al.* [106] have observed the particle vortices induced by the convection of neutral gas. Kroll *et al.* [107] have performed the experiments on the rotation of cloud as a whole in response to the neutral gas. The effect similar to the magnetization of the heavy dust particles in complex plasma, making use of the frictional coupling between a complex plasma and the neutral gas, has been seen by Kählert *et al.* [108]. Samsonov *et al.* [81] have reported an experimental observation of gas pulse induced shock formation in an rf produced 3D complex plasma under microgravity condition in the PKE-Nefedov device. The experimental result has been compared with the modified Rankine-Hugoniot equation taking into account the Coulomb pressure of strong coupling which has verified the structure as a weak shock with Mach number 1.2-1.4. In 2009, Heinrich *et al.* [109] have experimentally observed the repeated occurrence of dust acoustic shock waves in a dc glow discharge plasma. The shock waves have been excited when the dust fluid flows through two slits separated by very small distance. The self-steepening of nonlinear dust acoustic wave into the saw-tooth wave with sharp gradient in dust density is observed, which has quantitatively matched with the theoretical model of Shukla *et al.* [110]. Instead of slits, if a plate of 5 mm aperture is placed at that location and dust particles are allowed to flow through it, then a dust jet is observed having the velocity on the order of dust acoustic speed [111]. Nakamura *et al.* [112] have performed an experiment on bow shock formation in 2-D dusty plasma due to supersonic flow of charged dust particle through a conducting needle. The flow has been generated and controlled by tilting the experimental device. The structure has been confirmed as a bow shock by hydrodynamic theory as well as numerical simulation. Soon after, Fink *et al.* [113] have presented an experimental observation of well-developed tree like string structure supported by the gas flow in three-dimensional dc complex plasma. A built in nozzle has been used to redistribute the gas flow along the discharge axis which is used to control the effect of gravity and force due to electric field of the discharge on the microspheres. By using the similar configuration and with pulsed acceleration, the wave pattern have been observed behind the de Laval nozzle, which is called as autowave [114]. Later, Meyer *et al.* [115, 116] have extended the work carried out by Nakamura *et al.* [112] by using different method of flow generation. In their experiment, the dust particles have been initially confined in the L shaped grounded mesh and then flow has been generated by making it floating. They have observed the detached bow shocks in the upstream side of the cylinder, while an extended teardrop-shaped wake region is formed on the downstream side. In most of these experiments, the flow of dust fluid was initiated either by tilting the complete experimental set-up [112] to use gravity or by using gas puffs [81, 114]. Tilting the device can often be problematic as it can disturb optical alignments. In addition, it also limits the amount of control one has on the flow of particles. Likewise experiments with gas puffs also have limitations in the way of induced changes in the equilibrium configuration due to the sudden introduction of neutral gas into the device and the concomitant increase in the pressure. Additionally, in previous experiments, the fluid velocities have been measured in the context of specific experiments of structure excitations. A detailed investigation of different tools to measure the flow velocities in kinetic to fluid regime and their dependence on different parameters are still an unexplored topic of flowing dusty plasma research.

1.4 Contribution and Outline of the thesis

In this thesis, we have extended the flowing plasma research by performing the experiments on investigation of various techniques of flow generation without disturbing the optical alignment and equilibrium of the system and, the detailed measurements of the flow velocities in kinetic to fluid regime along with their variation with the flow rate and discharge parameters, which are relatively unexplored area of research. Further, we have performed the experiments to study the generation of nonlinear wave pattern in the fore-wake region such as precursor solitons and shock, which surprisingly has not received much attention so far in the plasma physics community and our findings should stimulate the further research in this area.

Chapter 2 discusses the design and development of an experimental set-up for flow studies, instrumentation and different diagnostics used in the experiments. It provides a detailed description of vacuum vessel, pumping and gas system, electrode geometry and power supply. The chapter also includes the details about plasma diagnostics such as Langmuir and emissive probes, circuits used for biasing the probe and the wave excitation circuit. Details of different dust particles used in the experiments and their characteristics are also given. The optical diagnostics used for viewing and capturing the dynamics of microsphere are described in this chapter.

Chapter 3 is devoted to the general properties of DC glow discharge plasma and the dusty plasma, which are relevant for the subsequent parts of the thesis. The detailed characterization of plasma (by using different diagnostics discussed in chapter 2) and dusty plasma for the measurement of different plasma/dusty plasma parameter are carried out in this chapter.

Chapter 4 appertain to various flow generation and velocity measurement techniques in kinetic and fluid regimes. A novel technique based on the excitation of dust acoustic wave is used for the first time to measure the flow speed in the case of dense dust fluid. A detailed discussion on the merits and demerits of the different techniques to initiate the flow and of the various measurement tools are presented. An estimation of the neutral drag force, which acts to either induce fluid flow or slow it down, is also provided.

Chapter 5 focuses on the precursor soliton excitation in dusty plasma medium caused by a supersonic flow of the dusty plasma over an electrostatic hill. These structures always go beyond the usual wake field excitations seen behind a moving charged object in a plasma and are a distinctly fore-wake phenomenon analogous to that observed in hydrodynamic experiments and are associated with transcritical flows. The propagation characteristics of this nonlinear structure is also studied by calculating the soliton parameter and time interval between the generation of two fully developed solitons. The experimental result are compared with theoretical forced Korteweg-de Vries (fKdV) model.

Chapter 6 deals with the neutral flow induced excitation of shock waves in dusty plasma. The technique of the excitation of the shock waves and detailed characterization of propagation characteristics of these structures by changing the perturbation strength in terms of the potential hill and background gas flow rate are described. The experimental results are compared with the theoretical model based on Generalized hydrodynamic equation, which includes the dust-dust interaction in the form of viscosity and an equilibrium flow in the velocity expansion. The effect of dust-neutral collision on the propagation of shock waves is also described in the chapter.

Finally in **chapter 7**, we provide a summary of the work carried out in the thesis. We further made an attempt to point out at some possible issues that merit future investigations.

Chapter 2

Experimental Set-up and Instrumentation

S. Jaiswal, P. Bandyopadhyay and A. Sen, Rev. Sci. Instrum., ***86****, 113503 (2015)*

This chapter provides the detailed description of versatile table top Dusty Plasma Experimental (DPEx) device with associated diagnostics and instrumentations [117]. The device has been built up at Institute for Plasma Research, which has several in-built facilities for studying flow induced excitation of wave patterns in liquid dusty plasma and different types of forces acting on the dust grains. In particular, there is an opportunity to effectively redistribute the gas flow along the discharge axis, which can be used as an active source to control and manipulate the dust particles. The basic geometry and design philosophy of this device has been inspired by the PK-4 experimental device [118, 119]. However, there are significant differences and enhancements in factors like the dimensions of the system, the electrode geometry and arrangement, as well as the plasma generation mechanism. In addition, the pumping and gas systems are also connected in a different manner so as to facilitate more precise control of particle flows for experimental investigations of flow induced excitations. As a basic requirement for flowing plasma experiments, the system dimension is chosen big enough so that it is much larger than the collisional mean free path (mainly dust-neutral), plasma Debye lengths, wavelength of the excited wave patterns and to make the plasma flow over the sufficient distance without any hindrance. Care has also been taken to ensure that the system size is not too large so as to require very high potential to be applied in order to produce a homogeneous dust cloud. The device is also designed with the concern of enough access for various diagnostics and instrumentations.

The chapter is organized as follows. The first section (Sec. 2.1) describes in details about the experimental set-up and accessories. Different types of dust particles used in the experiments along with their size distribution and dust dispenser are discussed in Sec. 2.2. Different power supplies used in the experiment are described in section (Sec. 2.3). Sec. 2.4 deals with the associated diagnostics and their instrumentations. We draw a concluding remark in Sec. 2.5.

2.1 Experimental Set-up

In this section, we provide a detailed technical and physical description of Dusty Plasma Experimental (DPEx) device used for the excitation of different waves and structures in a flowing dusty plasma [117]. The set-up mainly consists of a vacuum vessel, a pumping unit, electrodes *etc.*, which are described in detail in the following subsections.

2.1.1 Vacuum Vessel

The entire set of experiments are carried out in a DPEx device. A photograph of the experimental set-up is shown in Fig. 2.1 and its schematic diagram with associated diagnostics is depicted by Fig. 2.2. The vacuum chamber consists of a Π-shaped Pyrex glass tube which provide a very good access for optical diagnostics. The tube has several axial and radial ports for functional access. For various experimental convenience it is divided into two different parts, 1) **Experimental part** and 2) **Service part**. The main experimental area has a length of 65 cm and inner diame-

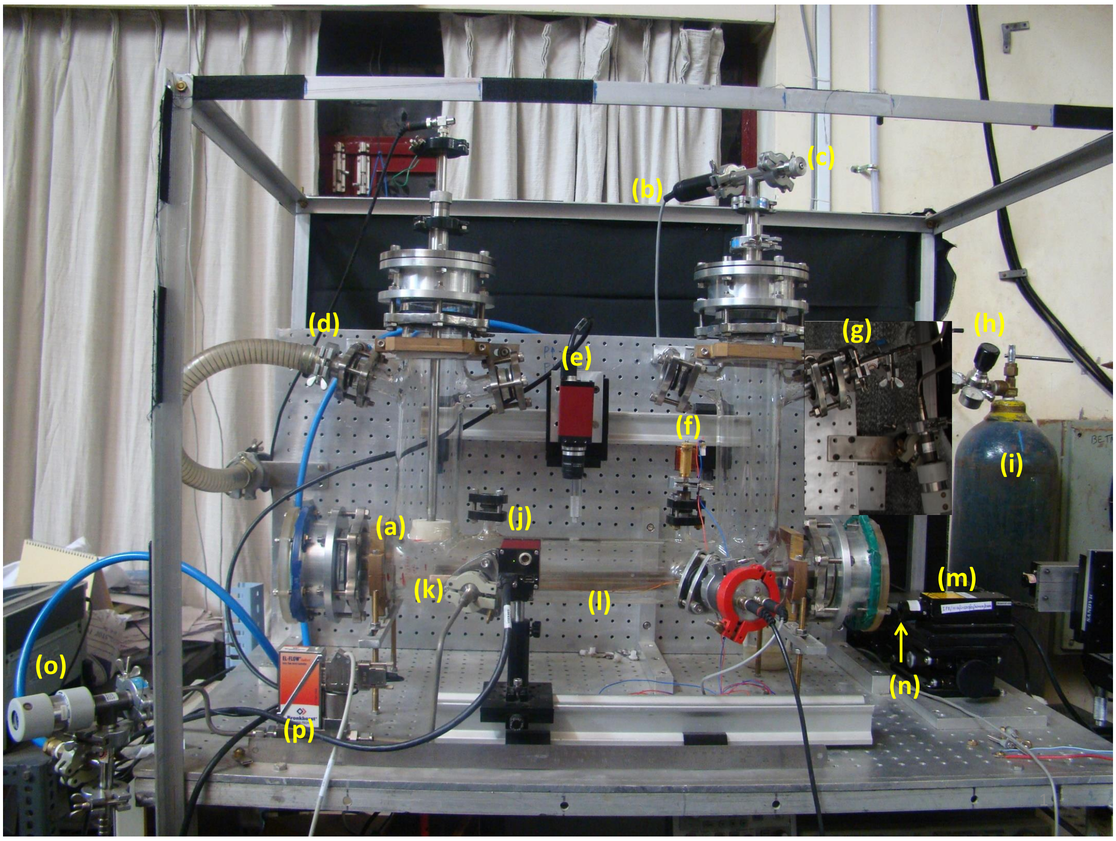

Figure 2.1: Photograph of the experimental set-up. a) Disc shaped anode (covered with ceramic holder), b) Pirani gauge, c) Vent valve, d) Pumping connection, e) Camera (top view), f) Dust dispenser, g) Second gas port (P_2), h) Gas regulator, i) Ar gas cylinder, j) Side view camera, k) First gas insertion port (P_1), l) Long grounded cathode tray, m) Laser, n) Line generator, o) Gas dosing valve, p) Mass flow controller .

ter of 8 cm in the horizontal section and it is terminated by two service parts of 30 cm length and of same diameter that form the vertical sections. All dusty plasma experiments are performed in the horizontal portion whereas the service part is intended for pumping, gas inlets, electrodes connections, pressure measurement and for venting the system. The axial ports of experimental portion are used for visualizing the dust particles dynamics by using laser and CCD cameras. A radial port (P_1) of the experimental part, very close to the left axial port, is used to introduce the gas into the chamber in a precisely controlled manner. Two other ports of the experimental portion are used to connect the cathode and to inject the dust into the system using a dust dispenser. Unused ports of the whole device are all covered by PEEK (Polyether Ether Ketone) material to prevent hollow cathode glow discharge.

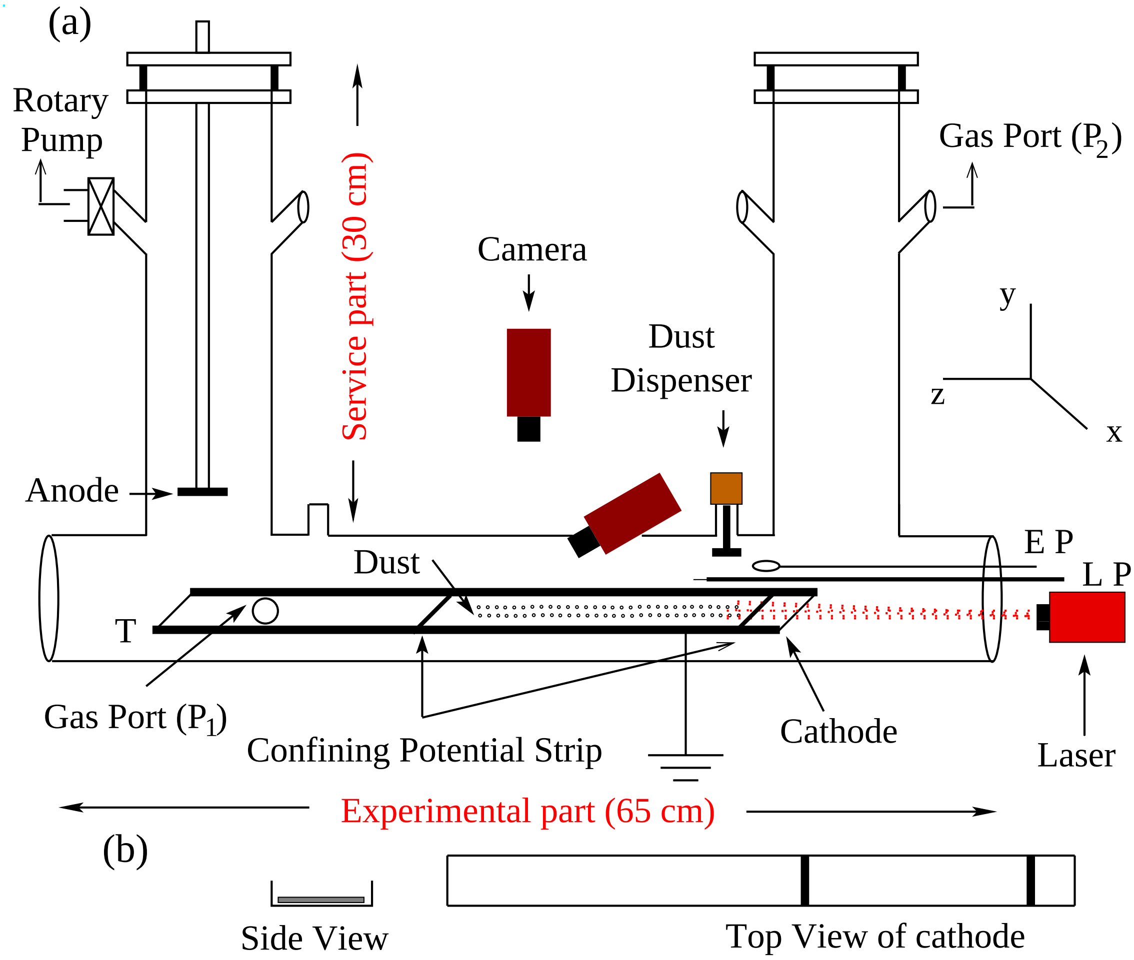

Figure 2.2: a) Schematic diagram of the Dusty Plasma Experimental (DPEx) device. LP: Langmuir probe, EP: emissive probe, T: grounded cathode tray. b) Cross sectional (side and top) views of grounded cathode tray.

2.1.2 Pumping and Gas system

The chamber is evacuated to a base pressure of $\sim 10^{-3}$ mbar by a rotary pump (ED-18, pumping speed = 250 lit/min and power 0.5 HP) connected to one of the radial ports of the left service part of the Π-tube. A gate valve connected to the mouth of the pump is used to control the pumping speed by adjusting the conductance of the pump. Couple of digital pirani gauges connected to the mouth of the pump and right service part of the tube, are used to measure the pressure at the mouth and inside the chamber respectively. These measurements help us to check the pressure difference between these two locations and hence the leak inside the system if any. A controlled amount of IOLAR grade-I Ar (99.99% purity) gas is fed into the glass tube through a Bronkhorst made mass flow controller, which is connected to one of the radial ports of the experimental parts of the tube and interfaced with a computer through a RS-232 cable. The mass flow controller can precisely control the gas flow rate and introduce the gas into the chamber in the step of 1.0 $\mathrm{ml}_s/\mathrm{min}$. Before performing the experiments, the gas is flushed several times and pumped down to its base pressure, $\sim 10^{-3}$ mbar. This process is useful to reduce the background contamination in the system. Finally the chamber is filled to the working gas pressure in a range 0.085 mbar to 0.24 mbar (according to the requirement) by adjusting the gas flow rate and the pumping rate. A gas dosing valve, connected at the service part (port P_2), is used to introduce extra amount of gas in the system in some of the flow related experiments (discussed in detail in Chap. 4). A venting valve connected to right service part is used to vent the experimental chamber.

2.1.3 Electrode configuration and Confinements

a) Electrodes

A stainless steel (SS-304) circular disc of 4 cm diameter and 5 mm thickness, hung from the axial port of the left service part of the vacuum vessel through a vacuum feed through, is served as an anode (shown in Fig 2.3). The outer portion of the SS disc is covered with a ceramic holder from the back side to prevent the micro-arcing from the edges of the disc. A long stainless steel tray of 2 mm thickness, 6.1 cm width, and 40 cm length placed inside the experimental portion of the tube along the axis serves as the cathode, which is connected to ground. A photograph of the cathode tray is shown in Fig. 2.4. With this specified cathode geometry, we are able to produce a two dimensional complex plasma whose size is $\sim 5 \times 30$ cm^2, which facilitates the observation of dynamical features involving macroscopic behaviour as well as microscopic structures of complex plasma such as observation of the spatial variation of the state of microparticles, flow of a dust fluid past an obstacle, propagation of different linear/ nonlinear waves and so on. The two sides of the cathode plate are bent 1.5 cm to give it the form of a tray that provides radial confinement of the dust particles through the radial sheath electric field.

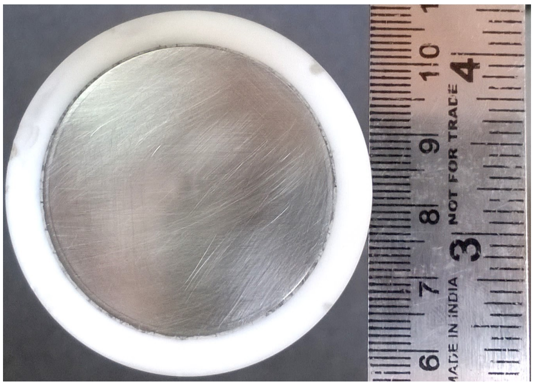

Figure 2.3: A photograph of anode covered with the ceramic holder.

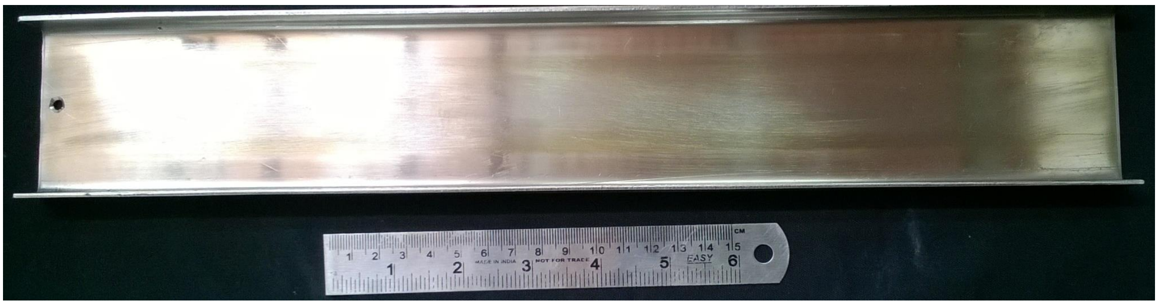

Figure 2.4: Photograph of long grounded cathode tray.

b) Confining strips

Couple of stainless strips of width 1.2 cm, thickness 0.5 cm and of different lengths (shown in Fig 2.5) are placed on the cathode tray to provide the axial confinement to the particles through their sheath electric field. Depending on the experimental requirements, they are placed 12 cm and 25 cm apart on the cathode to get the

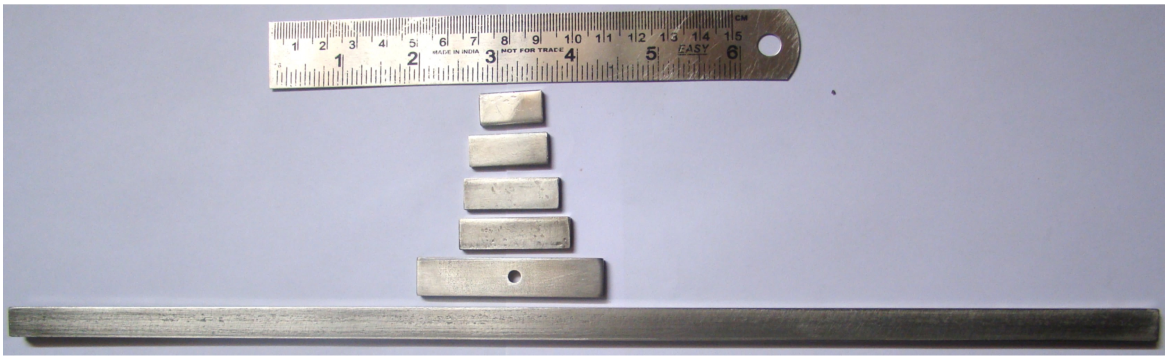

Figure 2.5: Different stainless steel strips used for radial and axial confinement.

particle cloud of different dimensions. Sometimes for better radial confinement, we have used two long strips of dimension 40 cm $\times$ 1.2 cm $\times$ 1 cm, which are placed $\sim$ 4 cm radially apart on the cathode.

2.2 Dust dispenser and Particles

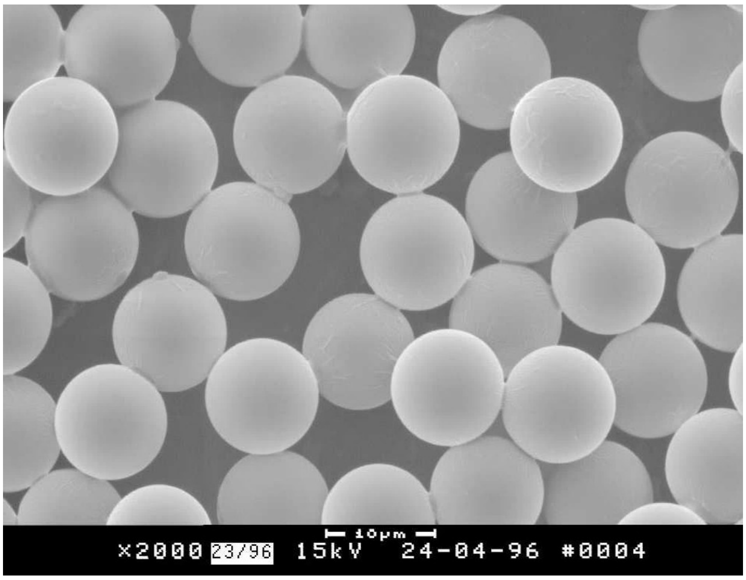

Figure 2.6: SEM picture of highly uniform, spherical Melamine Formaldehyde (MF) particles. image courtsey: Microparticle.de

In some of the experiments conducted at particle level, mono-dispersive Melamine-Formaldehyde (MF) particles of standard available sizes 9.19 ± 0.1 μm and 4.38 ± 0.1 μm diameter with the mass density of 1.51 g/cm^3 are used as dust grains due to their excellent mono-dispersivity (CV$<$ 2%) and highly uniform spherical shape.

Typical Scanning Electron Microscope (SEM) image of such particles are shown in Fig. 2.6. These particles are resistant up to high temperatures ($\sim 300°$) and hence do not agglomerate easily. In addition, due to their very small size distribution of the order of 0.1 μm, they mostly levitate in a single plane and form a monolayer dust cloud. Thus they are easily captured by the camera at the individual particle level and very useful for the particle level experiments.

To introduce these dust particles into the device a dust dispenser (shown in Fig. 2.7) is mounted on a radial port of the experimental area near the right arm of the Π-tube. The dispenser utilizes an electro-magnetic induction device that is wound using an enamelled copper wire. Particles are loaded in a cap of the dust dispenser. The cap is covered with a stainless steel mesh grid having an inter-grid spacing of 11 μm for 9.19 ± 0.1 μm and 6 μm for 4.38 ± 0.1 μm particles so that the particles can come out easily. Several spherical steel balls of 1 mm of diameter are also loaded in the cap along with the particles to shatter the powder into individual particles if they coagulate together. The dust dispenser is connected to a trigger circuit which is interfaced with the computer and operated using a LabVIEW based software.

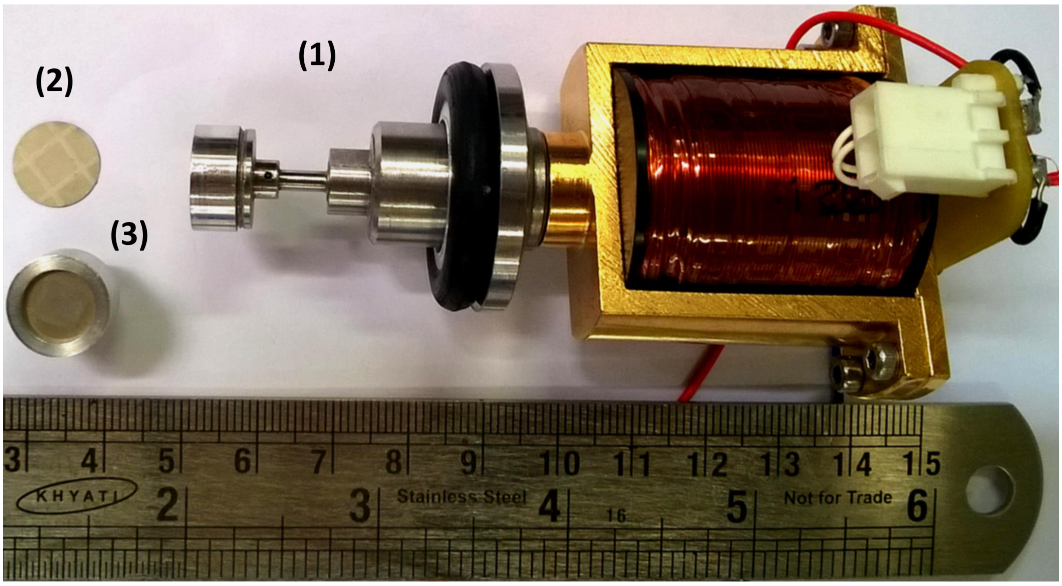

Figure 2.7: 1) A photograph of dust dispenser, which is used to introduce the micron sized particles into the system. 2) A SS mesh grid, 3) A cup to load the particles.

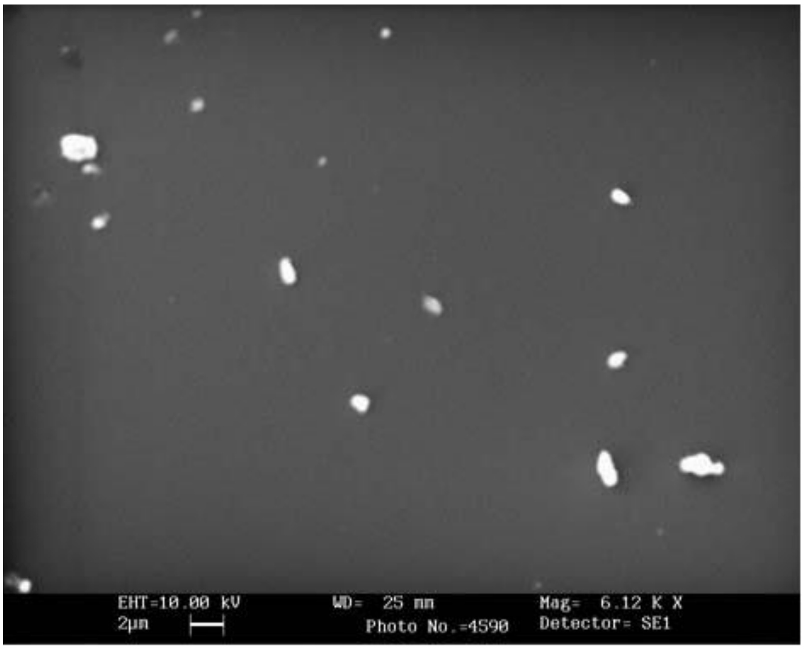

Figure 2.8: SEM picture of polydispersive kaolin particles.

In rest of the experiments at fluid level (as discussed in subsequent chapters), the laboratory graded poly-dispersive micron sized kaolin particles (hydrated aluminum silicate) are used as dust grains to get a dense dust cloud. The size distribution and shape of the dust grains are obtained by using Scanning Electron Microscope (SEM), which is shown in Fig. 2.8. It is found that the particles are non-spherical in shape and their size distribution are varied from 2 to 6 μm. Furthermore, the particles are very sensitive to the way they are distributed over the cathode and a small gap between the particles spread over the cathode can create a micro arcing, which may disturb the equilibrium of the whole dust cloud. Therefore, these dust particles are sprinkled uniformly on the cathode tray before closing the device. Due to their size variations they are levitated in different planes and constitute a highly dense dust cloud which is very helpful to conduct experiments on excitation of waves and structures. In all the experiments, these dust grains are pre-heated upto a certain temperature to remove the moisture before introducing them into the vacuum chamber.

2.3 Power Supplies

a) Plasma discharge power supply

An Ionics made regulated Direct Current (DC) power supply (voltage rating: 0 to +2 kV and current rating: 0 to 500 mA) is used in our experiments for producing the plasma. We have used a current limiting resistor of 1.6 kΩ connected in between the anode and output of the power supply for further protection to the power supply. With the help of this power supply, a high voltage (300 V- 500 V) is applied between anode and grounded cathode at the working pressure to produce a DC glow discharge plasma.

b) Power supply to excite the dust acoustic wave

For the pulse based excitation of dust acoustic wave, an exciter circuit consisting of power amplifier has been designed which is shown in Fig. 2.9. A low frequency AC voltage with a small DC offset is generated by using a Tetronix made AFG3022C dual channel Arbitrary Function Generator (25 MHz Bandwidth, 250MSa/s sampling rate, 10 Vpp to 50 Ω load). The output signal is then amplified 40 times by using a power amplifier (PA85A) to get the variable voltage from 40 to 360 V with variable amplitude of DC and AC voltage. For supplying the high voltage to the power amplifier, we have designed a power supply which can give an output of 380 V. The input and output voltage signals of the power supply are measured by 4 channel Agilent made DSO-X 3034 A Oscilloscope (350 MHz and 1 Gsa/sec) with the help of 10X probe that attenuate the output voltage by 10 times. The detailed circuit is discussed below:

A high voltage, high power bandwidth MOSFET operational amplifier (PA85A) is used to amplify the input AC+DC signal. This power amplifier is designed for the output currents up to 200 mA and the output voltage can swing up to ± 215 V with a dual supply and up to +440 V with a single supply. For our experimental

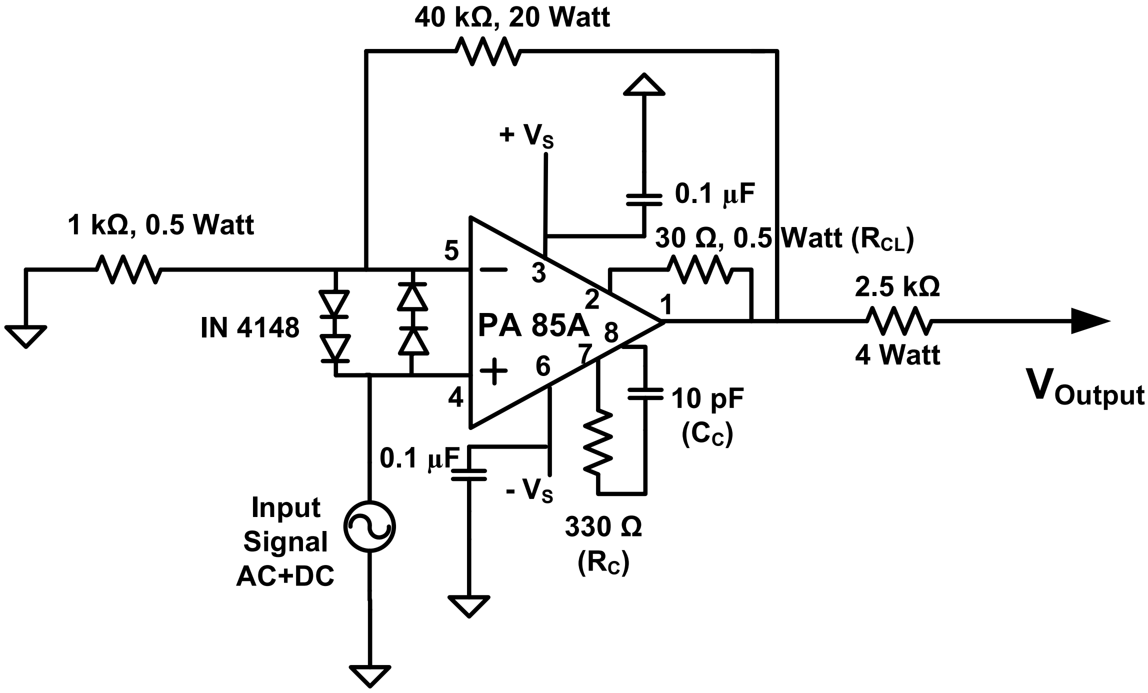

Figure 2.9: Typical connection of power amplifier (PA85A) used for the excitation of waves.

requirements we have used a negative power supply of -15 V (see Fig. 2.11) and a power supply of +360 V (Fig 2.10) to get the variable amplified output from -15 to +360 V. The amplifier is used in the non-inverting mode with the feedback resistance of 40 kΩ to amplify the input signal with the maximum gain of 41. R_c (=330 Ω) and C_c (=10pF) are the phase compensation resistor and capacitor, which are decided from the standard data sheet depending on the gain. R_{CL} is the current limiting resistor in the circuit which has been chosen from the data sheet. The minimum value of this resistance can be chosen to 1.4 Ω but for the optimum reliability it is recommended to set the value as high as possible. The maximum practical value can be chosen to 30 Ω. For the input protection of the amplifier, low leakage, low capacitance JFETs connected as diode is used, which can clamp the differential input voltage to ±1.4 V and hence produces the maximum power bandwidth. Capacitors of 0.1 μF (decoupling capacitor) are used in the biasing connection as a protection on the supply pins. The amplifier is equipped with the over current protection circuit and works upto 200 mA. Thus, for output protection of the circuit from the backward current of a plasma, a current limiting resistor of 2.5 kΩ is connected in the output of the amplifier circuit.

c) 360 V DC power supply to power the amplifier

A circuit diagram of 360 V power supply is given in Fig. 2.10. In this circuit, the output AC voltage of a step down transformer (230 V to 140-0-140 V) is given to the bridge rectifier circuit (MICBR1010). The rectified output DC voltage is then applied to a RC filter, made by capacitor (750 V, 333 μF) and combination of resistors (0.8 MΩ), to reduce the ripple. A resistor of 20 kΩ is connected in parallel to the capacitor to discharge the capacitor quickly (in ∼ seconds), when the input voltage is switched off. The output voltage of 360 V is supplied to bias the power amplifier (PA85A). Additionally a -15 V power supply is also used to supply the negative bias to the power amplifier.

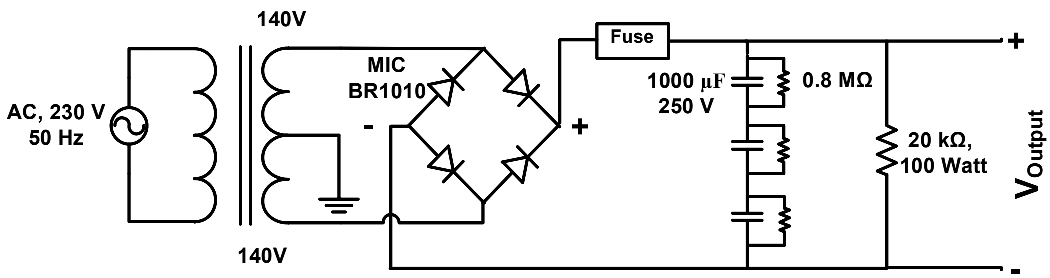

Figure 2.10: Circuit diagram of the 360 V power supply.

d) -15 V DC power supply to power the amplifier

In the circuit as shown in Fig. 2.11, the output of a step down transformer (230V to 15-0-15) is given to a full wave rectifier, which rectifies the AC input to provide the DC output. The output of the rectifier is applied to a filter capacitor (1000 μF, 63 V) to reduce the ripple. This DC signal is then supplied to a voltage regulator IC (7915) to get a regulated DC output of -15 V to be applied to power up the amplifier. Couple of ceramic capacitors of 0.1 μF (decoupling capacitor) are connected at input and

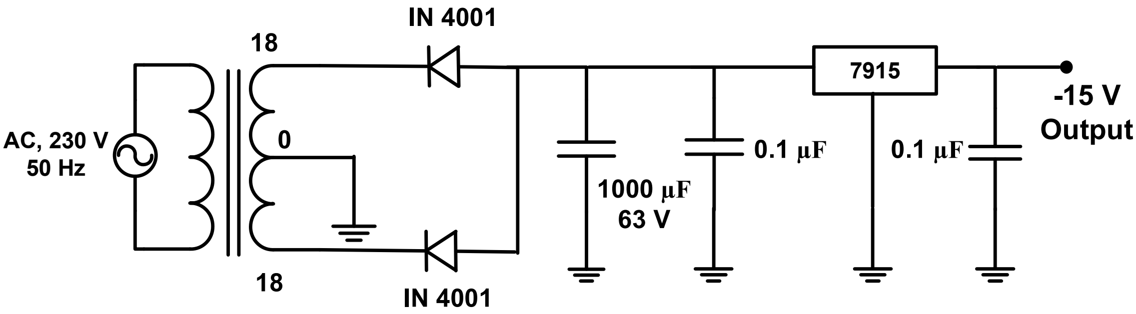

Figure 2.11: Circuit diagram of the -15 V power supply.

output of the IC for further protection from spikes.

2.4 Diagnostics and Instrumentation

We have used different electrostatic diagnostics namely Langmuir and emissive probe for plasma characterization and optical diagnostics for dusty plasma characterization. A single Langmuir probe is used to measure the plasma density, electron temperature, floating potential and to estimate the electron energy distribution function by means of collecting electrons and ions onto its surface. In addition, an emissive probe is used to measure the plasma and the floating potentials in the absence of dust particles. An optical unit, consisting of a diode laser, cylindrical lens, CCD camera and Zoom lens is used for visualizing and capturing the dust particles (or dust clouds) dynamics. The technical details of the diagnostics are described below.

2.4.1 Langmuir Probe

A cylindrical Langmuir probe [120–122], made up of a high melting point metallic wire and insulated by a ceramic holder (except at the tip), is used to measure the plasma parameters e.g., plasma density, electron temperature, floating potential and electron energy distribution function. The schematic of Langmuir probe [123, 124] along with the block diagram of associated circuitry is shown in Fig. 2.12. The probe having 1 mm of radius and 10 mm of length made up with a tungsten wire. The probe dimension (length (l) and radius (r_p)) in our case is found to be larger than the Debye length ($\lambda_{De} = 0.21 - 0.48$ mm) and hence the thin sheath collision less approximation ($l \gg r_p \gg \lambda_{De}$) is valid for low-pressure. Therefore, the conventional probe theory is applicable to estimate the plasma parameters in our experiments. The probe is electrically biased with respect to grounded cathode by using a voltage source and exposed inside the plasma to collect ions and electrons. Hence, it draws current from the plasma which varies with the variation of applied bias voltage. The amount of current flowing through the probe depends on the plasma parameters and the collecting area of the probe. The different regions of the V-I characteristics of the Langmuir probe give the information of various plasma parameters (n_e and T_e), which will be described in detail in Chap. 3.

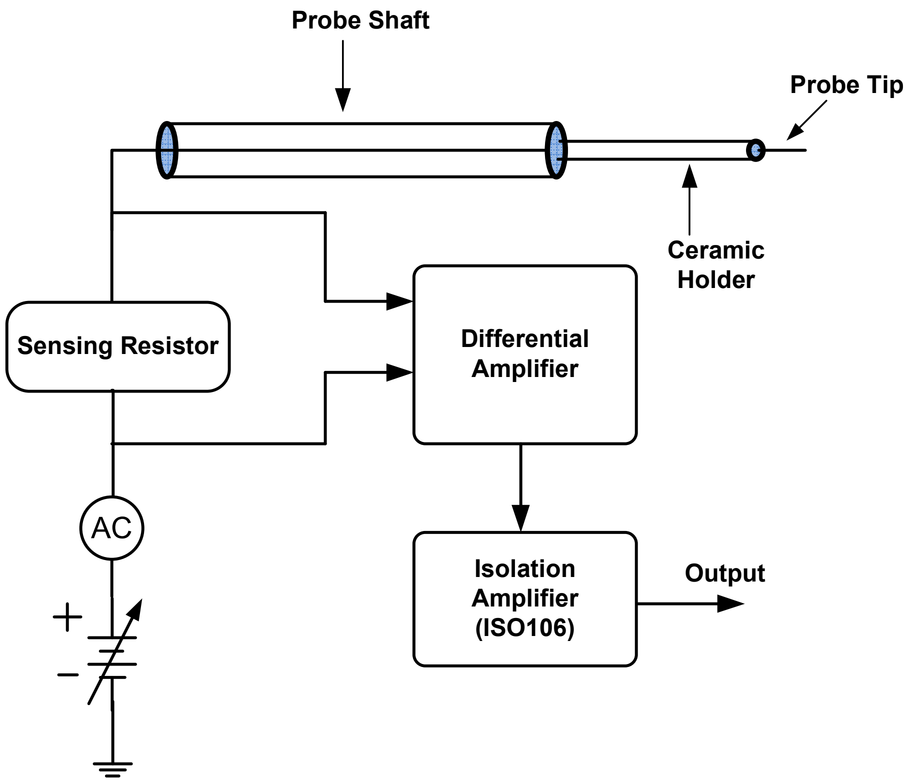

Figure 2.12: Schematic diagram of Langmuir probe circuit.

The V-I characteristic of the probe can be obtained by giving a sweep potential to the probe with respect to grounded cathode. When the probe is exposed to the plasma, it acquires a potential at which the net current becomes zero. This potential is known as **floating potential**. The value of floating potential depends on the plasma sources and discharge conditions. To get an idea about the sweep voltage range, initially the floating potential (V_f) is measured directly for a given set of discharge parameters. A ramp voltage of amplitude $V_f - 100$ V to $V_f + 100$ V is then applied to the probe to get a complete information of the ion saturation region to electron saturation region in the probe current. The electronic circuits used to operate the Langmuir probe are discussed below:

(i) Voltage source to bias Langmuir probe

In order to bias the langmuir probe, a ramp generator circuit has been designed which gives a sweep output voltage (30-350 V) at 50 Hz frequency with a variable DC shift of 0 V to 250 V. A block diagram of complete ramp generator circuit is shown in Fig. 2.13. A saw tooth pulse of ± 1 V is generated by a high frequency waveform

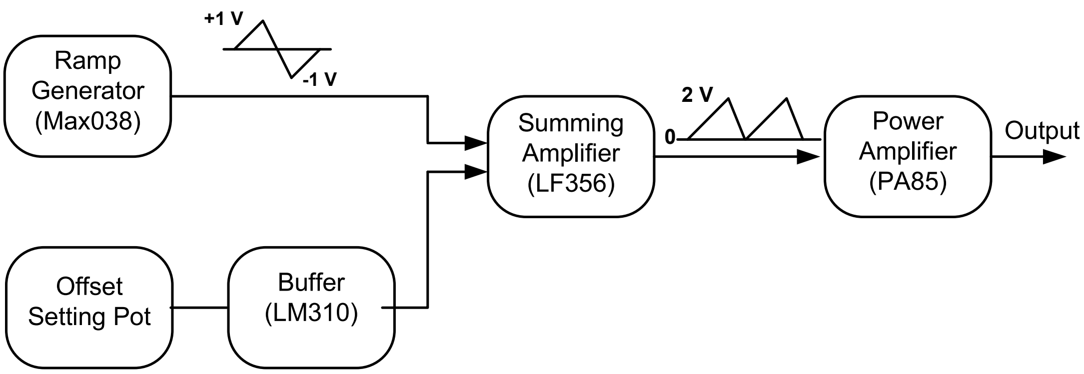

Figure 2.13: Block diagram of ramp circuit used to generate the ramp signal for our experiment.

generator Max038 (f= 0.1 Hz to 20 MHz, variable duty cycle). A buffer circuit is designed by using unit gain operational amplifier IC (LM310) with a potentiometer ($R_{in} = 0 - 1\ k\Omega$) in the input to shift the DC voltage up to 3 V. The output of pulse generator and buffer circuit is then applied to an adder circuit which is wired using a JFET Input Operational Amplifier (LF356). This combination gives a DC shifted output (0-3 V). The output voltage is then applied to a high voltage power amplifier circuit fabricated by using IC PA85A with the maximum gain of 86, which gives a variable output of 30-350 V. The DC shift can be adjusted by changing the resistance R_{in} according to the required electron or ion current.

(ii) Current measurement circuit to measure the probe current

The current measurement circuit (shown in Fig. 2.14) is used to measure the current drawn by Langmuir probe. It consists of mainly sensing resistors, differential amplifier and an isolation amplifier. The details of each component are described below:

a) Sensing resistor

The biasing voltage to the Langmuir probe is applied via different combination of resistors connected through a switch. The resistor can be switched to $R_1 = 0$ kΩ, $R_2 = 1$ kΩ, $R_3 = 3$ kΩ, $R_4 = 5$ kΩ and $R_5 = 10$ kΩ depending on the plasma parameters. The potential drop developed across the resistor is measured using a differential amplifier circuit.

b) Differential amplifier

The voltage drop across the sensing resistor is fed to the input of the differential amplifier circuit, which is designed by using an IC OP27. The differential amplifier circuit measures the potential difference across the sensing resistor and provides an output, which is proportional to the current drawn by the probe corresponding to the applied voltage. OP27 is a high precision amplifier with high speed and low noise. This amplifier also has high common mode rejection ratio and provides the required differencing sensitivity.

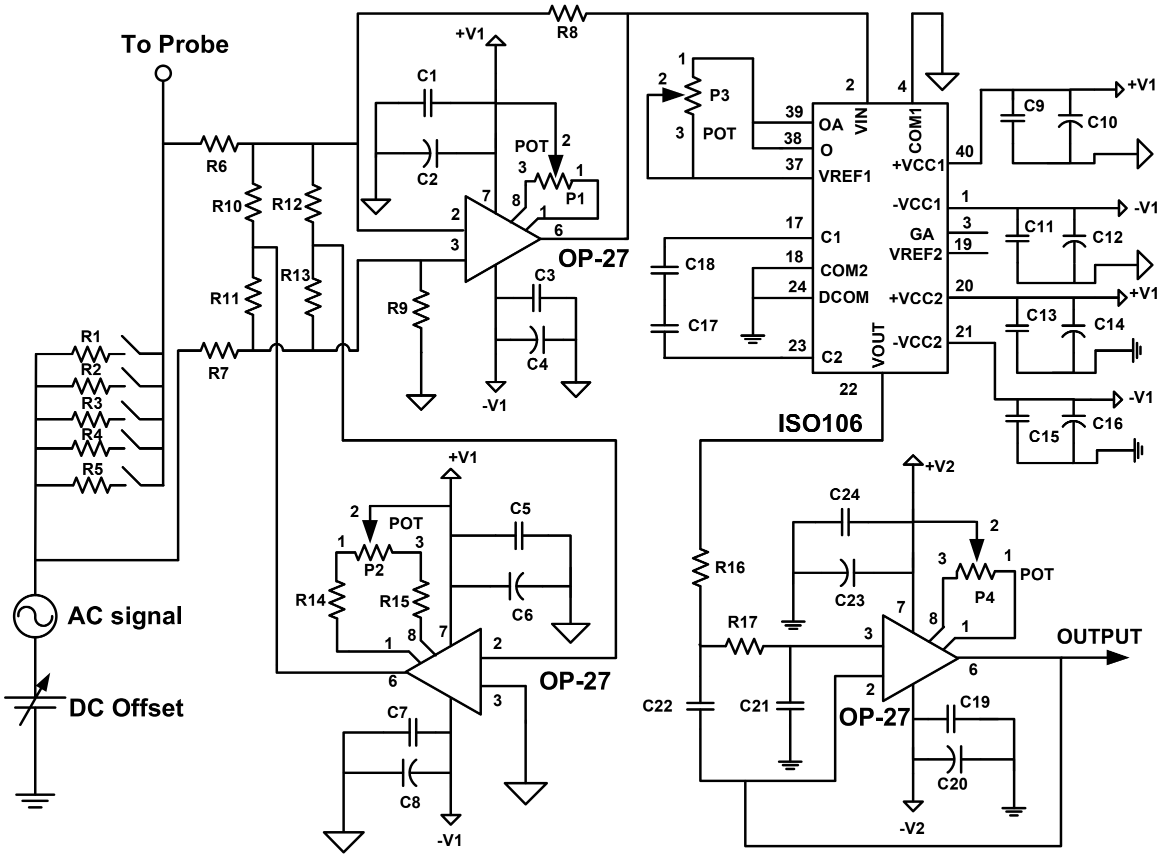

Figure 2.14: Current measurement circuit diagram.

c) Isolation amplifier (ISO 106)

In the Langmuir probe circuit, the sensing resistor is connected in series with the output of signal generator and probe. Thus to acquire the probe current more precisely and to prevent the effect of reference on probe signal an isolation amplifier IC ISO106 is used.

The output of the isolation amplifier is fed to an oscilloscope through a voltage follower circuit, developed by using IC OP27. The applied voltage to the probe is attenuated through a 10X probe and fed to an Agilent made 4 channel oscilloscope (350 MHz and 1 GS/sec). The data can directly be stored in a pendrive or transferred to the computer using a RS-232 connection.

In our experiment, the cylindrical Langmuir probe is inserted axially 2.5 cm above the cathode (or 2 cm above the strip, as the strip thickness is 0.5 cm) to scan the plasma parameters in axial direction. Before taking the measurements, we have cleaned the Langmuir probe by applying a positive voltage, higher than the plasma potential.

In addition to the langmuir probe, a hot emissive probe is used for further estimation of plasma parameters (plasma and floating potential). The details of emissive probe is described in the next subsection.

2.4.2 Emissive Probe

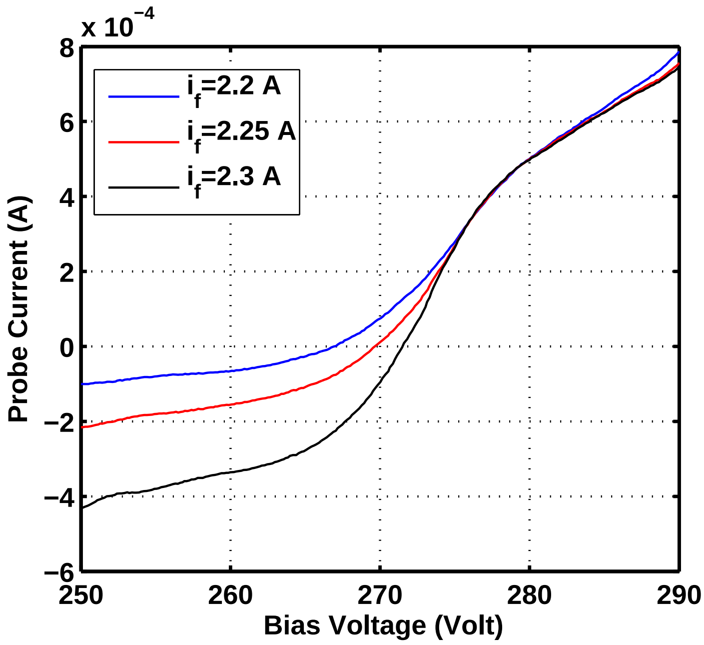

Figure 2.15: Emissive probe traces showing the effect of increasing filament current.

A direct and more precise measurement of plasma potential (V_p) and floating potential (V_f) can be obtained by using an emissive probe, a hot particle flux probe, which also emits electrons due to thermionic emission. In this diagnostic technique, a high current is applied to the filament (probe), heating it to the point where electrons are thermionically emitted. In this situation if the probe is swept for V-I characteristics, the characteristics tend to deviate form the typical characteristics shown for the cold probe in one region and remain unchanged in other region as shown in Fig. 2.15. The point of deviation at which separation of these two regions occurs on voltage axis is defined as the plasma potential.

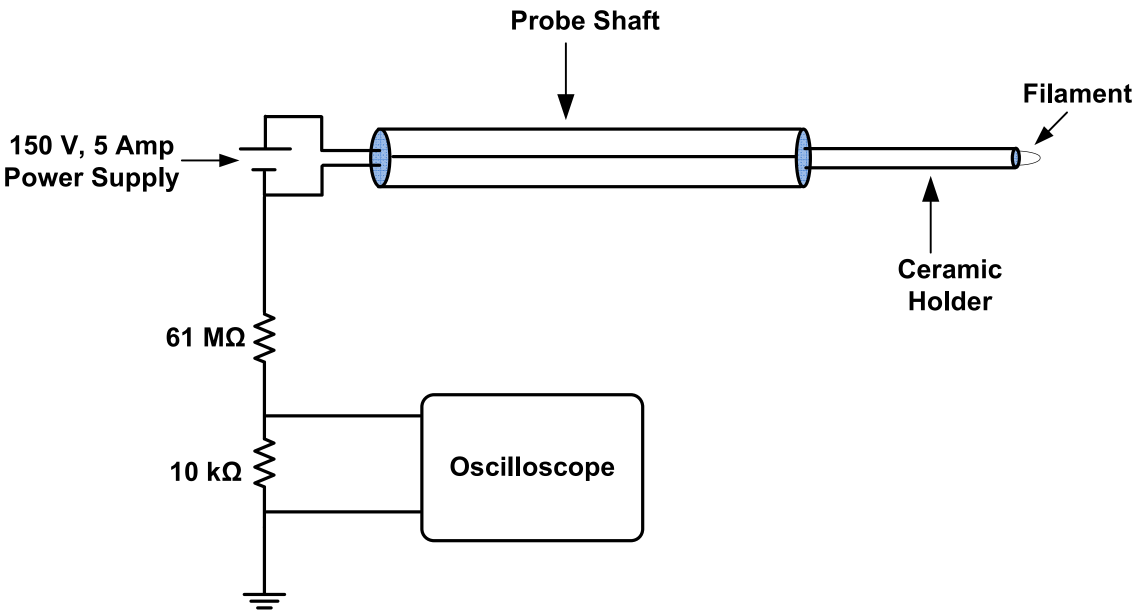

Figure 2.16: Schematic of emissive probe connections.

In our experiment, the emissive probe made of a tungsten wire of 0.125 mm diameter with loop of 4 mm length is exposed to the plasma. The wire is drawn from a twin bore ceramic tube to form a loop and the ends are pressed against copper wires of sufficient thickness to fit in tightly in the bores of the tube, to make a good electrical contact. This method of electrical contact is reliable and long lasting, even when the tungsten is heated to high temperatures. The twin bore ceramic tube of 4mm outer diameter is fixed on a ceramic block which is mounted on an axially movable shaft as shown in Fig. 2.16. A DC power supply (150 V, 5A) is used to supply the current to filament for heating. Two resistances with 61 MΩ and 10 kΩ is used to keep the probe floating and by using the potential divider method, the output voltage is measured. The different techniques to operate the emissive probe and the axial variation of plasma/floating potential at different discharge condition are discussed in Chap. 3.

2.4.3 Optical Diagnostics

The main diagnostic convenience of dusty plasma is the optical visualization. The particles are bigger in size and hence they scattered sufficient light while illuminating through laser, which can be easily detected by our naked eyes. In addition to that, due to higher mass, their motion is very slow thus their dynamics can be captured at individual particle level by using normal CCD camera. Therefore, video imaging is usually the primary source of acquiring the data in the dusty plasma experiments. The video imaging enables the continuous study of dust dynamics, such as structure formation, propagation of linear and nonlinear waves, void formation etc.. The particle cloud is illuminated by the combination of red (or green) diode laser and line generator. The scattered light from the dust particles is captured by couple of CCD cameras placed at different locations. The still images recorded by the camera with the variable speed are stored in a workstation through RS-232 cable. The stored data is analysed by using different mathematical softwares and video editor such as ImageJ, IDL based super Particle Identification and Tracking (sPIT) code, Matlab based open source Particle Image Velocimetry (PIV) tool etc.. The details are discussed in the following subsections.

a) Dust particle imaging

The particle cloud is illuminated by a green line-laser light (532 nm, 100 mW) sheet of thickness 1 mm and $\approx$ 60 mm width at a distance of 50 cm. In some of the experiments, a combination of red diode point laser (650 nm, 50 mW) with 1.5 mm diameter, spread into line with line generator mounted on the laser head, is shined along the axial length of the connecting tube in X-Z plane so that the dust cloud can be seen over its entire length. In this combination, there is an option to change the angle of the line generator to 90° which enables the laser to shine into Y-Z plane. The Mie-scattered light from the dust particles is captured by couple of normal CCD cameras with different resolutions and speed of the camera. The high speed camera (60fps, 1000 × 1000 Pixels) is placed at an angle of 15° with the y-axis and the high resolution camera (15fps, 2048 × 2048 Pixels) is placed exactly perpendicular to the dust cloud. The speed of the cameras can be further increased at the cost of lowering their resolutions.

b) Magnification of the object

Couple of **Fujifilm made** ‘C’ mount zoom lenses HF25HA-1B (focal length of 25 mm, iris range F1.4–F25) and HF16HA-1B (focal length of 16 mm, iris range F1.4–F16) with maximum aperture ratio of 1:1.4, are attached in front of different cameras for a more clear view of the dynamics of dust grains. The aperture and focal length of these lenses can be varied according to our requirements. Magnification of the zoom lens is increased by using C-rings in series to it. It is worth to mention that the increase in number of ‘C’ rings corresponds to more magnification.

c) Data storage and analysis

The CCD camera is interfaced with a high speed computer by using Allied vision made firewire to PCI Express Host Adapter card mounted on the motherboard. The camera is operated by using VIMBA 2.0 software which is a future-proof platform-independent SDK for all Allied Vision cameras with GigE Vision, FireWire (IEEE1394), USB3 Vision, and camera link interface. It is compatible with Windows and Linux operating system. The software provides the facility to set the sutter speed, resolution, gain and frame rate which helps to record the high quality images with desired speed. The data is stored into the high speed workstation (HP, 32 GB RAM, core i5 intel processor) in ‘jpeg’ format.

We have used ImageJ for calculating the distance between pixel points, as well as for scaling of the images. The software has the capability of subtracting, dividing, adding or multiplying two or more frames. For single particle analysis we have used an IDL based super Particle Identification Code which is a very efficient single particle tracking code, enables the estimation of position and velocity accurately and also useful to plot the trajectory of particles frame by frame, by different colours in the colour sequence of rainbow. For flowing denser particles cloud we have used MATLAB based open-source Particle Image Velocimetry (PIV) software. The time variation of flow velocity and vorticity can be calculated by using this software. The details of sPIT code and PIV analysis is provided in Chap. 4. For the wave analysis and plotting, we have used MATLAB software.

2.5 Conclusion

A table top experimental device, named DPEx, for the study of dusty plasma physics is presented. One of the unique features of the device is its ability to induce a flow in the dust component in a controlled fashion by adjusting the vacuum pumping speed and the gas flow rate of the device. This facilitates an experimental study of flow induced instabilities and the associated formation of nonlinear structures in a dusty plasma-an area of research that is relatively unexplored till date. The geometry and construction of the device also facilitate viewing and making optical measurements of the dynamics of the dusty plasma. The device has been commissioned and is operational at the Institute for Plasma Research. Various electrostatic diagnostics such as Langmuir probe and emissive probe along with associated circuitry have been discussed. An optical diagnostic consisting of lasers and cameras is also described.

Chapter 3

Plasma and Dusty plasma production and Characterization

S. Jaiswal, P. Bandyopadhyay and A. Sen, Rev. Scientific Instrum, ***86****, 113503 (2015)*

Before performing the experiments on flow induced excitation of linear and non-linear structures in dusty plasma, it is always important to have the knowledge of plasma and dusty plasma production mechanism and their equilibrium properties in the device. In addition, it is also essential to characterize these media to get an idea of the basic plasma and dusty plasma parameters and their variation with the different discharge conditions. This helps us to understand the parametric regime at which these structures are generated. In this chapter, we discuss the details about the production of DC glow discharge plasma in Dusty Plasma Experimental (DPEx) device. The detailed measurement of different plasma parameters such as plasma density, electron temperature, plasma and floating potentials and electron energy distribution function are measured in the absence of dust particles by using Langmuir and emissive probes. The variation of these plasma parameters along the axis of the experimental part of the device is described, that provides the necessary background for the creation of dusty plasma. Subsequently, the generation of dusty plasma at single particle level and fluid level along with their levitation and equilibrium properties are described. A full characterization of dusty plasma in terms of measured and/or inferred values, such as pair correlation function, inter-particle distance, dust density, thermal velocity of the dust particles, kinetic temperature component in axial and radial direction and Coulomb coupling parameter by using the single particle tracking code and other mathematical software is provided. The variation of dusty plasma parameters such as thermal velocity and temperature with the background pressure is also discussed. These measurements provide the necessary information about the parametric regime for the excitation of waves and structures of interest.

The chapter is organized as follows. In the first section (Sec. 3.1), we explain the plasma production and Paschen curve in our experiments. In Sec. 3.2, we describe the detailed characterization of plasma and the axial variation of plasma parameters over a range of discharge parameters. Characterization of dusty plasma is discussed in Sec. 3.3. Conclusions of this work are provided in Sec. 3.4.

3.1 Plasma production

Initially the system is evacuated to a base pressure of $\sim 10^{-3}$ mbar. Then the Ar gas is introduced into the device by mass flow controller as described in Chap. 2. A high DC voltage is applied between disc shaped anode and long grounded cathode tray to produce the plasma [125, 126]. To know the discharge parameter range in our device, we have performed the experiment on Paschen curve. Paschen law $U_{dc} = f(Pd_e)$ [125] describes the breakdown voltage of a glow discharge. According to this law, the breakdown voltage U_{dc} is a function of the product of the gas pressure P and the inter-electrode distance d_e. Fig. 3.1 illustrates the Paschen curve for three different inter-electrode spacing (4 cm, 6 cm and 8 cm) for our experiments. We have measured the minimum voltage for discharge in Ar gas of $\sim$ 270 V at $\sim$ 0.9 mbar-cm. It is also clear from the figure that at same pd value, the breakdown voltage differs depending on the inter-electrode spacing d_e, which agrees well with the measurement shown in Ref. [127]. The discharge voltage in our experiment is in the range of 290-450 V for neutral gas pressure 0.085 to 0.24 mbar at the inter-electrode spacing of 6 cm. At this discharge range, a homogeneous plasma glow is formed into the whole area of interest. Photograph of a typical stable glow discharge is shown in Fig. 3.2. Fig. 3.2(a) corresponds to the axial view, whereas Fig. 3.2(b) represents the radial view of glow discharge plasma formed in between the electrodes.

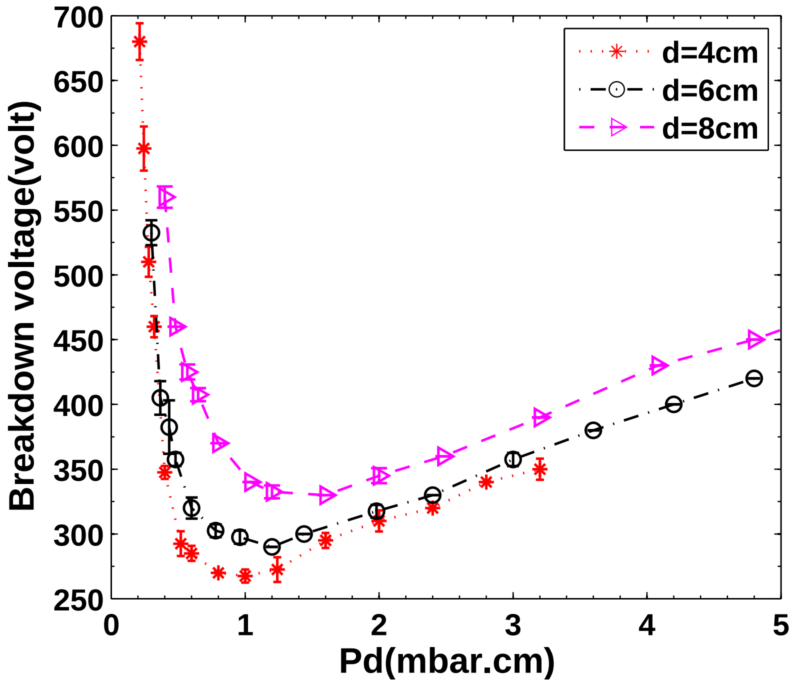

Figure 3.1: Paschen's curve obtained by varying the Ar gas pressure and distance between the electrodes.

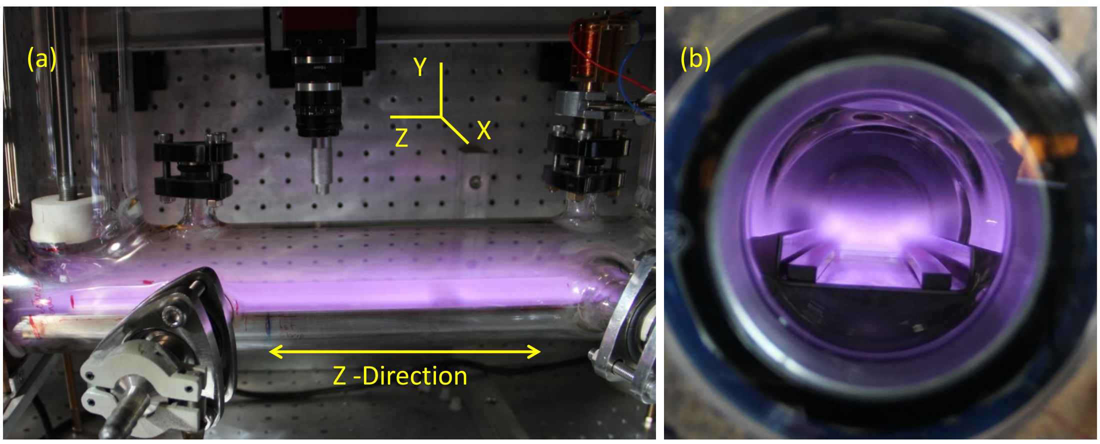

Figure 3.2: A photograph of DC glow discharge Ar plasma in Dusty Plasma Experimental (DPEx) device: a) axial view b) radial view.

3.2 Characterization of Plasma

We have made measurements of the plasma properties in the absence of dust particles by using a couple of electrostatic probes, namely a Langmuir probe and an emissive probe. In principle, the plasma characteristics can change in the presence of dust particles. However, when the number density of dust particles is quite low compared to the electron density the floating and plasma potentials remain relatively unaffected. In our experiment, both the probes are introduced into the plasma from the right sided axial port of the experimental part as shown in Fig. 2.2 of Chap. 2. The Langmuir probe is used to estimate the plasma density, the electron temperature, electron energy distribution function by using its V-I characteristics. The emissive probe is used to measure the floating/plasma potentials and hence the electron temperature. The details are given in the following subsections:

3.2.1 Variation of Plasma parameters

a) Langmuir probe measurements

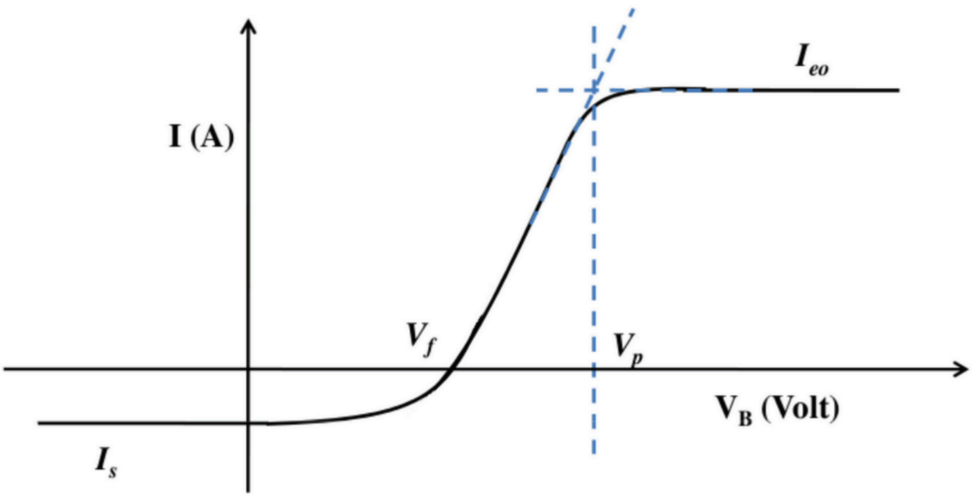

Figure 3.3: The ideal probe current variation sketch with the bias voltage V_B.

The plasma parameters such as plasma density and electron temperature in our experiments are measured by using single Langmuir probe. The construction and detailed circuitry of the Langmuir probe is described in Chap. 2. Initially, the probe is cleaned by applying a high voltage (higher than plasma potential) to the probe for longer time. Then at first, the floating potential (a potential at which the net probe current becomes zero because of exact balance between the electron and ion flux to the probe) is measured to get an idea about the range of applied biasing voltage. If the applied bias voltage to a probe is sufficiently positive with respect to the floating potential the probe draws electron current whereas it draws ion current if the biasing voltage is negative with respect to the to the floating potential. After the measurement of floating potential, a sweep voltage is applied to the probe to get the probe current. We have chosen the current sensing resistance by switching the resistor, connected in series with the probe, in such a way that it can draw a significant ion saturation current. In our case the current sensing resistance is set to 5 kΩ. The current (I) drawn by the probe is measured as a function of the applied bias voltage (V_B). The resulting relation between the probe current and the bias voltage is called the Langmuir probe characteristics. A sketch of ideal probe characteristics is shown in Fig. 3.3. The flat part of the V-I characteristics (for $V_B \ll V_f$) shows the ion saturation current (I_{is}) collected by the probe when the bias voltage V_B, is sufficiently negative with respect to the floating potential V_f. The ion saturation current, I_{is} is given by

$$I_{is} = 0.6 e n_i v_{Bohm} A_{probe}. \tag{3.1}$$

Where, n_i is the ion density, $v_{Bohm} = \sqrt{8k_BT_e/m_i}$ is the *Bohm velocity*, m_i is the ion mass, and A_{probe} is the probe collecting area. In the vicinity of a negatively biased probe, in order to enter the positive sheath region, the ions must approach the sheath with a speed exceeding the Bohm velocity (v_{Bohm}). To achieve this speed, ions must acquire an energy corresponding to the electron temperature T_e. The factor of 0.6 in Eq. (3.1) is due to the reduction in the density of the ions in the pre-sheath, which is the region over which the ions are accelerated up to the Bohm speed [126]. The transition region is a combination of both ion and electron current but electron current is dominated in this region. This region contains the information of electron energy. In the right part of the V-I characteristics (for $V_B > V_f$), there is a 'knee' on the probe current. The potential corresponds to this 'knee' is called the plasma potential at which the electrons and ions come randomly to the probe. If the bias voltage is more positive than the plasma potential then the current saturates because at this point virtually there is no sheath around the probe exists (no electric field to be shielded). So, all the electrons in the Maxwellian distribution are collected randomly. This is the maximum current and is called the electron saturation current. The electron saturation current I_{es} is given by [126],

$$I_{es} = (1/4)en_eV_{Te}A_{probe}. \tag{3.2}$$

Where n_e is the electron density, $V_{Te} = \sqrt{8k_BT_e/\pi m_e}$ is the electron thermal speed, and m_e is the electron mass. Figs. 3.4(a) and 3.4(b) show the typical bias voltage applied to the probe and current drawn by the probe in our experiments. The X-axis represents the number of data points (in our case 2000 data points), which corresponds to real time. Fig. 3.5 depicts a typical Langmuir probe characteristics at a discharge voltage V_d = 320 V and P=0.15 mbar. Before calculating the electron temperature, we have eliminated the contribution of ion current by subtracting a DC voltage equivalent to ion saturation current from the entire probe characteristics. Then we fit the exponential curve on the measured V-I characteristics by considering the electrons are Maxwellian at the transition region of Langmuir probe characteristics. The slope of $log(I - I_{is})$ Vs probe bias voltage is used to determine the electron temperature. The inverse of the slope gives the electron temperature

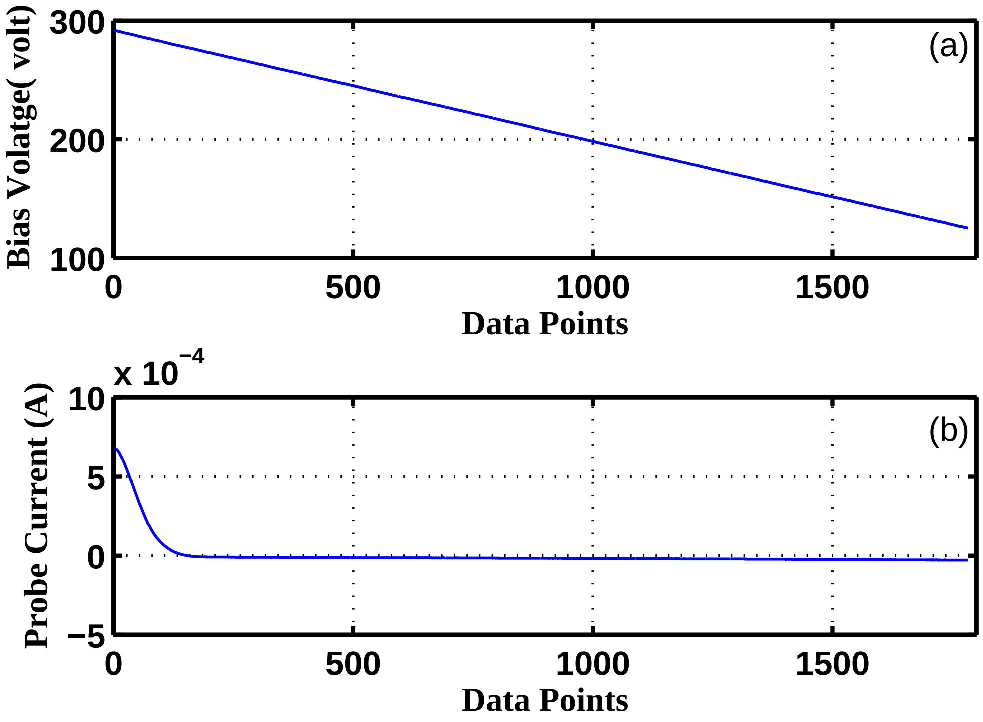

Figure 3.4: Langmuir probe data: a) Bias voltage applied to the probe, b) The current drawn from the probe.

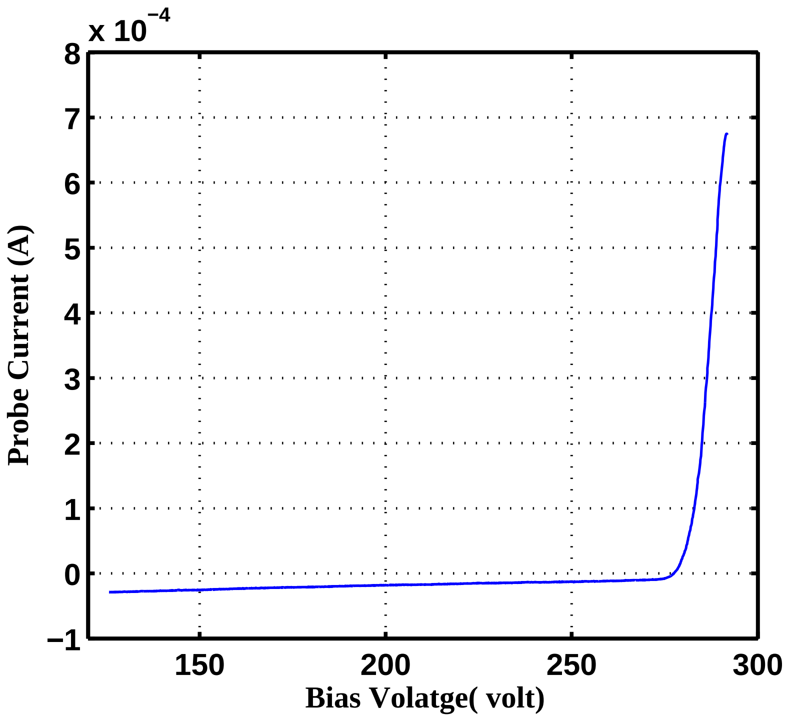

Figure 3.5: A typical probe characteristics.

at that particular discharge condition. The plasma density is calculated from the ion saturation region (following Eq. 3.1) with the help of the estimated electron temperature. It is observed that the electron temperature changes from 2 eV to 4 eV, whereas the plasma density is of the order of $10^{15}/m^3$ for a range of discharge voltages between 250 and 350 V and working pressures between 0.1 and 0.2 mbar. The Langmuir probe is then scanned axially to get the temperature and density profiles along the axis of the experimental part. The variation of the density and the temperature in axial direction is shown in Fig. 3.6 for three different values

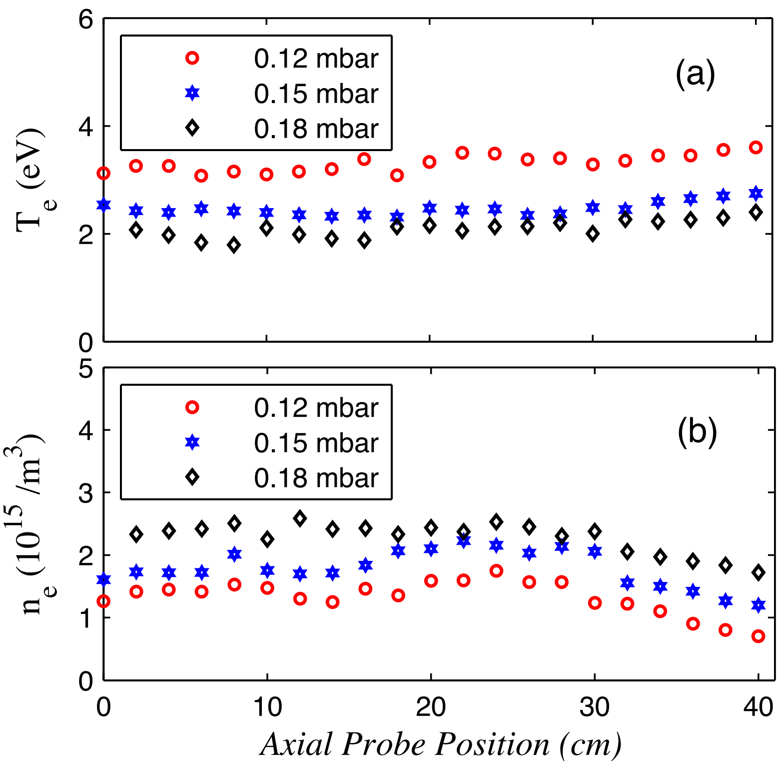

Figure 3.6: Axial profile of (a) electron temperature and (b) plasma density for different values of working pressure. The measurement errors are within ±5%.

of working pressures, namely, P = 0.12, 0.15, and 0.18 mbar for a given value of discharge voltage (V_d = 310 V). Fig. 3.6 also shows that the density increases and the temperature decreases with the increase of neutral pressure. The variation of discharge and plasma parameters of the current interest of this thesis is summarize in table 3.1.

Table 3.1: Discharge and plasma parameters

Parameters	Values
Discharge voltage (V_d)	$290 - 450$ V
Discharge current (I_d)	$2 - 20$ mA
Neutral Gas Pressure (P)	$0.085 - 0.24$ mbar
Floating potential (V_f)	$240 - 310$ V
Plasma potential (V_p)	$270 - 330$ V
Plasma Density (n_e)	$(0.5 - 3) \times 10^{15}$ m^{-3}
Electron Temperature (T_e)	$2 - 5$ eV
Ion Temperature (T_i)	0.03 eV

b) Plasma and floating potential measurements by emissive probe

In addition to the Langmuir probe, a hot emissive probe is also used to measure the plasma and floating potentials [120, 128] in our experiments. The difference of plasma potential (V_p) and the floating potential (V_f) gives the electron temperature. The temperature variation is compared with the temperature obtained from Langmuir probe data. The construction and the circuitry of the emissive probe are described in the previous chapter (Chap. 2).

The relation between the difference of plasma and floating potential with the electron temperature for Ar is given as [126],

$$V_p - V_f = 5.2 \times k_B T_e / e \tag{3.3}$$

There are different standard techniques available for the operation of emissive probe to determine the plasma potential [128]. These are **separation point** method, **inflexion point** method and **floating point** method. Among these three methods, the inflexion point method and floating point method are the more familiar and commonly used techniques. The inflexion point method is based on obtaining the full V-I characteristics of emissive probe with finite emission. According to the floating point method, at strong emission the probe floats close to the plasma potential.

With the further increase of filament current, the floating potential saturates and this value is considered as **plasma potential** (shown in Fig 3.7).

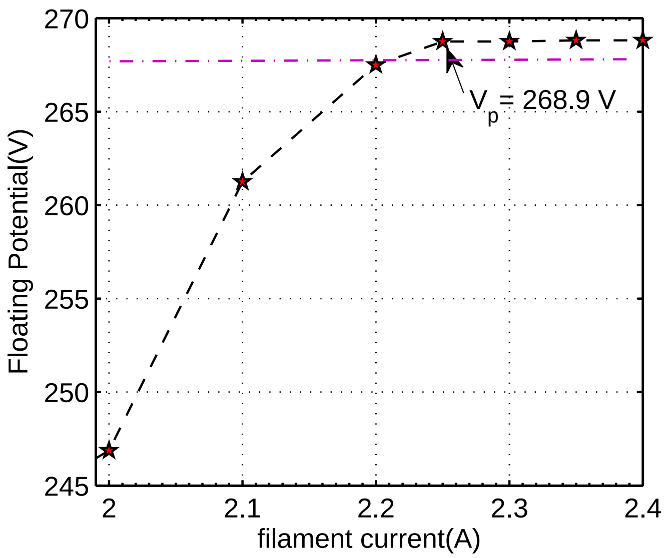

Figure 3.7: Measurement of plasma potential by floating point method.

For a particular position and discharge condition ($V_d = 290$ V and $P = 0.12$ mbar), the floating potential and the plasma potential are measured by following all these three mentioned techniques. It is found that the measured plasma potential, using the floating method is 269 V at a distance of 15 cm axially away from the anode. The separation point and the inflection point methods also give the plasma potential to be 269 ± 5 V for the same position and discharge condition, which is very close to that of the floating method. Hence, the easiest technique, namely the floating method is chosen to measure the floating potential and plasma potential profiles. Fig. 3.8 shows the variation of floating (open symbols) and plasma (solid symbols) potentials along the axial direction at a particular value of the neutral gas pressure (P=0.12 mbar) in the absence (Fig 3.8(a)) and presence (Fig 3.8(b)) of confining potential strips respectively. Four different symbols represent different values of discharge voltages ($V_d = 290, 310, 330$ and 350 V). The first point represents the floating/plasma potential when the probe is kept just under the anode whereas the

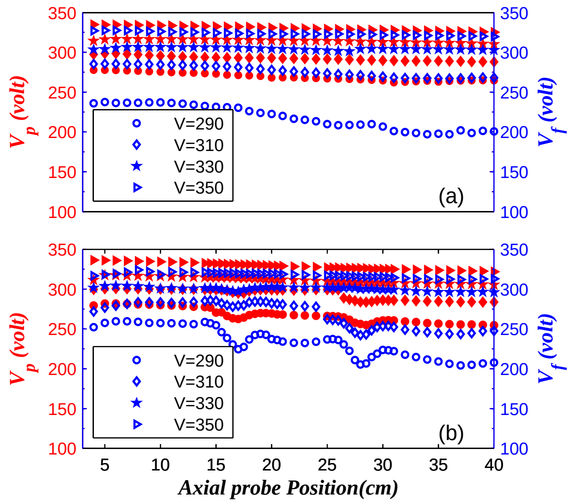

Figure 3.8: Axial profile of plasma, V_p (closed symbols) and floating V_f (open symbol) potential for different discharge voltages at P = 0.120 mbar (a) without confining strips (b) with confining strips placed at 10 cm apart. The measurement errors are within ±5%.

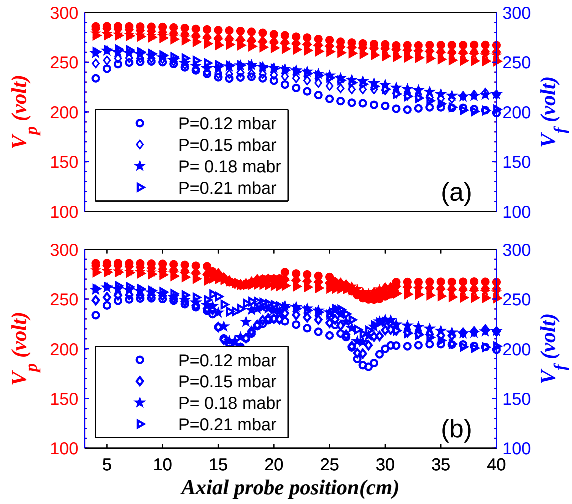

Figure 3.9: Axial profile of plasma, V_p (closed symbols) and floating V_f (open symbol) potential for working pressures at Vd = 310 V (a) without confining strips (b) with confining strips placed at 10 cm apart. The measurement errors are within ±5%.

last point represents the same at the position near the right edge of the cathode. It is seen that both the potentials have a small negative gradient when the probe is scanned away from the anode. It is to be noted that the plasma/floating potential decreases with the decrease of the discharge voltage at a given value of pressure. Furthermore, the difference between the plasma potential and the floating potential increases when the discharge voltage is decreased, which indicates that the electron temperature increases with the decrease of discharge voltage. Additionally, a couple of wells are observed in the potential profiles just above the confining potential strips as shown from Fig. 3.8(b). These confining strips are placed on the cathode at 12 cm apart for the purpose of confinement of the dust particles during dusty plasma experiments. It is also clear from the figure that the depth of the potential wells (plasma as well as floating potential) decreases with the increase of discharge voltage. Beyond $V_d = 350$ V the effect of the confining potential strips becomes insignificant. In all the cases, the emissive probe is scanned axially 2.5 cm above the cathode (or 2 cm above the strip, as the strip thickness is 0.5 cm). The electron Debye length (estimated from the electron density and temperature) for the discharge condition, V_d = 350 V and P = 0.120 mbar pressure, comes out to be 0.21 mm whereas it is 0.48 mm for V_d = 290 V and P = 0.120 mbar. The sheath thickness for these two specific discharge conditions (calculated from Fig. 3.8(b)) come out to be 2.21 cms for case-I (V_d = 350 V and P = 0.120 mbar), whereas 2.75 cm for case-II (V_d = 290 V and P = 0.120 mbar). For these two extreme cases the sheath thickness is also measured by using the dusty plasma which is given in Sec. 3.3.1. The measured values are consistent with past experimental results under similar experimental conditions [126] as well as with theory/simulation model sheath calculations [129]. As has been pointed out in [129], depending on the extent of collisionality in the plasma the sheath thickness can vary from a few Debye lengths to upto 100 Debye lengths. It is also clear from these measurements that the probe scans over the sheath in case-I, whereas it scans through the sheath in case-II. As a result, we find couple of dips in plasma/floating potential profiles shown in Fig. 3.8(b) for the 2nd case (open and closed circles), whereas no dips are found in the first case (open and closed triangles).

The axial profiles of the floating potential (indicated by open symbols) and the plasma potential (indicated by closed symbols) at a constant discharge voltage, V_d = 310 V, are shown in Fig. 3.9. The different symbols represent different values of background pressures (P=0.12, 0.15, 0.18 and 0.21 mbar). The profiles plotted in this figure show that there is a small gradient in plasma/floating potential while going away from the anode similar to Fig. 3.8(a) that is caused by a small negative gradient in the plasma density along the axis. We have confirmed this by measuring the density over the entire length, using a Langmuir probe and found the value to vary by 5×10^{14} /m^3 over a distance of 40 cms at a discharge voltage of 310 V and P = 0.12 mbar and thereby ascertained the existence of a density gradient. Our conjecture for the cause of the gradient in the plasma/floating potential is also consistent with the trend seen in the ion saturation current which decreases gradually when the probe is moved away from the anode. It is also to be noted that both the plasma and floating potentials decrease with the increase of neutral gas pressure although the change is not significant. In the absence of potential strips a smooth curve is obtained throughout the axis whereas in presence of strips, a couple of potential wells are found in the potential profiles as similar to those found in Fig. 3.8(b). These wells are more prominent in case of floating potential profiles compared to the plasma potential profiles. The depth of the wells decreases when the working pressure is increased which implies that the strength of the confining potential decreases with the increase of pressure.

Hence, it can be deduced from Figs. 3.8(b) and 3.9(b), that lower pressure and/or lower discharge voltages provide a favourable condition for confinement of dust particles in the axial direction at a particular height from the cathode. The description of dusty plasma confinement is given in later section (Sec. 3.3.1).

c) Electron energy distribution function

The electron energy distribution function (EEDF) also provides useful information about the plasma parameters [130, 131]. It can be used to know whether the electrons are Maxwellian or not. In addition, the multipeaks in EEDF indicates presence of hot electrons in the plasma. Here, the EEDF is estimated using the Langmuir probe to sample the electron population by drawing a small current from the plasma. The electron energy distribution function can be defined as given in reference [131],

$$f(\epsilon_e) = 2(2m_e)^{1/2}(e^3A)^{-1}\epsilon_e^{1/2}\frac{d^2I}{dV^2}. \tag{3.4}$$

$\frac{d^2I}{dV^2}$ is calculated from the Langmuir probe characteristics, which also gives the information about electron energy. The ratio of electron energy distribution function to the $\sqrt{\epsilon_e}$ gives the electron energy probability function (EEPF). The probability function is plotted in Fig. 3.10 as a function of the electron energy using the Lang-

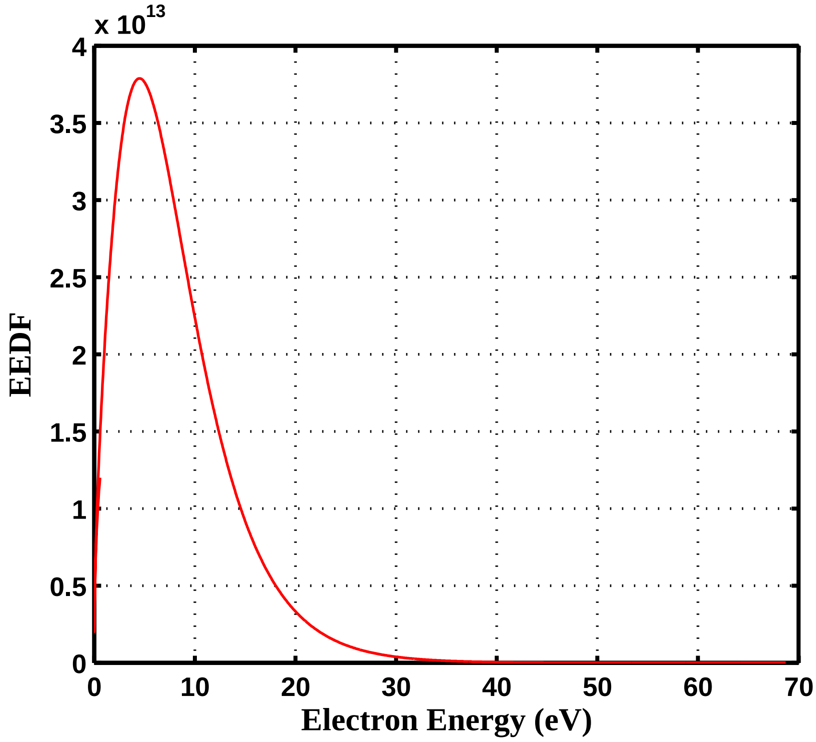

Figure 3.10: Electron energy distribution function at $P = 0.11$ mbar and $V_d = 310$ V. The distribution shows the electron temperature is ~ 5 eV.

muir probe data. The single peak in the probability distribution function shows the presence of mono-energetic electrons in the plasma which have an average energy of about 5 eV. The plasma density, which is also calculated with the help of EEDF comes out to be $\sim 1 \times 10^{15}$ m^{-3}.

3.3 Characterization of Dusty Plasma

The dust particles when immersed into the plasma get charged and levitate in the plasma sheath boundary. The addition of this extra component affect the plasma and add much richness to the collective dynamics of the system. Therefore, they are often called as complex plasma and the dust component, in particular, displays a variety of equilibrium states. Thus to understand the dynamical features of dusty plasma it is important to characterize them and know about the basic parameters, which play a very important role in any physical phenomenon associated with the dust into plasma. In this section we will discuss some of the dusty plasma parameters like dust temperature, thermal velocity, dust density, Coulomb coupling parameter etc. for our experiments and their variation with the discharge parameters such as background pressure and discharge voltage.

3.3.1 Dust cloud Equilibrium

When the dust particles are introduced into the plasma they collect electrons and ions. Due to high mobility of the electrons, more electrons get attached to the particles than ions and hence they acquire negative charge. There are various other charging mechanisms exist but in laboratory plasma the charge collection is the dominant charging mechanism. In this process the electron density decreases and quasi-neutrality condition also gets modified.

The negatively charged particles get trapped in the plasma sheath boundary region above the grounded cathode. By adjusting the pumping speed and the gas flow rate, a steady-state equilibrium dust cloud can be formed in between the stainless steel strips. In this levitated condition, the vertical component of the inhomogeneous sheath electric field provides the necessary upward electrostatic force $\vec{F}_E$ to the particles to balance the downward gravitational force $\vec{F}_g$ as shown in Fig. 3.11. This figure (Fig. 3.11) shows the horizontal view $(X - Z)$ of the stable dust cloud equilibrium. For the micron sized dust particles at equibrium, the other forces like drag forces and thermophoretic force do not play a major role as described in Chap. 1 [5, 49]. The force balance condition gives the relation between the equilibrium height of a dust particle with its dimension. The force balance condition is given as:

$$Q_d(Y)E(Y) = m_d(Y)g. \tag{3.5}$$

From above equation (Eq. 3.5), it is found that the particles of different sizes (different mass) achieve equilibrium at different heights (i.e. different Y position). In our experiments, the kaolin particles have a size distribution of $2 - 6$ μm, which

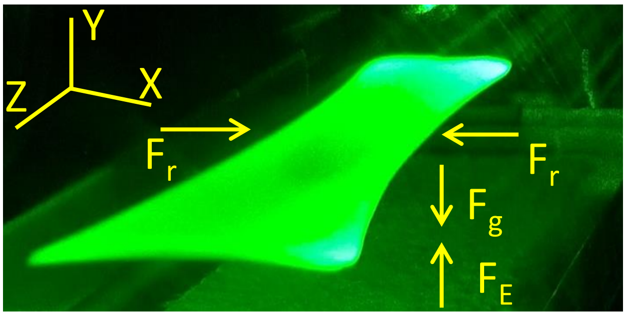

Figure 3.11: A photograph of horizontal ($X - Z$ plane) view of stable dust cloud .

results in the distribution of mass (as $m_d \propto r_d^3$) and charge (as $Q_d \propto r_d$). Due to size variation, the smaller particles levitate near the sheath boundary, whereas the bigger particles levitate near to the bottom of the cathode. Therefore in the case of kaolin particles, multiple layers are formed depending on the size distribution and discharge parameters. The radial (along X) and axial (along Z) sheath electric fields due to confinement strips provide the electrostatic force in the radial and axial direction and are responsible for confinement of the dust particles in respective directions against their mutual Coulomb repulsive force.

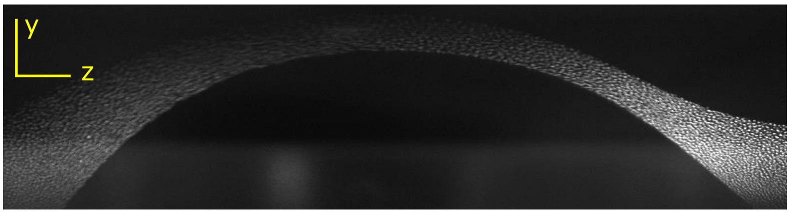

Figure 3.12: A photograph of particles flowing over a strip in $X - Z$ plane.

To see the effect of various SS strips used for particle confinement, we have measured the sheath thickness from emissive probe data over a wide range of discharge parameters (as discussed in Sec. 3.2.1). To ascertain the result shown by emissive probe measurement, the sheath thickness for the specific discharge condition (at $V_d = 290$ and 350 V and $P = 0.120$) are measured experimentally by examining the snap shots of the motion of the poly-dispersive particles over the confining strips (shown in Fig 3.12). Inside the plasma, most of the particles are found to be confined by the same confining potential strips, which are also used in emissive probe measurements. Some of the lighter particles which are levitated in the top most layer are found to flow over the potential hill. By capturing this image, we are then able to measure the sheath thickness very precisely knowing the height of the potential hill from the cathode. The estimation of sheath thickness agrees well with the emissive probe measurements.

3.3.2 Dusty plasma Parameters

In order to estimate the parameters of dusty plasma, we have carried out some initial experiments in which few particles (approximately 100) are introduced in the plasma and these are seen to be levitated at the plasma sheath boundary which is about 1-1.5 cm above the grounded tray. Then we adjust the pumping speed and gas flow rate in such a way that we can achieve an equilibrium steady state dust cloud of single layer. To study the dynamics of the particles, a series of images of dimension 1000 pixels × 1000 pixels are captured into a computer from the CCD cameras. A sample image of such a collection of dust particles in crystalline form is shown in Fig. 3.13. The detailed description of calculation of dusty plasma parameters are given in below subsections.

3.3.3 Dust charge and Sheath electric field

The charge on a dust particle can be estimated by considering it as spherical capacitor and following the relation (detailed discussion given in Chap. 1):

$$Q_d = CU = 4\pi\epsilon_0 r_d U. \tag{3.6}$$

Where C is the capacitance and U is the surface potential of the dust particle. The above equation (Eq. 3.6) is valid when $r_d \ll \lambda_D$. In our experiments λ_D varies from $30 - 50$ μm and r_d lies in the range: 2-6 μm. An expression for surface potential

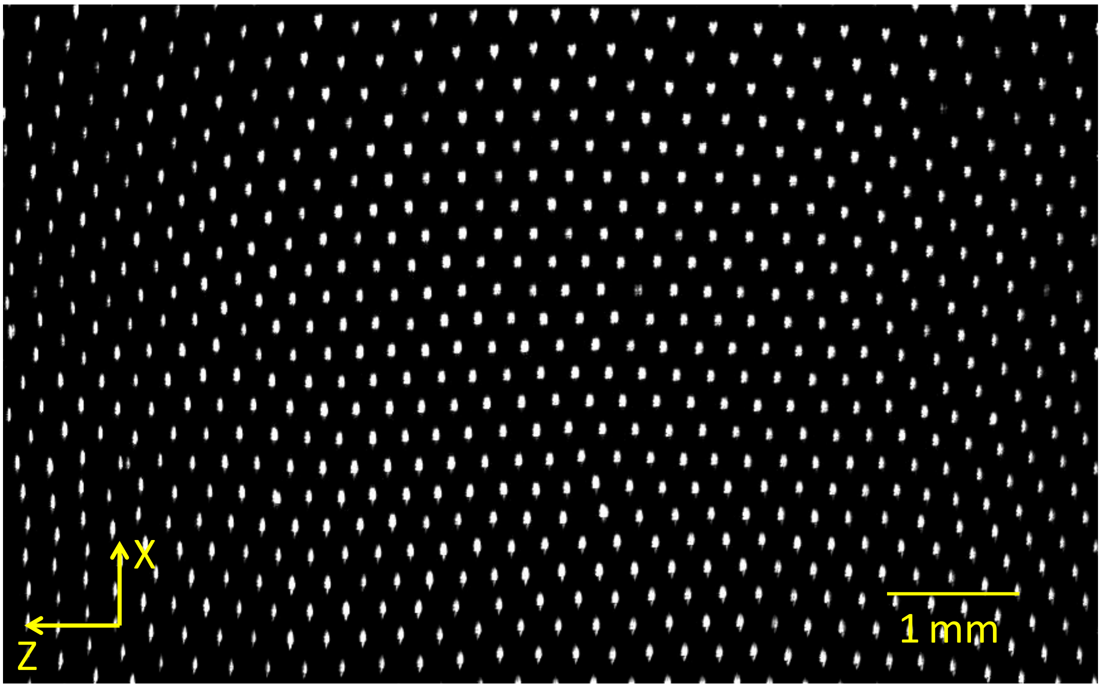

Figure 3.13: A photograph of horizontal ($X - Z$ plane) view of dust particles arranged in an ordered structure.

with respect to plasma potential for Ar gas when $T_e > T_i$ and $n_e \approx n_i$ is given as [47, 49]:

$$U = 0.73\frac{k_B T_e}{e} ln\left(\frac{m_e T_e}{m_i T_i}\right)^{1/2}. \tag{3.7}$$

For a singly charged Ar plasma, the simplest form of surface potential is given as $U = 4.0 \times k_B T_e/e$ (from Ref. [47]). Thus, for the typical value of plasma parameters, $T_i = 0.03$ eV, $T_e = 4$ eV, the charge on each particle of radius 2 μm comes to be $Q_d = 2 \times 10^4 e$.

By using the value of charge in the force balance equation (Eq. 3.5), we can estimate the sheath electric field responsible for the levitation of the dust particles. For our experimental condition, $m_d = 8.7 \times 10^{-14}$ kg (for a dust grains of radius 2 micron) and $Z_d \sim 2 \times 10^4$. Putting these values in equation 3.5 then the estimated electric field E comes out to be ~ 2.66 V/cm.

3.3.4 Pair correlation function and Inter-grain distance

We have used an idl based (super) Particle Identification and Tracking (sPIT) code [132, 133] to extract the coordinate of all the particles for a given span of time. By knowing the coordinates of each particle for a single frame (e.g., for Fig. 3.13), it is very straightforward to evaluate the pair correlation function, which represents the probability of finding two particles separated by a distance d. This is a very important parameter, which tells the ordering between the dust grains and inter-particle distance. It is generated by measuring the distance from each particle to every other particle and then counting the number of particles in the region between d and $d + \delta d$ from the particle. This is repeated for every particle until an average value is determined which is then normalised by dividing by the annular area between d and $d+\delta d$. Fig. 3.14(a) shows the pair correlation function calculated for

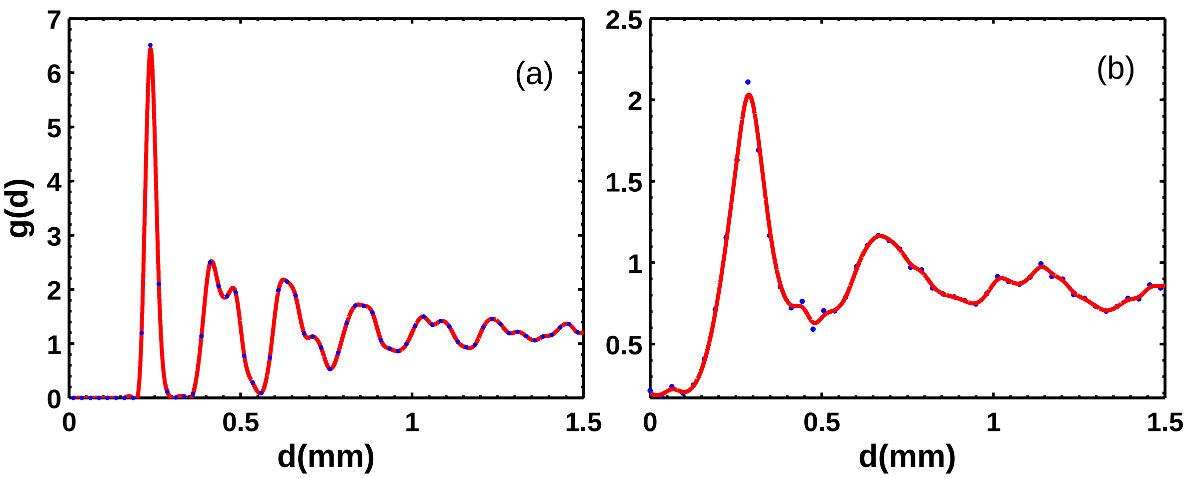

Figure 3.14: Pair correlation function calculated (a) from Fig 3.13 taken at P = 0.14 mbar and $V_d = 310$ V, (b) for P = 0.11 mbar and $V_d = 310$ V.

the Fig. 3.13, which is taken at background pressure P = 0.14 mbar and discharge voltage V_d = 310 V. As we can see in the Fig. 3.14(a), the correlation function exhibits several distinct peaks. This indicates that the system ordering is several times the nearest neighbour distance. This corresponds a long-range correlation among the particles which is indicative of the system being in a crystalline state. The first peak in Fig. 3.14(a) is much larger than the others. This is due to the fact that even in systems with long-range ordering, the correlation between nearest neighbours is stronger than that of more distant pairs. Due to this correlation, the primary peak is significantly narrower causing a corresponding increase in the height of the peak. Fig. 3.14(b) corresponds the correlation function calculated at background pressure P = 0.11 mbar and discharge voltage $V_d = 310$ V. It is clearly seen in this figure that there is only one primary peak or a primary peak followed by a small second or third peaks. In the present case the nature of the correlation function shows the existence of short range ordering between the particles which is the indication of strongly coupled liquid state. Thus at pressure 0.11 mbar or below this, the dusty plasma found to be in its liquid state. Keeping this fact into the mind we performed all the wave related experiment near (or even less) to 0.11 mbar.

From the first peak in Fig. 3.14(a) and (b) which shows the nearest neighbouring distance, we can estimate the inter-particle distance very accurately. From Fig. 3.14, the inter-particle distance is estimated as $\sim 250\ \mu m$. The inter-particle distance has also been calculated for the particles of different sizes and of different materials (MF, Kaolin) over a wide range of discharge parameters. In our experiments it varies from $500 - 160\ \mu m$ for a range of discharge parameters, different sizes and shapes of the particles.

3.3.5 Dust density calculation

The dust density n_d is estimated from the measurement of inter-particle spacing. It is considered that a single dust particle is contained in a sphere of radius d. The dust density can be estimated as,

$$n_d = \frac{3}{4\pi d^3}. \tag{3.8}$$

It can be seen from the above equation that the dust density is proportional to d^{-3}. In out experiment the density lies in the range $(0.5 - 6) \times 10^{10}/m^3$ depending on the discharge voltage and background pressure and particles of different sizes and shapes.

3.3.6 Dust thermal velocity and Temperature

The thermal velocity of the particles is estimated by dividing the displacement of the particles by time in consecutive frames (the time interval of two consecutive frames is known). In our experiments, for better statistics, we have chosen approximately hundred particles for a few hundred frames to calculate the velocity distribution function. Figs. 3.15(a) and 3.15(b) show a velocity distribution of dust particles along Z and X directions for the discharge parameters of $V_d = 290$ V and $P = 0.13$ mbar. The dotted line in the figures show the experimentally obtained velocity distribution. A Maxwellian function is fitted (shown by solid line) on the experimental data points to estimate full width at half maximum of the distribution function.

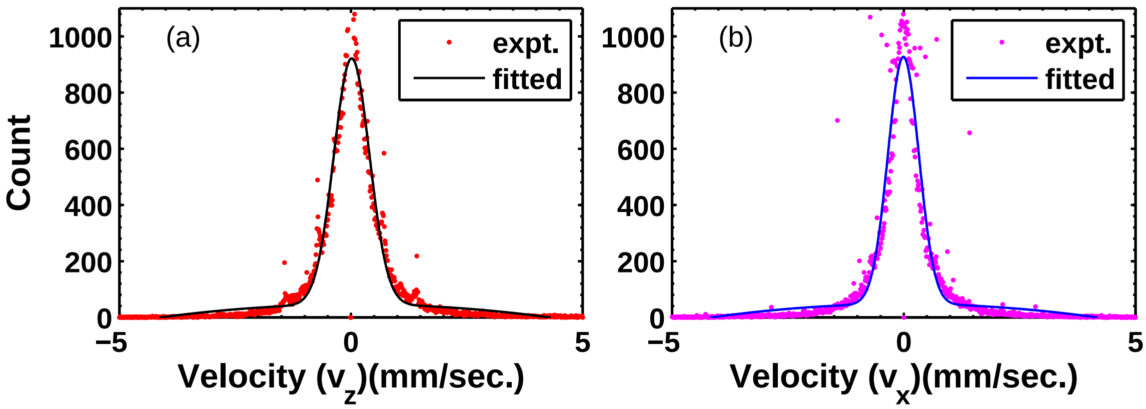

Figure 3.15: Velocity distribution of particles (a) in Z direction (b) in X direction

From this calculation we can estimate the temperature of dust particles by using the relation.

$$\frac{1}{2}m_d\langle v_{z,x}^2\rangle = \frac{1}{2}k_B T_{z,x} \tag{3.9}$$

Fig. 3.16 shows the variation of average thermal velocity of the particles with neutral pressure. The velocity is calculated from $v = \sqrt{v_z^2 + v_x^2}$. Here v_z and v_x are the thermal velocities of particles in Z and X direction respectively. It has been found

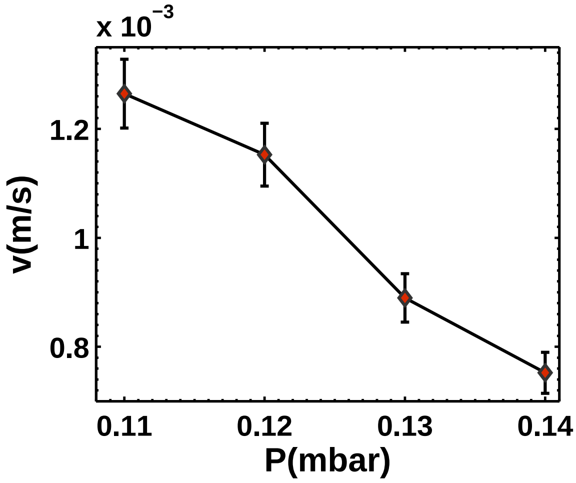

Figure 3.16: Variation of average velocity of the dust particles with neutral pressure

that the thermal velocity decreases with the increase of the neutral pressure. This is due to frequent dust neutral collisions.

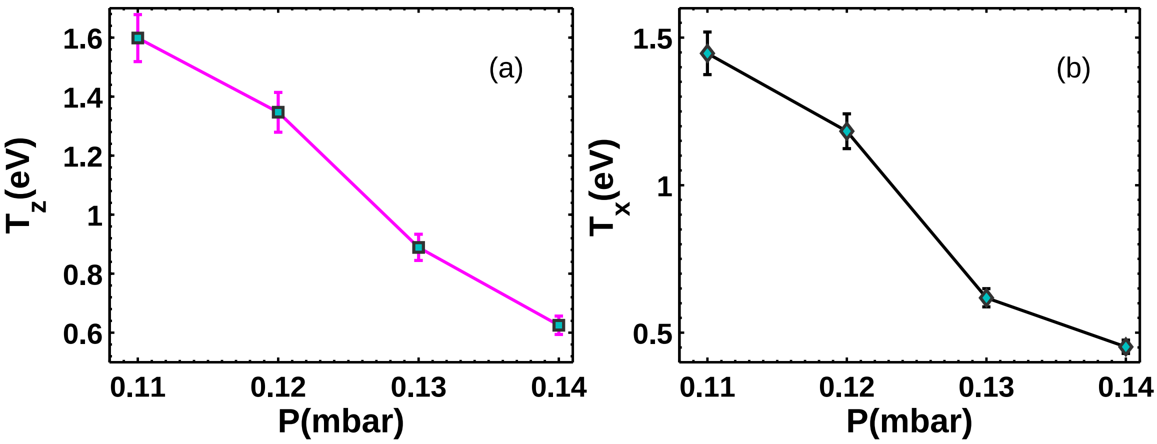

Figure 3.17: Variation of kinetic temperature components (a) T_Z and (b) T_X of the particles as a function of neutral gas pressure.

Using the Eq. 3.9, we have calculated the dust temperature for the range of discharge parameters. A variation of the dust temperature with the neutral gas pressure is shown in Fig. 3.17. In our experiments, the kinetic temperature along Z direction varies from 0.6 to 1.5 eV where as in X direction it varies from 0.4 to 1.4 eV. In both the directions, temperature decreases with the increase of neutral pressure. This is due to the fact that increase in pressure increases the dust-neutral collision probability and hence particles transfer their energy to the neutral atoms and cool down. It is also worth to mention that in our experiments levitation of the dust particles and hence the calculation of these parameter with the wide range of discharge voltage is difficult because at higher/lower discharge voltage, the force balance condition is not maintained in a particular plane.

3.3.7 Coulomb coupling Parameter

The Coulomb coupling parameter Γ defines the state of a dusty plasma, whether it is crystalline, fluid or gas [25, 134]. Its variation depends on the inter-particle distance (d), Debye length (λ_D) and charge over the dust particles. The detailed discussion is given in Chap. 1. In our experiment the coupling parameter varies from 80 to 220 for the range of temperature shown in Fig. 3.17 keeping other parameters fixed.

3.4 Conclusion

In this chapter we have discussed the characteristic features of a glow discharge plasma in the absence and presence of dust particles. The glow discharge is produced by applying a DC potential between the electrodes. The breakdown voltage follows Paschen's law, which shows that the minimum breakdown voltage is $\sim$ 270 V at $Pd_e = 0.9$ mbar.cm. The plasma parameters such as the plasma density, electron temperature, plasma potential, floating potential, and electron energy distribution function are estimated from measurements made by a single Langmuir probe and a hot emissive probe. The electron temperature is obtained by Langmuir probe analysis which is in the range of $2 - 5$ eV whereas the plasma density come out to be $(0.5 - 3) \times 10^{15}\mathrm{m}^{-3}$. The plasma density increases, whereas electron temperature decreases with the increase of background pressure. The plasma and floating potential, measured with the help of an emissive probe, show a small negative gradient in the axial direction. Furthermore, both the potential decrease with the decrease of discharge voltage and increase of neutral pressure.

The micron sized dust particles are immersed in the plasma, got negatively charged and levitated in the sheath region. The dusty plasma is characterized by estimating the parameters like inter-grain spacing, dust density, dust temperature and Coulomb coupling parameters over a wide range of discharge parameters. It is observed that in our experiments, the pair correlation function changes its nature with the change of background pressure and several peaks are observed for 0.14 mbar whereas a single peak followed by 2^{nd} and 3^{rd} peak are observed in the case of 0.11 mbar. It shows that the dusty plasma are in a fluid regime at lower pressure. The inter-particle distance comes in the range of $500 - 160$ μm, whereas dust density varies from $(0.5-6)\times 10^{10}/m^3$ for the range of discharge voltage and background pressure. The highly charged dust particles are influenced by a small sheath electric field and as a result the dust particles acquires a finite temperature in both axial and radial direction. The dust thermal velocity and temperature decreases with the increase of background gas pressure due to enhanced dust neutral collisions. The Coulomb coupling parameter (Γ) calculated over the range of discharge parameters is in the range of $80 - 220$ for a range of background pressure of 0.1-0.15 mbar. It suggests that we have a dusty plasma in a strongly coupled fluid regime upto pressure 0.12 mbar whereas it arranged in ordered structure on and above to 0.14 mbar.

Chapter 4

Flow generation and Measurement Techniques

*Surabhi Jaiswal and P. Bandyopadhyay and A. Sen, PSST, **25**, 065021 (2016)*

4.1 Introduction

A very interesting feature of complex plasmas is that they can exist in crystalline and liquid phases, as well as in the gaseous state. The complex liquids, which are essentially a one-phase system, are well suited for dust flow related studies as they have many properties similar to those of classical fluids as well as their dynamical behaviour can be investigated at the single particle level at high spatial and temporal resolution using laser illumination and video imaging. Thus, liquid complex plasmas have been widely used by several researchers for studying the fluid flows [29, 30, 135], measurement of drag forces [90, 136, 137], flow induced excitation of linear and nonlinear structure [81, 112, 114], hydrodynamic instabilities [94] etc.. For performing these type of flowing plasma experiments it is important to have a good control over the flow of particles/fluids. Thus it is necessary to explore an efficient technique of flow generation for pursuing such studies.

After generating the flow in the dust fluid, it is equally important to accurately measure the velocity of the flow so as to properly decipher the underlying physical mechanism responsible for the flow induced excitations of linear/nonlinear waves and vortex structures. To study the properties of these waves/structures in a detailed manner, it also sometimes becomes essential to make a coordinate transformation from the laboratory frame to the fluid frame for which it is necessary to know the fluid velocity. Furthermore, several theoretical studies predict that the wave behaviour undergoes drastic changes when the fluid flow velocity changes its magnitude from subsonic to supersonic values. In some of the dusty plasma experiments, in which the dust dynamics plays an important role, the estimation of different forces (e.g. neutral drag force, ion drag force, electrostatic force etc.) [90, 136, 137] acting on the flowing dust particles are very crucial. For such experiments, time varying measurements of the fluid velocity can provide useful information to estimate these forces. Thus precise measurements of the fluid velocity are crucial for the investigation of propagation characteristics of flow induced excitations of linear/non-linear waves as well as for estimating the fundamental forces acting on the dust particles.

In this chapter, we discuss the different techniques that we have implemented to initiate the dust flow in our experiments and also describe the variety of tools that we have employed to measure the flow velocity in different regimes. Among these measurement techniques, the use of low amplitude Dust Acoustic Waves has not been tried before and our findings should motivate further research and development in this area. This novel technique allows us to measure the velocity of a dense fluid which flows with a very high velocity. The result obtained by these different techniques are compared with each other. Further, a detailed discussion on the merits and demerits of different techniques of flow generation and velocity measurement tool are presented. An estimation of the neutral drag force responsible for the generation as well as the attenuation of the dust fluid is also made.

The chapter is organized as follows: In the next section (Sec. 4.2), we overview some of the earlier work carried out on the flow generation and their implementations. In Sec. 4.3, we describe the experimental set-up and associated diagnostics used for flow generation and measurement experiments. Sec. 4.4 describes the different techniques that we have followed to generate the flow in dusty plasma. The measurement of fluid velocity using different tools with their merits and demerits are presented and discussed in Sec. 4.5. In Sec. 4.7, we discuss the estimation of neutral drag force acts opposite to the direction of fluid flow. We draw a concluding remark in Sec. 4.8.

4.2 An Overview of Previous Works

In recent times, a series of experiments has been carried out world wide for studying shear flows, estimation of drag forces, excitation of different linear and nonlinear structures etc. in a flowing dusty plasma. In 2004, Morfill *et al.* [29] experimentally studied the kinetic flow topology around an obstacle in a rf produced plasma under microgravity condition where thermophoresis was used to compensate the effect of gravity. In that experiment, they observed the steady axially symmetric flow pattern with an upward and downward flow with a velocity $U_t = 0.8$ cm/sec. Soon after, Nosenko *et al.* [30] reported an experiment on shear viscosity measurement in two-dimensional liquid-state dusty plasma. In that experiment, two counter-propagating Ar^+ laser beams pushed the particles in the respective directions, which initiated a shear-induced melting in the monolayer and a shear flow in a planar Couette configuration. They measured the particle velocity profile in the shear flow and calculated the kinematic viscosity by comparing the experimental results with Navier-Stokes model. Later on in 2007, Ivlev *et al.* [135] investigated the shear flows in three-dimensional complex-plasma fluids produced in a DC glow discharge plasma by using "Plasma-Kristall-4" (PK-4) facility. The shear was induced either by an inhomogeneous gas flow or by a laser beam. They showed the non-Newtonian behaviour of complex plasma accompanied by substantial shear thinning. In 2012, Feng et al. [138] reported the profound temperature peaks in the region of high velocity shear in a laser-driven two-dimensional (2D) dusty plasma. The flowing dusty plasma had also been used as a source of perturbation for the excitation of different linear and non-linear structures in dusty plasma [81, 112, 114]. Samsonov *et al.* [81] reported the experimental observation of shock structures in a rf produced 3D complex plasma under microgravity conditions in the PKE-Nefedov device by applying a sudden gas pulse using an electromagnetic valve. Later, Nakamura [112] experimentally observed a bow shock like formation in a 2D flowing dusty plasma as a consequence of interaction of supersonically flowing dust fluid with the charged stationary object. In 2013, Meyer *et al.* [115] performed an experiment on transient bow shock formation by a supersonic dust fluid incident on the biased cylinder. In this experiment, the flow was generated by disconnecting the ground connection of the L shaped mesh and allowing the dust particles (which were trapped in the potential of the mesh) to expands towards anode. Very recently, Fink *et al.* [114] triggered auto waves in a complex plasma by injecting gas from a gas-flow controller. Several authors reported the experimental studies on the estimation of drag forces in flowing dusty plasma [90, 136, 137]. Thoma *et al.* [136] reported the experimental investigation of ion drag force acting on the particles over a wide range of neutral gas pressure. They also measured the flow velocity of the particles of different sizes (1.28 to 11.0 μm) and found that the velocity varies from $\sim$ 1 cm/sec to 12 cm/sec for different size of particles and discharge conditions. In addition, they observed that the flow velocity decreases with the increase of the neutral pressure. Nakamura *et al.* [137] experimentally measured the flow velocity ($\sim$ 0.25 cm/sec to 4cm/sec) and estimated the neutral drag force acting on dust particles of size 5 μm for a range of neutral gas pressure. They found that the velocity decreases with the increase of neutral pressure. In most of these experiments the flow of dust fluid initiated either by a mechanical arrangement such as tilting the complete experimental set-up [112] to use gravity or by using gas puffs and laser pulse [30, 81, 114, 135]. The mechanically generated gravity induced flow is somewhat limited in its range and also not easily amenable to control in a precise manner. In addition, it is very difficult to manage the optical alignments in such a configuration. Likewise experiments with gas puffs also have limitations in the way of induced changes in the equilibrium configuration due to the sudden introduction of neutral gas into the device and the concomitant increase in the pressure. In laser induced flows, the transport properties of complex plasma are no longer local and equilibrium and a high power laser is desirable for this kind of experiments, which is difficult to operate. Furthermore, in all these experiments the flow velocity is measured at single particle level with particle tracking techniques. The techniques for the measurement of flow velocity of relatively denser fluid moving with supersonic speed has not been explored earlier and it is necessary to investigate an efficient way of measuring the flow velocity in the case of high density complex plasma. This chapter is dedicated to investigate different flow generation techniques and measurement of flow velocity at single particle level and fluid level.

4.3 Experimental arrangement

The experiments are performed in a Π−shaped Dusty Plasma Experimental (DPEx) device (shown in Fig. 4.1), which is made of Pyrex glass. The detailed description of experimental set-up is given in Chap. 2. A rotary pump is used to evacuate the system up to its base pressure of 10^{-3} mbar and a gate valve connected at its mouth is used control the pumping speed. In this experiment, the Ar gas is introduced by a mass flow controller and gas dosing valve through the gas ports, P_1 and P_2. For most of the experiments, the port P_2 is kept closed and used only for some specific experiments. For flow experiments at particle level, we have used monodisperse Melamine Formaldehyde (MF) particles of sizes 9.19 and 4.38 μm that are injected into the plasma by using the dust dispenser. For fluid level flow experiments (exciting DAWs) poly-dispersive kaolin particles are spread uniformly on the cathode before closing the device. To operate the

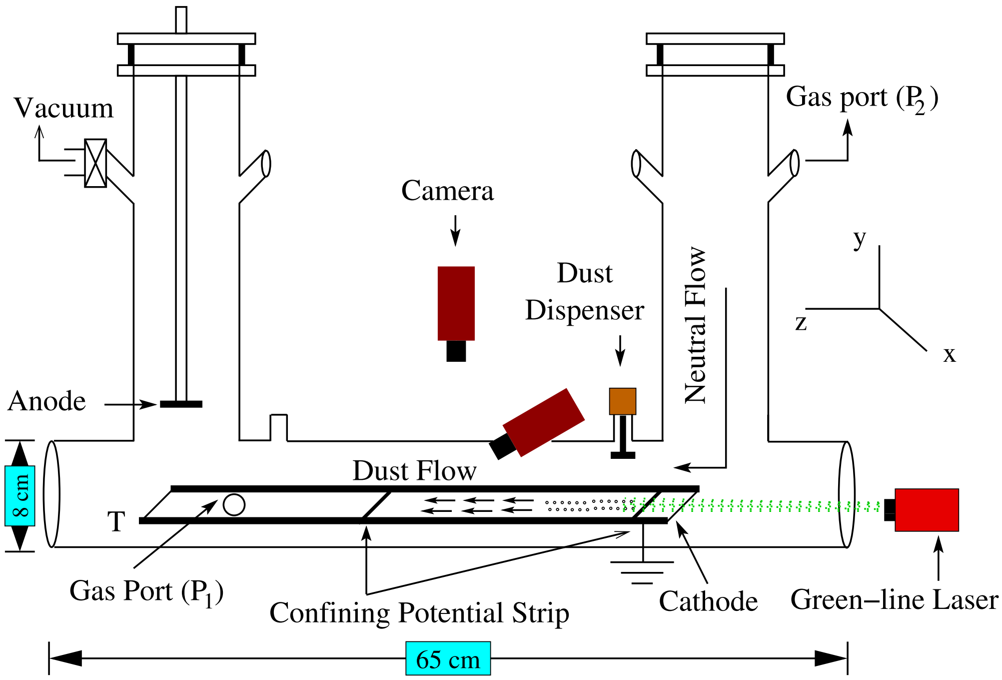

Figure 4.1: Schematic diagram of Dusty Plasma Experimental (DPEx) setup., T: grounded cathode tray.

device for flowing dusty plasma experiments, we begin with the evacuating the vacuum chamber. After achieving the required base pressure of $\sim$ 0.001 mbar, Ar gas is flushed several times and pumped down to its base pressure. Finally, the working pressure is set in the range of $0.1 - 0.2$ mbar by maintaining the pumping speed and the gas flow rate.

A DC glow discharge plasma is then formed in between the disc shaped anode and long grounded cathode tray by applying a discharge voltage in the range of $300 - 400$ V. The particles (MF or Kaolin) get negatively charged by collecting more electrons than ions and get trapped in the plasma sheath boundary above the grounded cathode as discussed in Chap. 3. By adjusting the pumping speed and the gas flow rate, a steady-state equilibrium dust cloud is formed over the cathode in between the stainless steel strips used for radial and axial confinements. The particle cloud is illuminated by a green line-laser light (532 nm, 100 mW) along the axial length of the connecting tube so that the dust cloud can be seen over its entire length. The Mie-scattered light from the dust particles is captured by a couple of CCD cameras and the images are stored into a high speed computer. The high speed low resolution camera (60fps, 1MP) is placed at an angle of 15° with the y-axis, whereas the low speed high resolution camera (15fps, 4MP) is placed exactly perpendicular to the dust cloud.

Plasma parameters such as plasma density, electron temperature, plasma and floating potential are measured by using cylindrical Langmuir and emissive probes, which have been discussed in detail in Chap. 2 and Chap. 3. In order to estimate the dust temperature, we have measured the dust thermal velocity by tracking the individual particles in consecutive frames as discussed in Chap. 3.

4.4 Flow generation Techniques

After attaining the equilibrium dust cloud, the flow of dust particles has been initiated by using different means of flow generation. In the subsequent subsections, we will discuss about the three different techniques that we have employed to generate the flow of dust particles.

4.4.1 Single Injection method

As mentioned above, a steady state equilibrium dust cloud can be formed when the pumping rate (~20% opening of the gate valve) and the gas flow rate (27.5 ml$_s$/min) through gas port P_1 are suitably balanced in a precise manner. If the pumping rate exceeds the gas flow rate, the particles are seen to flow from right to left and in the reverse direction if the gas feeding rate is increased beyond 27.5 ml_s/min. However, for our experimental convenience, the flow is always generated from right to left by reducing the gas flow rate in steps of 2.75 ml_s/min. from its equilibrium value. After initiating the flow of dust particles, the gas feed rate is set back to its original value within a second and hence the equilibrium condition is restored. As a result almost all the particles are found to return to their original position from where they had started their journey. In this process some particles always get lost during the experiments. The particle velocity in this procedure can be raised up to $20 - 25$ cm/sec by increasing the flow rate difference. When the flow rate difference is set to a higher value, the particles move towards the pump with very high velocity and hence they overcome the potential barrier and flow over the strip and finally fall down on the left edge of the glass tube where the cathode ends.

4.4.2 Dual injection method

In an alternative method, the flow of dust particles is initiated by using two gas feed ports P_1 and P_2 as shown in Fig. 4.1. As discussed, initially the steady state dust cloud is formed at a particular discharge condition, in between two confining potential strips by adjusting the pumping rate and the gas feeding rate through port P_1. In this equilibrium condition, the dust particles only show Brownian motion due to their thermal energy. It is to be noted that the gas dosing valve mounted at gas feeding port P_2 is kept closed at this point. To generate the flow of dust particles, this gas dosing valve is opened and as a result the particles are found to flow from right to left. In this dual gas injection technique, the flow velocity can be changed very precisely by changing the gas flow rate of port P_2. With the help of this method we can maintain a constant gas pressure while performing the experiments. In some of the experiments at lower gas pressure (below $P = 0.09$ mbar), we can produce a flow in the particles by first attaining the background pressure at equilibration by using both the ports and subsequently injecting the dust particles by the dust dispenser.

4.4.3 Withdrawing potential hill

In the third technique of flow generation, the equilibrium of the long dust cloud is first achieved in between the confining potential strips (located at right end of the cloud) and the grounded wire (located at left end of the cloud) as shown schematically in Fig. 4.2 (a). There is an experimental arrangement (connecting switch or variable resistance in between the wire and ground) by which this wire can be kept either at floating or at ground or at intermediate potentials. The grounded wire creates an electrostatic potential hill by which the dust particles get confined in the axial direction. To initiate the flow, the grounded wire is suddenly switched to the floating potential (or into a potential which has a higher value than the ground) and as a result the stationary dust cloud is found to flow over the wire. Fig. 4.2(b) shows a schematic diagram of this situation when the height of the potential hill is reduced by changing the wire potential from ground to floating. In this

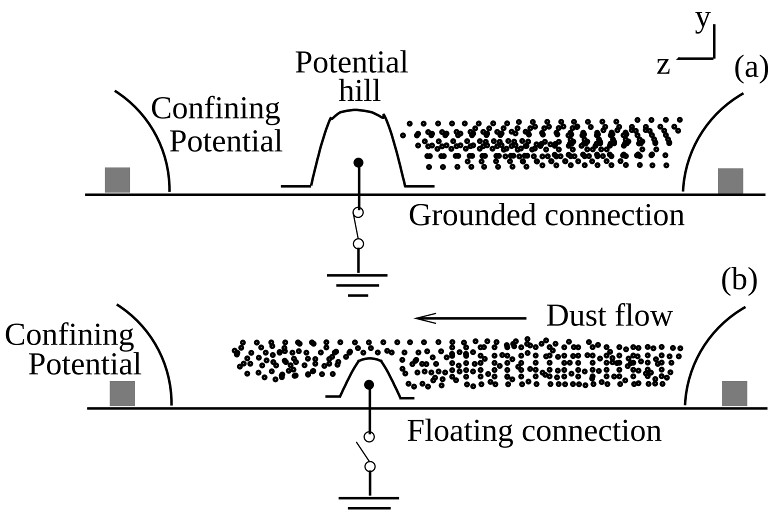

Figure 4.2: (a) Equilibrium dust configuration with the potential hill created by a grounded wire and b) dust flow induced by sudden lowering of the potential hill by switching the grounded connection to a floating connection.

condition, the particles cannot feel the presence of the wire and are observed to flow over it. To get the clear picture of the potential heights in grounded and floating condition respectively, we introduced extra gas to make the particles flow over the grounded/floating wire. Fig. 4.3(a) shows a snap shot of the particles flow in the Y-Z plane for the case of grounded wire, whereas (Fig. 4.3(b)) shows the same when the wire is kept at floating

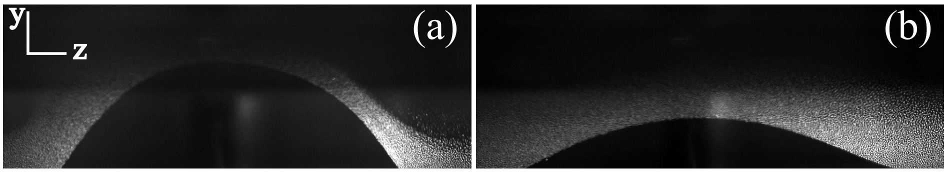

Figure 4.3: Real view of the potential profile for the a) grounded wire and b) floating wire. The height of the potential hill decreases considerably when the wire is switched to floating potential from grounded potential.

potential. The profiles of the particle trajectories in these two different situations are seen to closely follow the potential profiles created by the wire. It can be seen that the height of the potential hill is reduced significantly when the wire potential is switched from the ground potential to a floating potential. The height of the potential hill and hence the speed of flow of the particles, can be precisely controlled by drawing currents through different combinations of resistances connected between the wire and the ground. It is worth while mentioning that, in this scheme of flow generation the neutrals do not carry the dust particles.

Among these three different techniques, the single and dual gas injection techniques are used to generate a motion of dust particles by reducing or inducing a neutral gas flow in the experimental device. In other words, the dust particles flow from right to left due to the neutral streaming which carry the dust particles along their way. With the help of these schemes, the dust fluid velocity can be raised from subsonic (few mm/sec to cm/sec) to supersonic (few tens of cm/sec) values. However, in single gas injection technique, the sudden reduction of gas flow rate creates a momentary (for a time less than a second) change of the neutral gas pressure, which disturbs the steady state equilibrium during the course of the experiment. Although, this gradient of pressure is created for less than one second and the maximum instantaneous change of pressure (as measured in the pressure meter, whose response time is about 200 ms) is less that $\pm 5\%$. In fact sometimes this change cannot even be detected by the pressure meter if the flow rate is decreased by a small amount. This small-scale problem is further overcome in the second technique of dual gas injection by introducing the neutral gas in a continuous manner to maintain a constant gas pressure during the experiments. The third technique, namely flow generation by altering the confining potential is very useful for experiments which demand a stationary neutral gas. However this technique is limited by its inability to produce very high velocity fluid flows for long periods in comparison to the first two techniques.

4.5 Velocity measurement Technique

After the initiation of the fluid flow it is essential to measure the dust fluid velocity prior to conducting any further experiments. The fluid velocity measurement helps in estimating the fundamental forces that act on the particles and that influence the collective behaviour of the dusty plasma. The velocity measurement is also needed to determine the true velocity of the linear/nonlinear wave structure from the laboratory frame measurements. We now discuss various techniques of measuring the fluid flow velocity in the following subsections.

4.5.1 super Particle Identification Tracking (sPIT) Code

We begin with an Idl based super Particle Identification Tracking (sPIT) [133] code to measure the dust particle velocity from an analysis of video images of the flow. In this code, particle positions are first identified in each frame by plotting brightness contours at an adjustable threshold and determining the centers of intensity of each local region found this way. Then the particle position is traced in consecutive frames for given number of frames. The particle velocity is then calculated from the information of particle position and frame rate [132]. This code efficiently measures the flow velocity when the individual particles are distinguishable in consecutive video frames. Hence, for an accurate measurement of the particle velocity using the sPIT code, one needs to restrict oneself to conducting experiments where the dust number density is low (not more than 30 particles in the field of view of 9.0 mm$\times$2.2 mm) and that move with a moderate velocity (not more than $\sim$ 8 cm/sec). This is to ensure that we focus on a small area at a maximum frame rate so that the particles can be detected very easily. The analysis shows that the particles start to move with zero velocity and then accelerate to a certain value and finally attain a terminal velocity within this region. The proper threshold and background values are

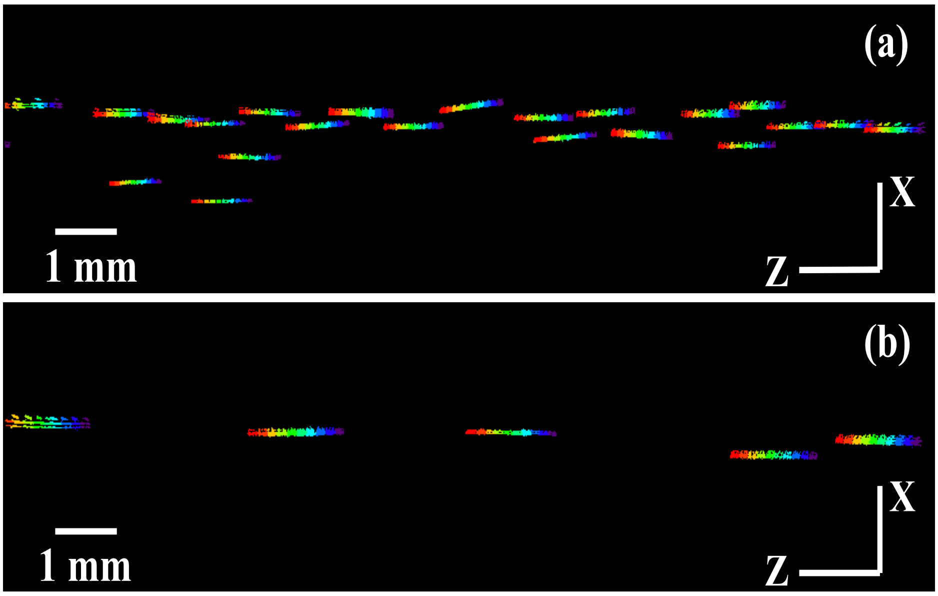

Figure 4.4: Color plot showing the particle trajectory at (a) 0.15 mbar and b) 0.13 mbar respectively at discharge voltage (V_d) of 300 V.

set for the consecutive images to trace the particle with maximum probability for all the frames. Fig. 4.4 depicts the trajectory of the particles for two different pressures at a discharge voltage of 300 V. This figure is created by overlapping ten consecutive frames that are marked in different colors in the color sequence of a rainbow. The violet colour corresponds to the positions of the particles in the first frame whereas the red colour corresponds to their positions in the tenth frame. From such a sequence it is clear that the particles are moving from right to left. Fig. 4.4(a) represents the particle trajectory for 0.15 mbar pressure whereas Fig. 4.4(b) represents the same for 0.13 mbar pressure. It is clearly seen in the figure that the average particle trajectory becomes shorter at higher pressures. It essentially indicates that the particles undergo a larger number of collisions with the neutrals at P = 0.15 mbar and as a result they are not able to travel a longer distance. It is also to be noted that by calculating the distance travelled in 10 frames, we are able to estimate the velocity of the particles.

The spatial variation of the velocity of an individual particle is depicted in Fig. 4.5. It shows that the particle experiences an acceleration in the beginning and then it attains a terminal velocity which is approximately equal to 1.3 cm/sec. The particles achieve the terminal velocity due to the neutral drag force which always opposes the motion of the

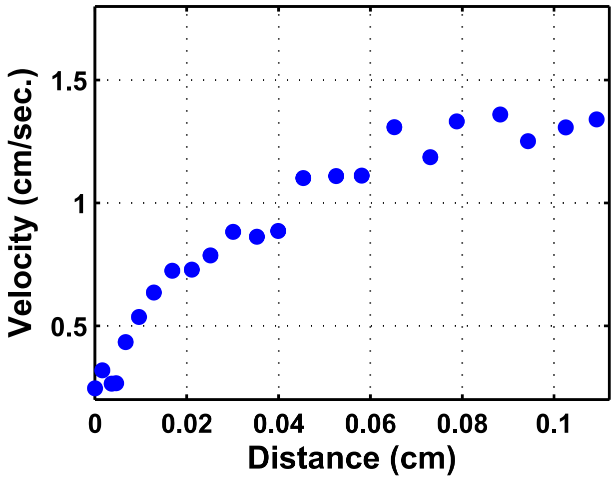

Figure 4.5: A plot showing the variation of velocity with the distance travelled by the particles at P = 0.13 mbar, discharge voltage (V_d) = 310 V and for the flow rate difference of 2.75 ml_s/min.

dust particles when they travel faster than the neutrals.

4.5.2 Particle Image Velocimetry (PIV) analysis

In addition to the sPIT code, a Matlab based open access Particle Image Velocimetry (PIV) [139] analysis has also been carried out to estimate the average velocity of the particles. For the present PIV analysis, 50 still frames of pixel resolution 1000×225 in the interval of 30.7 m sec of flowing dust particles are considered. A 2-pass algorithm is used in which 64×64 sq. pixel interrogation area in steps of 32 pixel followed by 32×32 sq. pixel interrogation area in steps of 16 pixel are chosen to construct the velocity vector fields. The velocity vector and its components are estimated by taking the mean of all the frames with a proper velocity vector validation. Fig. 4.6 shows the velocity vector fields along with the magnitude of the velocity components v_z (Fig. 4.6(a)) and v_x (Fig. 4.6(b)). The magnitude of the velocities are represented by color code of HSV where the blue color corresponds to the minimum value of velocity and red corresponds to the maximum value. It is clearly seen in the figure that all the particles move from right to left almost in the axial direction as the x-component of the velocity (v_x) is almost negligible compared to the axial component of the velocity (v_z). It is also found that the length of the velocity vector field ($v = \sqrt{v_z^2 + v_x^2}$) is very small at the right edge (Z-position $\sim$ 0 cm) and later gradually increases till $Z \sim 3$ cm and finally it acquires an almost constant length. The

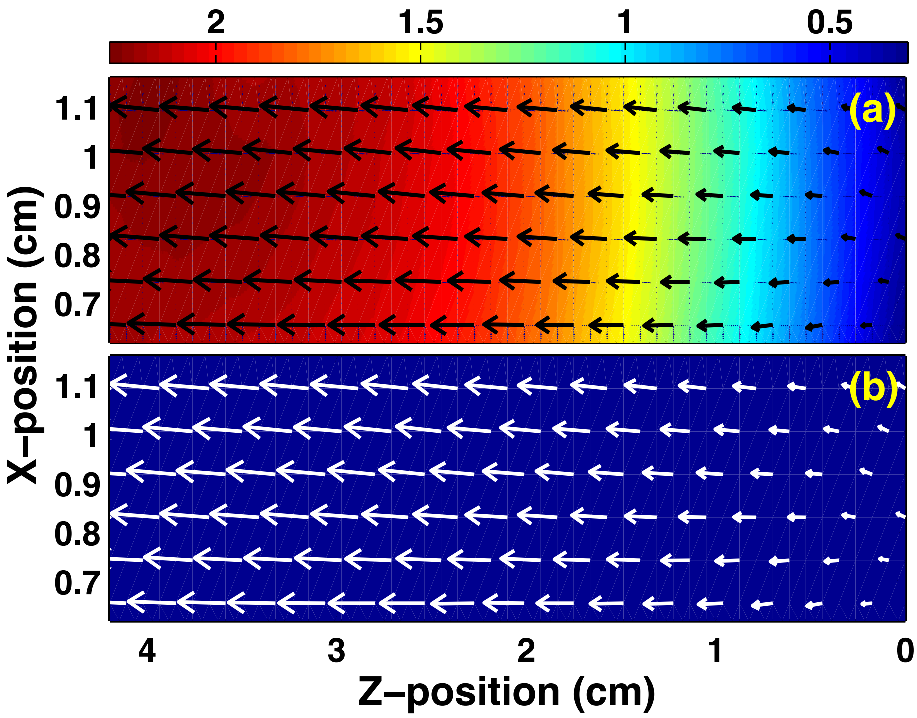

Figure 4.6: velocity vector fields along with the magnitude of the velocity components v_z (Fig. 4.6(a)) and v_x (Fig. 4.6(b)) respectively.

velocity components (v_x, v_z) are depicted separately in Fig. 4.7. The solid line represents the variation of v_z whereas the dashed line represents v_x with distance from the right edge. It is clear from the figure that significant contributions to the magnitude of the velocity vector comes from the v_z component as the particles rarely move in the other direction. It is seen in the experiments that the particles start from their initial velocity and then accelerate towards the port P_1 due to neutral streaming and then they attain a terminal velocity. The main force responsible for bringing the dust particles to a terminal velocity is the neutral drag force (an opposition force due to background stationary/moving neutrals) which always acts opposite to the direction of the particle motion. In figure (Fig. 4.7) the solid line shows the particle starting with a finite velocity (at the extreme right edge of the image) and accelerating (up to 2 cm) and finally (beyond 3 cm) achieving an almost constant velocity.

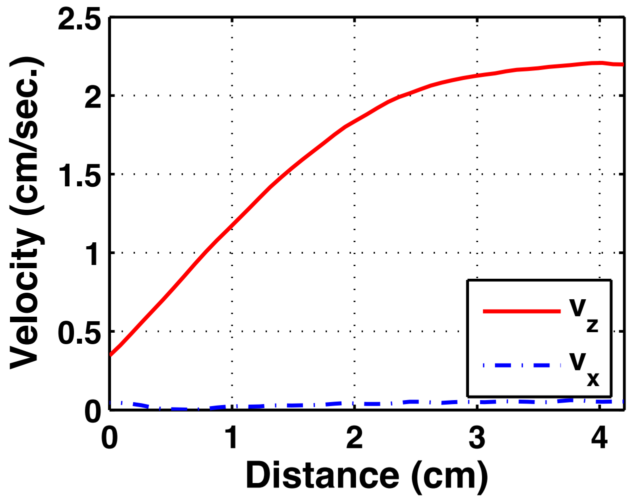

Figure 4.7: The variation of velocity component v_z (shown by solid line) and v_x (shown by dashed line) with distance travelled by the particles.

4.5.3 By inducing flow on Dust acoustic waves

In this subsection we discuss a new technique to measure the dust fluid velocity that is based on the excitation of a low amplitude Dust Acoustic Wave (DAW) in the medium. This novel technique is applicable even when the particles move with a high velocity and have smaller inter-particle distances as it is independent of the requirement of distinguishing individual particles that is necessary for using the sPIT code method or the PIV analysis. In this technique, after the equilibrium of dust cloud is achieved by adjusting the pumping and gas feeding rate at lower pressure (P=0.097 mbar) between a mesh and the potential strip, a DAW is excited by applying a sinusoidal voltage (V_{pp} = 100 V at a frequency of f = 0.8 Hz) on a mesh at a discharge voltage of V_d = 350 V. The excitation of the Dust Acoustic Waves (DAW) and their subsequent propagation away from the mesh are shown in Fig. 4.8 and Fig. 4.9. The measured phase velocity of these waves is around $4 - 5$ cm/sec and is dependent upon the applied frequency and the plasma and dusty plasma parameters. The experimentally obtained phase velocity is then compared with the theoretical value, $v_{ph} = Z_d\sqrt{\frac{k_BT_in_d}{m_dn_i}}$[1] [140] where, Z_d, n_d, n_i, k_BT_i, m_d are the dust charge number, dust density, ion density, ion temperature and dust mass, respectively. For $Z_d \sim 2\times10^4$, $n_d \sim 5\times10^{10}/m^3$, $n_i \sim 1.2\times10^{15}/m^3$, k_BT_i = 0.03 eV and

[1]the derivation of phase velocity is given in appendix B

$m_d = 8.7 \times 10^{-14} kg$ (for a dust grains of radius 2 micron), the phase velocity comes out to be 4.2 cm/sec which agrees well with the experimentally obtained phase velocity.

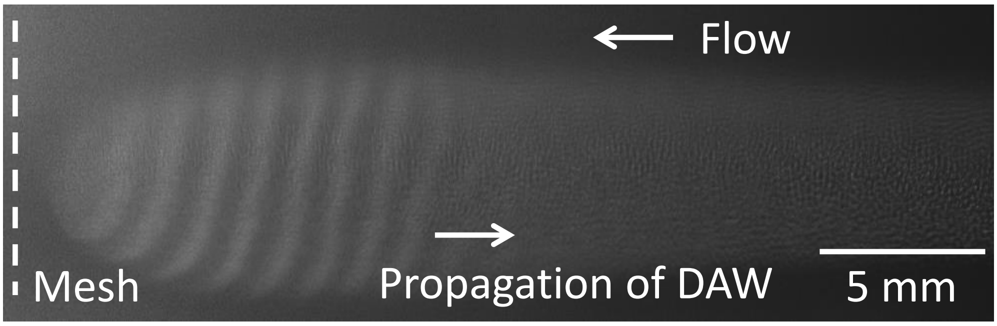

Figure 4.8: Typical image of propagation of dust acoustic wave (DAW)

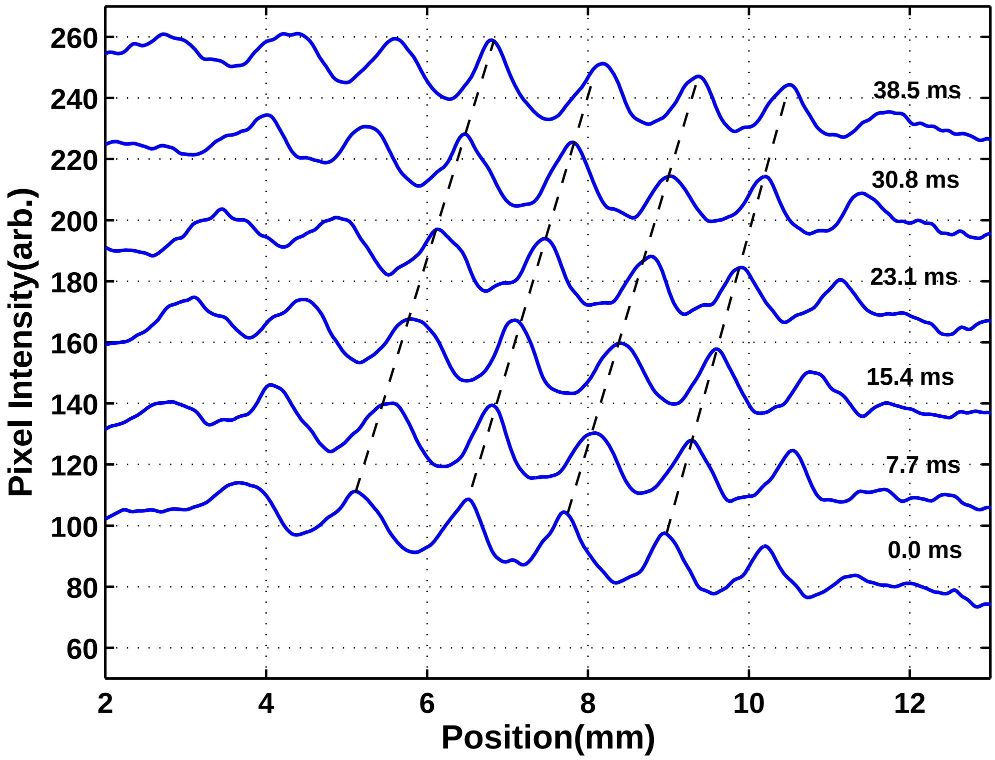

Figure 4.9: Propagation of dust acoustic wave at 7.7 msec. intervals

After the excitation of the DAW, the flow of dust is generated with the help of the single gas injection method (discussed in the earlier Sec. 4.4.1) in small steps of the flow rate. As the direction of fluid flow is opposite to the direction of propagation of the DAW, we find that initially the phase velocity of the DAW decreases with the increase of flow rate difference. For a particular higher flow rate difference the DAW becomes almost a standing wave (phase velocity becomes almost zero). Then for a further increase in the flow rate difference, the DAW changes the direction of propagation i.e., it travels in the direction of the neutral flow. The variation of the phase velocity of the DAWs with the flow rate difference is shown in Fig. 4.10(a). This figure clearly indicates that the DAW velocity decreases almost linearly with the flow rate change. Subtraction of the original phase velocity (v_{ph}) from this velocity (which is the sum of the flow velocity and the v_{ph}) directly gives the dust fluid velocity. Fig. 4.10(b) shows the dust fluid velocity with the gas flow rate change. However, this method also has its disadvantage in that the DAW cannot be excited at higher pressures due to strong damping arising from higher dust neutral collisions. Hence, to measure the flow velocity by this technique, we need to perform the experiments in a pressure range between 0.07 mbar to 0.11 mbar for a particular voltage (V_d) $\sim$ 340 V.

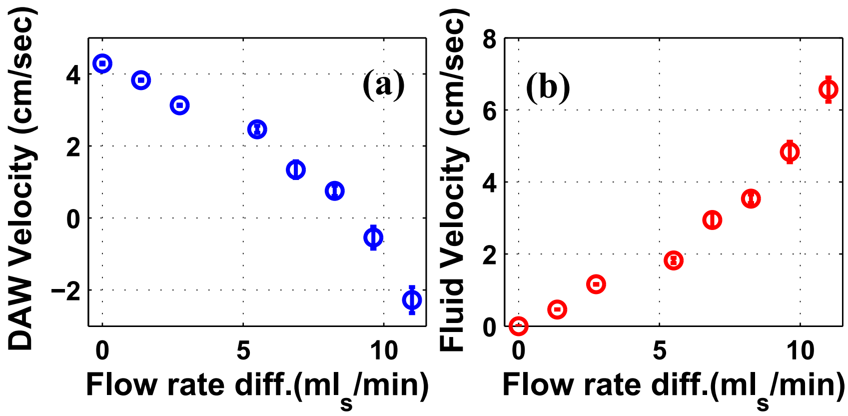

Figure 4.10: Variation of (a) phase velocity of dust acoustic wave (DAW) b) and fluid flow velocity with the flow rate difference.

Thus the above three techniques to measure the flow velocity, as discussed in this section, have their individual merits and limitations. The sPIT code method is a very efficient and powerful technique to measure the flow velocity as long as one is able to distinguish individual particle motions in the dust component and the flow is not too high so that the trajectory of each individual particle can be traced in consecutive frames. For a higher density dusty plasma and/or a dust fluid moving with a higher velocity, the sPIT code method fails to measure the velocity accurately. For this reason, it is always recommended to zoom into a small area so that very few number of particles can be tracked for a number of frames. This however limits the information on the spatial variation of flow velocity measurement. Some of these issues can be addressed by using the PIV analysis. With the PIV tool one can measure the velocity profile for a reasonably larger field of view. However, this technique also gives better results when in the input images one can clearly identify the motion of individual particles otherwise the measurement of high velocity by this technique becomes difficult. Both these techniques collapse when the fluid velocity turns out to be high and/or the density of the flowing particle is too high so that the particles become indistinguishable. Their efficacy depends on using very high resolution cameras along with high frame rates. In the absence of such a facility, the 3rd technique associated with the excitation of DAWs assumes significance. In this procedure, the DAW acts as a diagnostic tool to provide the information of the fluid velocity albeit with the limitation that its application is limited to lower pressure discharges (less than 0.12 mbar for the present experiments). Hence an accurate measurement of the flow velocity at higher pressures still remains a challenge and an open issue that needs to be addressed.

4.6 Results and Discussion

In this section, we compare some of the results that we have obtained by employing different techniques to measure the terminal velocity, varies from $\sim$ 0.5 cm/sec. to 7.0 cm/sec., which is in good agreement with the measurements made in past [114, 136, 137]. In the present set of experiments the dust particles attain a flow velocity due to their interaction with flowing neutrals. The force associated with the momentum transfer from the neutrals to the dust particles is given as $F_{dn} = -m_d \nu_{dn}(v_d - v_n)$ where m$_n$ is the mass of the neutrals, ν_{dn} is the dust neutral collision frequency and $v_d - v_n$ is the relative velocity of the dust particles with respect to the velocity of the neutrals. Initially at equilibrium, the dust cloud is nearly stationary except for small random velocities associated with the thermal energy of the dust particles. When the neutrals with very high velocity are then introduced in the system their collisional impact with the dust particles impart the latter with an average unidirectional momentum that makes them move in the forward direction along the neutral flow. This momentum transfer diminishes as the relative velocity between the two species decreases ultimately leading to a terminal velocity for the dust particles. In the single (Sec. 4.4.1) and dual (Sec. 4.4.2) gas injection techniques the neutral streaming always carry the particles in its direction whereas in the 3rd technique (Sec. 4.4.3), the flow is generated due to a sudden alteration in the confining potential and there are no streaming neutrals. But in all these three processes, the opposing force comes from a background of moving/stationary neutrals and as a result the dust particles ultimately attain a terminal velocity [136]. In our experiments, it is found that depending on the plasma and discharge parameters, the particles achieve terminal velocity after travelling a maximum distance of about 2 cms. Furthermore, the terminal velocity of the dust particles is dependent on the flow rate difference and background pressure of the neutrals.

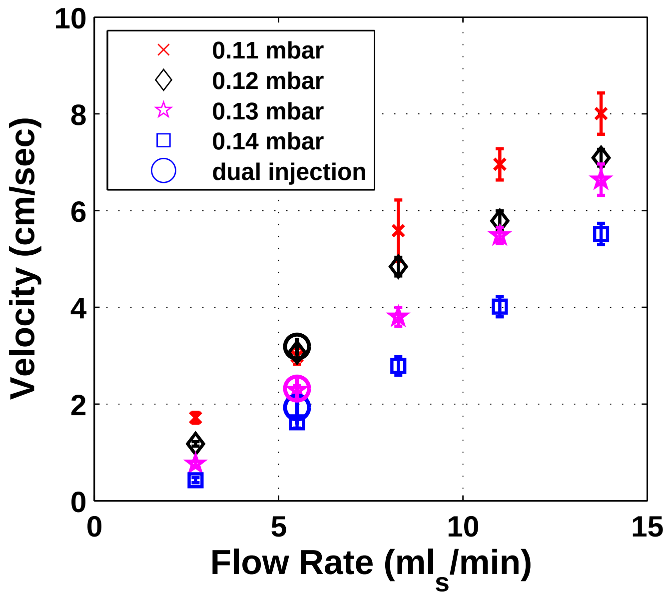

Figure 4.11: Variation of particle velocity with the difference of gas flow rate.

Fig. 4.11 shows the variation of the average particle velocity with the change of gas flow rate from the equilibrium conditions for four different background pressures. The average velocity is plotted in this figure when the particles achieve their terminal velocities. It is to be noted that the pressure mentioned here is the pressure just before disturbing the equilibrium condition. For a given value of neutral gas pressure (P = 0.110 mbar), the velocity increases almost linearly with the change of gas flow rate from the equilibrium condition. To validate our measurements, we have compared the velocity data taken from different flow generation techniques namely, single gas injection and dual gas injection method. We find excellent agreement between the particle velocities obtained by these two independent methods which is reflected from the overlapping of the data point 'o' (represents the dual injection) with the data points '$\star$', '$\square$', '$\diamond$' that corresponds the data taken from single gas injection method. Fig. 4.12 shows the variation of the terminal

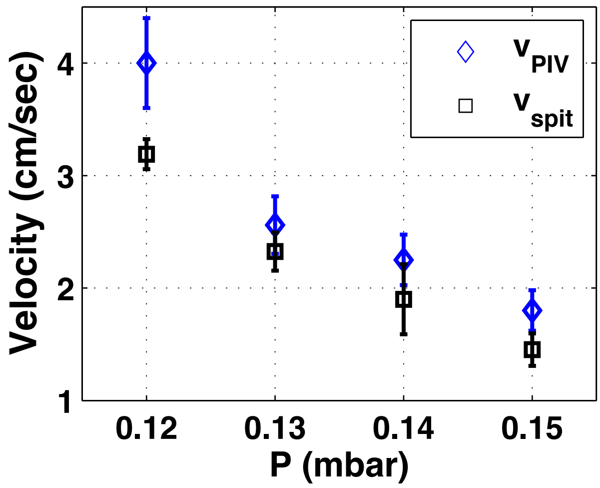

Figure 4.12: Variation of fluid flow velocity with neutral pressure. Blue diamond corresponds velocity measurement by sPIT code and black square corresponds the velocity measurement by PIV tools.

velocities with the background neutral gas pressure when the other discharge parameters are kept constant. Data point with '□' represents the sPIT data whereas the '◇' represents the PIV data. It is to be noted that the terminal velocity estimated by both the techniques decreases with the increase of gas pressure. Both the analyses of estimating the flow velocity give almost the same value except when the particle velocity increases (see the data points for $P = 0.12$ mbar). As we have discussed, the sPIT code becomes inefficient when the particle velocity becomes higher and this could be the reason why it gives a lower value of the terminal velocity at $P = 0.12$ mbar as compared to the PIV analysis. For other pressure regimes the measurements using both the techniques give almost comparable values, although PIV data always gives a slightly higher value of the terminal velocity compared to the values analysed using sPIT code.

4.7 Estimation of Neutral drag force

We now estimate the forces that are acting on the flowing dust particle using the measurement of the fluid velocity. In the first two experiments, the basic mechanism responsible for generating the dust fluid flow is the neutral gas streaming which always carries the particles along its direction. From the sPIT data analysis it is shown in Fig. 4.13, that

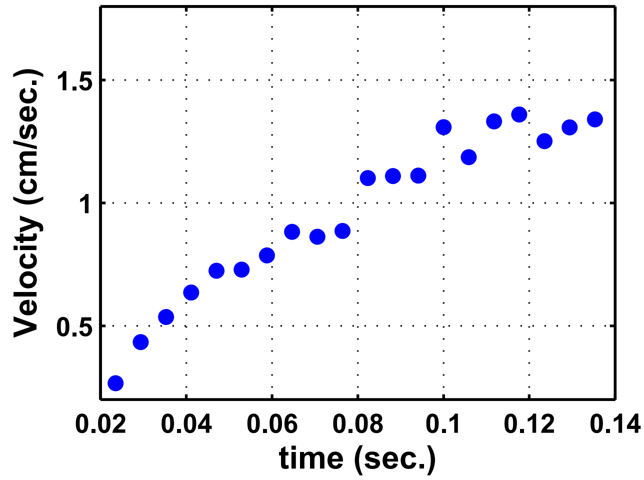

Figure 4.13: Change of the flow velocity with time for pressure (P) = 0.13 mbar, discharge voltage (V_d = 310 V) and for the flow rate difference of 2.75 ml_s/min.

the particles are initially accelerated towards the port P_1 from a steady state equilibrium position. After travelling a distance of less than about 1 mm, almost all the particles are found to attain a terminal velocity within about 100 msec due to the resultant opposing forces acting on them. The resultant force acting on the particles could be attributed due to electrostatic force, ion drag force or/and neutral drag force. In present set of experiments, the discharge is operated at a pressure where the neutral density is $10^5 - 10^6$ times more than the ion density. Hence, the ion drag force acting on the dust grains is considerably small compared to the neutral drag force [117]. To ascertain this we have estimated the ratio of the ion drag force to the neutral drag force [137] and found the neutral drag force to be always $\sim 10^3 - 10^4$ times higher than the ion drag force. A similar estimation has also been provided by Nakamura *et al.* [137]. From a detailed study on the variation of plasma and floating potentials at different discharge conditions [117], it is found that the axial component of electric field is very small and therefore the contribution of electrostatic force on the flow of dust particles can also be neglected. To verify this, an experiment is also performed to measure the flow velocity at different discharge voltages. It is observed that the particles changes only their equilibrium height with the voltages but the flow velocity remains unaffected. At the time when the particles acquire terminal velocity (U_t), the neutral drag force can be expressed as $F_{dn} = -\frac{4}{3}\gamma_{Eps}\pi r_d^2 m_n n_n V_{Tn} U_t$ [90], where, m_n, n_n, V_{Tn} and v_n are the mass, background density, thermal and drift velocities of the neutrals respectively. γ_{Eps} represents the Epstein drag coefficient which varies from 1 to 1.4 depending upon the types of reflection [51]. Therefore, the exact value of γ_{Eps} is essentially needed to find out the neutral drag force for our experiments. For the estimation of γ_{Eps}, we then calculate the slope ($\frac{dv}{dt}$) of the straight line of Fig. 4.13 till 80 msec and multiply it by the average mass of the dust particles ($m_d = 6.2 \times 10^{-13}$ kg for the dust particles of radius $\mathrm{r}_d = 4.59 \times 10^6$ μm) to get the accelerating force which is later equated with F_{dn}. For a given value of terminal velocity (in this present case it is $\sim$ 1.2 cm/sec) and plasma/dusty plasma parameters such as $m_n = 6.68 \times 10^{-26} kg$, $n_n = 2.7 \times 10^{21}$/m^3, $V_{Tn} = 427.7$ m/sec, γ_{Eps} comes out to be $\sim$ 1.07. With the help of γ_{Eps} and for a wide range of terminal velocities as shown in Fig. 4.12 the neutral drag force is estimated to be 1×10^{-13} N to 3×10^{-13} N.

4.8 Conclusion

In conclusion, we have presented and discussed a variety of experimental means of generating and measuring flows in a dusty plasma fluid. The techniques have been tested in a series of experiments carried out in the DPEx device for a dusty plasma of MF/kaolin particles embedded in a DC glow discharge Ar plasma. The initial steady state equilibrium dust cloud formed in a confining potential well by adjusting the pumping speed and the gas flow rate can be made to flow by using streaming neutrals introduced from single or duel gas injection ports or by suddenly lowering the confining potential. The resultant dust fluid velocity can be measured by using a sPIT code or a PIV analysis. Another novel way is by exciting DAWs - a technique that we have successfully tried out for the first time in our experiments. Each method has its strengths and limitations which we have pointed out on the basis of our experimental findings. We have also provided estimates of the terminal velocities that the dust component can acquire based on a theoretical evaluation of the neutral drag force that acts on the dust. These findings can be usefully employed to facilitate experimental explorations of linear/nonlinear wave and other phenomena associated with flowing complex plasmas which will be described in subsequent chapters.

Chapter 5

Excitation of Precursor Soliton

Surabhi Jaiswal, P. Bandyopadhyay and A. Sen, Phys. Rev. E, ***93****, 041201 (R) (2016)*

5.1 Introduction

The phenomenon of wave patterns generated by an object moving in a fluid have long been a classical topic of research both for its fundamental significance as well as for its numerous practical implications in oceanography, atmospheric dynamics and various other engineering applications [141–144]. A well known phenomenon is that of wakefields generated behind a moving object such as a boat traveling on a lake surface. An important question, that has received much attention in hydrodynamics, is what happens when the speed of the moving object approaches and crosses the phase speed of the characteristic linear mode of the medium. Theoretical and numerical studies [145–148] have shown that for speeds above this critical velocity the object generates not only wake patterns behind it but also radiates a steady stream of solitons ahead of it in the upstream region that move away from it at a faster speed. This type of solitons are known as *precursor solitons*. This fascinating phenomenon that has also been observed experimentally (using ship models moving in shallow channels) has been successfully modeled using nonlinear evolution equations like the forced Korteweg deVries (fKdV) equation or the forced Boussinesque equation [39, 149–152]. These precursor solitons are also seen to be excited if instead of moving the object the fluid is made to flow at a supercritical speed over a stationary object resting at the bottom of the fluid channel [39, 152].

Wakefield patterns also occur behind a charged object (particle) moving in a plasma medium [153–159]. An open and interesting question to ask is whether the phenomenon of precursor wave excitations can occur in a plasma? In a recent theoretical investigation [43] a model calculation predicts the excitation of precursor solitons in a plasma due to the passage of a charged object travelling faster than the ion acoustic velocity. However, to the best of our knowledge, there has so far been no experimental observation or demonstration of *precursor* solitons in a plasma medium although standard dust acoustic solitons triggered by short pulse excitations have been studied in a number of experiments [83, 84, 160–162]. The existence of upstream solitonic excitations could have wide ranging applications and also open up new areas of fundamental research in flowing plasma dynamics. Hence it is important to establish the experimental feasibility of such a phenomenon.

In this chapter we discuss the first experimental observation of precursor soliton in a flowing dusty plasma a spectacular phenomenon in hydrodynamics has surprisingly not been investigated in the plasmas as before. These wave patterns have been generated by a supersonic mass flow of dust fluid passing over an electrostatically biased object. In a frame where fluid is stationary and the hill is moving the solitons propagate in the upstream direction as precursors while wake structures consisting of linear DAWs are seen to propagate in the downstream region. A theoretical explanation of these excitations based on the forced Korteweg-de Vries model equation is provided and their practical implications in situations involving a charged object moving in a plasma are discussed.

The chapter is organized as follows. In the next section (Sec. 5.2), we review some earlier theoretical and experimental studies of precursor soliton and wake formation in fluids and plasmas. In Sec. 5.3, we describe the experimental arrangement briefly which has been used for the precursor soliton experiments. Sec. 5.4 is concerned with method to excite these nonlinear structures. Experimental findings are described in Sec. 5.5. The theoretical model for our experimental observation are given in Sec. 5.6. Finally, we conclude the whole chapter in Sec. 5.7.

5.2 An Overview of Previous Works

Various theoretical and experimental investigations on wave patterns formation ahead of moving object have been done in hydrodynamics. C. Katis *et al.* [145] in 1986 theoretically studied the three-dimensional wave pattern generated by a moving pressure distribution of finite extent acting on the surface of depth h_0. For a speed near the linear-long-wave speed they found that the response was governed by a forced nonlinear Kadomtsev-Petviashvili (KP) equation, which describes a balance between linear dispersive, nonlinear and three dimensional effects. Numerical solution based on the KP equation indicated that a series of straight-crested solitons were radiated periodically ahead of the source and three-dimensional wave pattern formed behind. They also compared the relation between width of soliton amplitude and period of soliton formation with the experimental observation of Ertekin, Webster and Wehausen (1984). Ertekin *et al.* [146] numerically investigated the flow created by an impulsively started pressure distribution travelling at a constant velocity in a shallow channel. They used Green-Naghdi theory of fluid sheets to perform the three dimensional calculations. Their calculations predicted the periodic generation of two-dimensional soliton in front of and travelling faster than the disturbance along with the doubly corrugated set of waves behind the disturbance if the disturbance was large enough. N. F. Smyth [147] theoretically studied the formation of these waves in two-dimensional shallow channel and found that these upstream waves become straight crested due to geometrical effects aided by the presence of side walls. In a combined experimental, theoretical and, numerical study by Seung *et al.* [150], phenomenon of forced generation of nonlinear waves by disturbances moving steadily with a transcritical velocity through a layer of shallow water was observed. They have conducted a series of experiments with a cambered bottom topography impulsively started from rest to a constant transcritical velocity U, the corresponding depth Froude number $F = U/(gh_0)^{1/2}$ being nearly the critical value of unity. They modelled the experiments with generalize Boussinesq equation and forced Korteweg-de Vries (fKdV) equation and found a broad agreement between theory and experiment, both in respect of the amplitudes and phases of the wave generated when the speed was nearly critical (0.9<F<1.1) and the forcing was sufficiently weak (the topography-height to water-depth ratio less than 0.15) to avoid breaking. In a combined theoretical and experimental study, Wu *et al.* [39] explored the formation of this fore-wake phenomenon in different scenario. They observed the

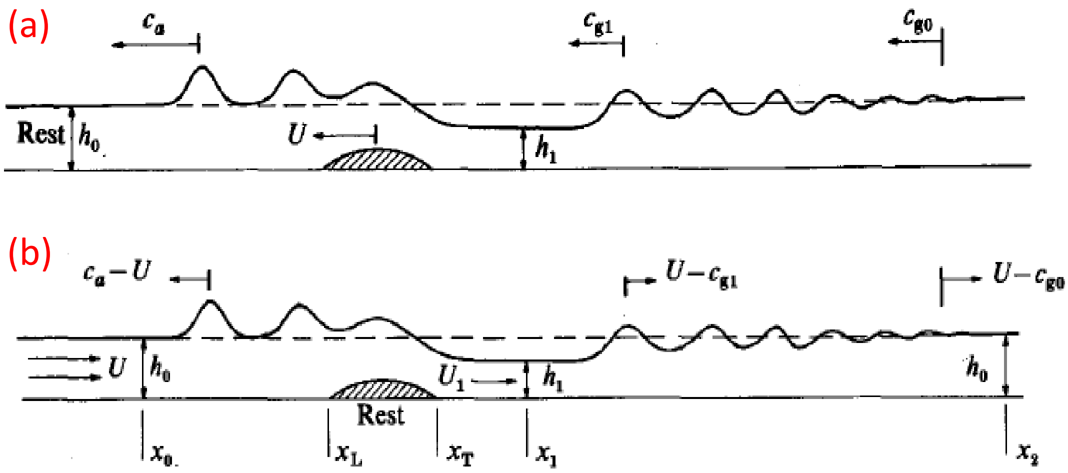

Figure 5.1: Illustration of transcritical water-wave problem: (a) an obstacle moving at constant transcritical velocity U in a uniform layer of water initially at rest; (b) obstacle fixed in a uniform stream of velocity U (see Wu *et al.*, Journal of Fluid Mechanics, 1987).

generation of wave pattern ahead of a body moves with supercritical speed in a shallow water channel which was stationary. In an alternate way they demonstrated that if instead of moving body, the stream of water flows over the object kept at rest then in that situation this kind of wave structure can be observed as shown in Fig 5.1(b).

In a plasma medium, a common occurrence of wake patterns generated behind an object were observed by several authors. Brattli *et al.* [155] observed wake pattern formed behind an electrically charged builder moving in plasma. It was found that when the speed of travelling object becomes supersonic the boundaries of wake were defined by a shock structure and the resultant trailing structure was called Mach cones. Hutchinson *et al.* [158] theoretically studied the formation of wake behind a spherical particle smaller than the Debye length in flowing plasma by using particle-in-cell code. Engwall *et al.* [156] observed the wake formation behind the positively charge space craft in flowing tenuous plasmas.

Very recently a forewake phenomenon i.e; the formation of precursor solitons was theoretically studied by few authors. In a theoretical investigation by Sen *et al.* [43], it was found that the forewake phenomenon existed ahead of charged object if the object travel faster than the ion acoustic velocity. Hutchinson *et al.* [163] theoretically studied the flow of magnetized plasma past an obstacle, and found that the obstacle created a traditional wake along with a forewake region from the shadowing of electrons. Sanat *et al.* [164] studied the phenomenon of precursor solitons and wakes in plasma by performing a MD simulation. However, there has not been any experimental observation on the formation of precursor soliton in the plasma medium reported till now thus it is necessary to facilitate an experiments to study this novel phenomenon which is associated with transcritical flows. This chapter is dedicated to discuss the first experimental observation of the formation and propagation characteristics of precursor soliton in a flowing dusty plasma.

5.3 Experimental Set-up and Operation

The experiments have been carried out in DPEx device which is described in detail in Chap. 2. For the excitation of nonlinear compressive modes along with the wake, some modifications have been made in the experimental arrangement as shown in Fig. 5.2. The electrodes geometry and their positions are similar to the previous arrangement whereas a couple of SS strips are placed approximately 25 cm apart on the cathode to confine the dust particles in the axial direction by means of their sheath electric fields. The reason for choosing this distance is to facilitate the formation of a long dense dust cloud in between these two strips and also to provide a sufficient space so that the dust fluid can be made to flow for a longer distance without any obstruction. In order to model the charge obstacle, a copper wire of 1 mm diameter, insulated to the cathode by ceramic beads, is mounted midway between these two strips at a height of 1 cm from the cathode. The wire can be kept either grounded or floating via a switch connected in between the wire and ground. A DC glow discharge plasma is produced between electrodes in a similar way as described in Chap. 3. To create the dusty plasma, micron sized kaolin particles (with a size dispersion ranging from 4 to 6 μm) are sprinkled on the cathode tray before closing the experimental device. The sheath formation over the wire creates a potential hill which act as an obstruction to the dusty plasma flow. The potential hill is used initially to confine the dust particles between the right SS strip and the wire as shown in Fig. 5.3 (a).

We have operated the device at a working pressure of $P = 0.090$ mbar and a discharge voltage of $V_d = 350$ V at which the discharge current is $I_d \sim 2\ mA$. At this discharge condition, a high density stable long dust cloud is formed over the cathode which is confined between the potential strips if the wire is kept on floating. It is occasionally seen that a spontaneous excitations of [118] dust acoustic waves (DAWs) is developed when the background pressure is below ~ 0.07 mbar. We therefore maintain our background pressure at ~ 0.09 mbar and above to inhibit such spontaneous excitations. We have also ascertained that the dust density does not influence the spontaneous excitation process by examining equilibria with different dust densities under the same discharge conditions and found no excitations even for low dust densities as long as the neutral pressure is maintained at ~ 0.09 mbar and above. Therefore at this particular discharge condition the dust cloud remain in equilibrium which is the demand of the present experiment. Plasma parameters are measured using single Langmuir and emissive probes (as described in Chap 3) and typical experimental values are plasma density $n_i \approx 1 \times 10^{14} m^{-3}$, electron temperature $T_e \approx 5eV$ and ion temperature $T_i \approx 0.03eV$. From the video images of the cloud the dust density is estimated to be $n_d \approx 1 \times 10^9 m^{-3}$. The average dust mass is $m_d \approx 1.7 \times 10^{-13} kg$ and the average charge on a dust particle is approximately $Q_d \approx 4.5 \times 10^4 e$. Based on

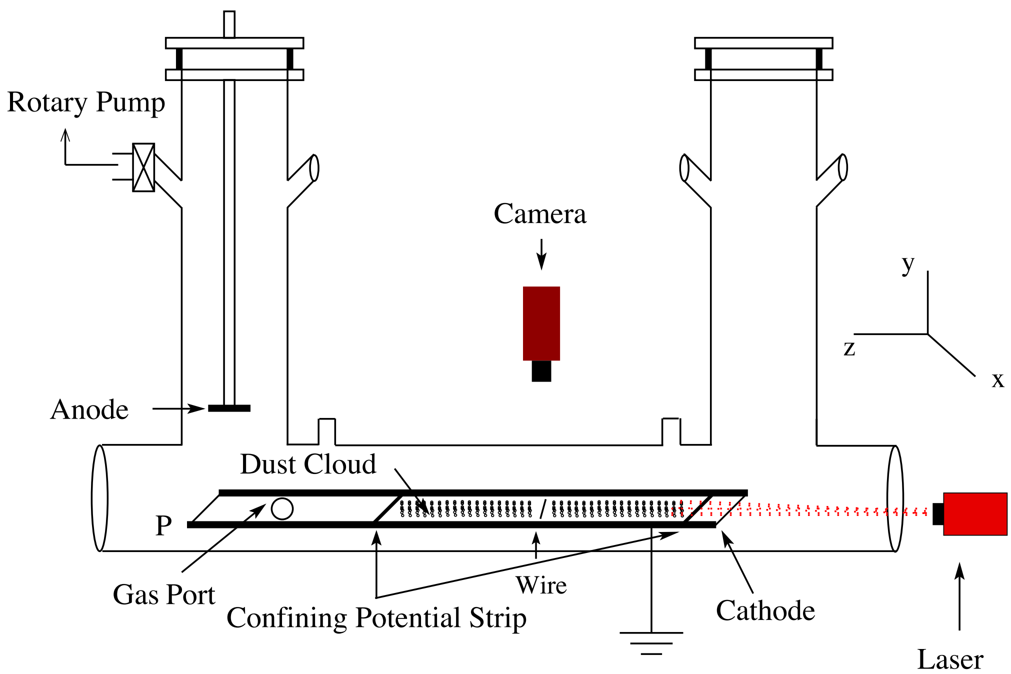

Figure 5.2: A schematic of the Dusty Plasma Experimental (DPEx) Device

these parameter values the typical magnitude of the linear phase velocity of a DAW turns out to be $v_{ph} \approx 2.4cm/sec$. Our estimated values of the dust charge and the phase velocity of DAW agree quite well with earlier investigations that were carried out in dusty plasmas with similar experimental parameters [71, 112]. We have also independently measured the phase velocity by analysing the propagation speed of spontaneously excited DAWs and obtained a value of $\approx 2.5cm/sec$ which is very close to the theoretically estimated value.

5.4 Method of Precursor soliton Excitation

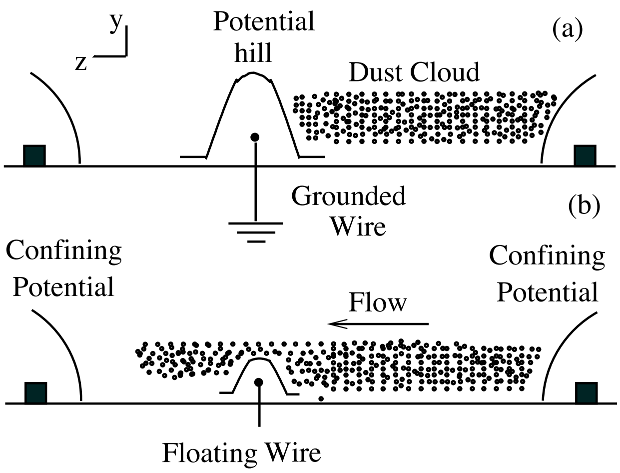

Figure 5.3: (a) Equilibrium dust configuration with the potential hill created by a grounded wire and b) dust flow induced by sudden lowering of the potential hill by a floating wire.

To initiate the flow in the present experiment, we follow the third technique of flow generation as described in Sec. 4.4.3 of Chap. 4. We start with an equilibrium of dust particles that are trapped between the right SS strip and the potential hill created by the grounded wire. This trapped stationary dust cloud is then made to flow from right to left by suddenly reducing the height of the potential hill above the wire and thereby removing the barrier that obstructs them from getting to the left half of the cathode region. Fig. 5.3(b) shows a schematic diagram of this situation when the height of the potential is reduced by removing the grounding from the wire and allowing it to have a floating potential. The height of the potential and hence the speed of flow of the particles, can be precisely regulated by drawing different amounts of currents from the wire using an external resistance. The flow speed of the dust cloud is determined by the amount of initial lowering of the height of the wire potential, the density of the dust particles and the magnitude of the neutral pressure in the chamber. In our experiment, we hold the dust density as well as the neutral pressure at constant values and change the flow speed by lowering the potential hill to different heights. Upon release from the potential barrier the flowing dust particles quickly attain a terminal velocity U_t due to the slowing down effect from the neutral drag force [117]. This velocity is found to remain uniform over a substantial region of the device till the time that the cloud runs out of dust particles. The fluid velocity is measured by analyzing a few successive frames of the video image near the copper wire by using the Particle Image Velocimetry (PIV) tool in the Matlab software package [139] which is discussed in detail in Chap. 4.

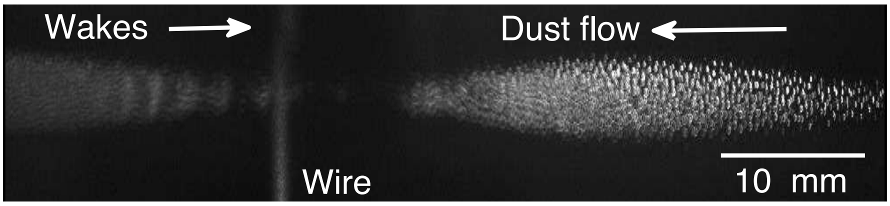

Figure 5.4: Generation of wakes due to the subsonic flow of the dust fluid over the wire.

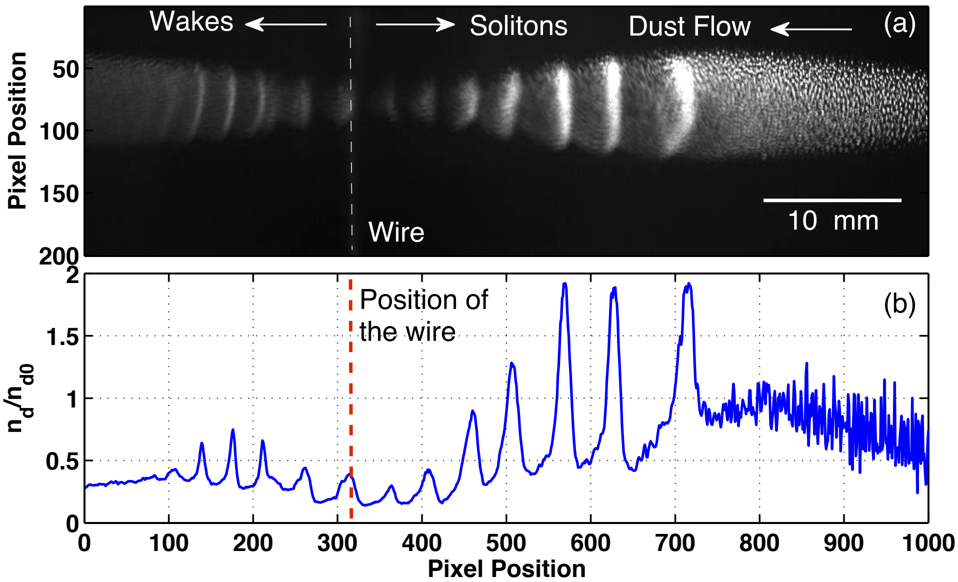

Figure 5.5: (a) An experimental image of the excited precursor solitons and small amplitude wakes. (b) The intensity profile of Fig 5.5(a).

5.5 Experimental Findings

Using the above technique we have made a number of experimental runs to study the flow induced excitations of the dusty plasma as it passes over the potential barrier. For flows that are slow compared to the DAW phase speed (subsonic) wakefields are excited in the left side of the wire travelling in the direction opposite to the flow. In the frame of the fluid where the hill is moving from left to right these wakefields are in the downstream region. The actual velocity of the wake is given by $U_t - v_{wm}$ where U_t is the flow velocity and v_{wm} is the measured velocity of the wake fronts [39]. A typical experimental image of a subsonic flow case is shown in Fig. 5.4 for $U_t \approx 1.8\ cm/sec$ and $v_{wm} \approx -0.5\ cm/sec$. These excitations thus travel at a speed of $U_t - v_{wm} \approx 2.30\ cm/sec$ which is close to the phase velocity of the linear DAWs. When the flow is made supersonic we notice a dramatic change in the nature of the excitations. In addition to the wake fields to the left of the wire we observe large solitary wave excitations to the right of the wire that travel in the direction opposite to the flow or in the frame of the fluid in the upstream direction of the moving potential hill. An experimental image of such excitations is shown in Fig. 5.5(a) for the case when fluid velocity $U_t \approx 2.65\ cm/sec$. The measured velocity of these structures is $v_{sm} \approx -1.5\ cms/sec$ and their actual speed after taking account of the flow is $v_s = U_t + v_{sm} \approx 4.15\ cms/sec$ which is about 1.6 times the DAW speed. Thus the speed of the flow (whether subsonic or supersonic) determines whether solitons are excited or not. Once the solitons are excited (for supersonic flow conditions) they continue to propagate at their characteristic nonlinear speed and the speed of the flow has no influence on their shape or propagation speed. The laboratory frame measurement of the speed of the soliton structure, v_{sm}, would however change if the flow speed changes in order to preserve the constancy of the soliton speed, namely, $v_s = U_t + v_{sm}$. As can be seen from Fig. 5.5(b), the space interval between successive solitons is nearly constant indicating that U_t is uniform over the region of propagation of the solitons. Note that since the flow velocity in this case is larger than the DAW speed the wake structures to the left of the wire are carried forward in the direction of the flow. Such excitations of precursor solitons and wakes have been observed over a range of supersonic values of the

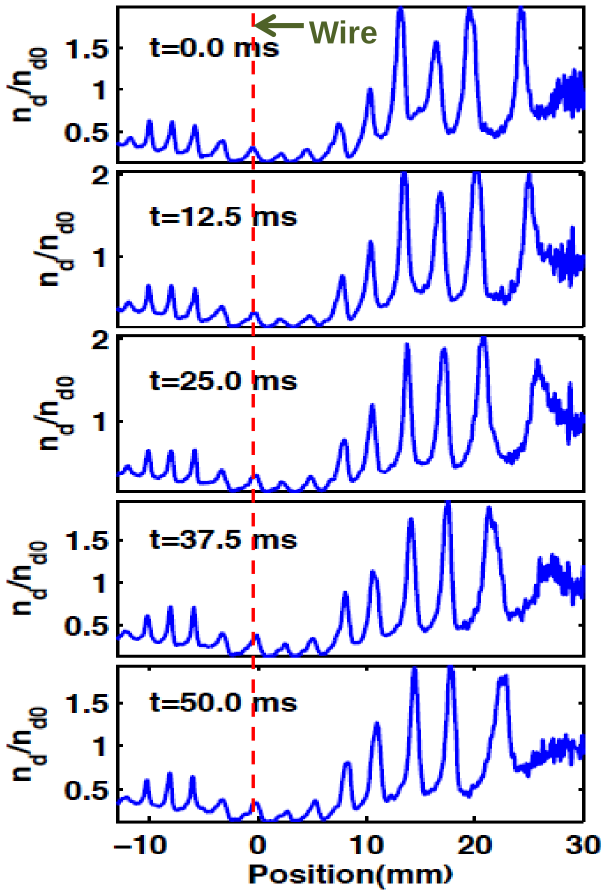

Figure 5.6: Time evolution of precursor solitons. The '0' position in the plot corresponds to the position of wire.

flow velocity and for various values of the dust densities resulting in solitons of varied amplitudes. It is also found that the precursor pulses are emitted in regular time intervals and keep growing in amplitude as they travel to the right till they attain a saturated amplitude value as can be seen in Fig 5.6. After attaining the saturation they travel faster than the dust acoustic speed. Furthermore, their speed also depends on the size of their amplitude - a property typical of KdV solitons [84]. These observations are consistent with theoretical predictions given by Sen *et al.* [43] for the charged moving object through a plasma medium.

5.6 Theoretical Model

To model our experimental observation we have derived a corresponding forced Korteweg-de Vries (fKdV) equation for the charged object moving subsonically or supersonically with respect to linear mode of the dusty plasma medium. To derive this equation we consider an unmagnetized weakly collisional dusty plasma consist of electrons, ions and negatively charged dust grains. The lighter electrons and ions are assumed to follow the Boltzmann distribution. The one dimensional fluid equations for dust dynamics are written as:

$$\frac{\partial n_d}{\partial t} + \frac{\partial}{\partial x}(n_d u_d) = 0, \tag{5.1}$$

$$\frac{\partial u_d}{\partial t} + u_d \frac{\partial u_d}{\partial x} = \frac{\partial \phi}{\partial x}, \tag{5.2}$$

$$\frac{\partial^2 \phi}{\partial x^2} - n_d - \alpha_e e^{\sigma\phi} + \alpha_i e^{-\phi} = S(x - v_d t) \tag{5.3}$$

where n_d, u_d are the density and velocity of the dust fluid respectively and ϕ is the electrostatic potential. α_e and α_i are the constants defined as $\alpha_e = n_{e0}/Z_d n_{d0}$ and $\alpha_i = n_{i0}/Z_d n_{d0}$ where Z_d the number of charge residing on the surface of the dust particles and $\sigma = T_i/T_e$. The term $S(x-v_d t)$ is the charge density source term arising from the charged object moving at the speed v_d from the frame of the fluid. The above equations have been normalized using:

$$x \to \frac{x}{\lambda_D}, \quad t \to t\omega_{pd}, \quad \phi \to \frac{e\phi}{k_B T_i}, \quad n_d \to \frac{n_d}{n_{d0}}, \quad u_d \to \frac{u_d}{C_D}.$$

where $\lambda_D = (k_B T_i/4\pi n_{d0} Z_d e^2)^{1/2}$ is the Debye length, $\omega_{pd} = \left(4\pi n_{d0} Z_d^2 e^2/m_d\right)^{1/2}$ is dust plasma frequency and $C_D = (Z_d k_B T_i/m_d)^{1/2}$ is the dust acoustic speed. Following standard reductive perturbation technique, we now expand the dependent variables in a power series in terms of a small expansion parameter ϵ which is a measure of the weakness of the amplitude or dispersion,

$$\begin{aligned}
n_d &= 1 + \epsilon n_d^{(1)} + \epsilon^2 n_d^{(2)} + \epsilon^3 n_d^{(3)} + O(\epsilon^4) \\
u_d &= \epsilon u_d^{(1)} + \epsilon^2 u_d^{(2)} + \epsilon^3 u_d^{(3)} + O(\epsilon^4) \\
\phi &= \epsilon \phi^{(1)} + \epsilon^2 \phi^{(2)} + \epsilon^3 \phi^{(3)} + O(\epsilon^4) \\
S(x - v_d t) &= \epsilon^2 S_2(x - v_d t)
\end{aligned} \tag{5.4}$$

defining the stretched coordinates,

$$\xi = \epsilon^{1/2}(x - v_{ph}t), \qquad \tau = \epsilon^{3/2}t \tag{5.5}$$

where v_{ph}[1] is the phase velocity normalized by C_D.The differential operators in terms of these stretched variable (Eq. 5.5) can be written as:

$$\frac{\partial}{\partial x} = \epsilon^{1/2}\frac{\partial}{\partial \xi}, \qquad \frac{\partial}{\partial t} = \epsilon^{3/2}\frac{\partial}{\partial \tau} - v_{ph}\epsilon^{1/2}\frac{\partial}{\partial \xi}. \tag{5.6}$$

In lowest order, equations (5.1) - (5.3) give

$$v_{ph}n_d^{(1)} = u_d^{(1)}, \qquad -v_{ph}u_d^{(1)} = \phi^{(1)}, \qquad -v_{ph}^2 n_d^{(1)} = \phi^{(1)}. \tag{5.7}$$

From above equation (Eq. 5.7), we get

$$v_{ph} = \frac{1}{\sqrt{Q}}. \tag{5.8}$$

The 2nd higher order of the equations (5.1) - (5.3) give

$$\frac{\partial n_d^{(1)}}{\partial \tau} - v_{ph}\frac{\partial n_d^{(2)}}{\partial \xi} + \frac{\partial u_d^{(2)}}{\partial \xi} + \frac{\partial}{\partial \xi}(n_d^{(1)}u_d^{(1)}) = 0, \tag{5.9}$$

$$\frac{\partial u_d^{(1)}}{\partial \tau} - v_{ph}\frac{\partial u_d^{(2)}}{\partial \xi} - \frac{\partial \phi^{(2)}}{\partial \xi} + u_d^{(1)}\frac{\partial u_d^{(1)}}{\partial \xi} = 0, \tag{5.10}$$

$$\frac{\partial^2 \phi^{(1)}}{\partial \xi^2} - Q\phi^{(2)} - n_d^{(2)} - \frac{R}{2}(\phi^{(1)})^2 = S_2 \tag{5.11}$$

where $Q = \sigma\alpha_e + \alpha_i$ and $R = \sigma^2\alpha_e - \alpha_i$. Using the above equations (5.7 - 5.11) we obtain the fK-dV equation,

$$\frac{\partial \phi^{(1)}}{\partial \tau} + A\phi^{(1)}\frac{\partial \phi^{(1)}}{\partial \xi} + B\frac{\partial^3 \phi^{(1)}}{\partial \xi^3} = B\frac{\partial S_2}{\partial \xi} \tag{5.12}$$

[1] $v_{ph}/C_D = Z_d\left(n_{d0}k_BT_i/n_{i0}m_d\right)^{1/2}/\left(Z_dk_BT_i/m_d\right)^{1/2} = (Z_dn_{d0}/n_{i0}) = \left(1 - \frac{n_{e0}}{n_{i0}}\right) \approx 1$ for $n_{i0} \gg n_{e0}$

with the coefficients

$$A = -\frac{v_{ph}^3}{(\delta-1)^2}\left[\delta^2 + (3\delta+\sigma_i)\sigma_i + \frac{1}{2}\delta(1+\sigma_i^2)\right], \qquad B = \frac{v_{ph}^3}{2}. \tag{5.13}$$

The equation 5.12 is known as fK-dV equation where $S_2(\xi + Ft)$ is the moving charged source term that is moving at a velocity v_d and $F = 1 - v_d$. In the absence of source term ($S = 0$) this equation simply becomes a well known KdV equation which is nonlinear through the convective term $\phi^{(1)}\frac{\partial\phi^{(1)}}{\partial\xi}$ and dispersive through the term $\frac{\partial^3\phi^{(1)}}{\partial\xi^3}$, widely used to describe the evolution of weakly nonlinear dispersive waves in a dusty plasma.

Table 5.1: Plasma and dusty plasma parameters

Parameters	Value
Electron Temperature (T_e)	$\approx$5 eV
Ion Density (n_i)	$\approx 1\times10^{14} m^{-3}$
Particle radius (r_d)	2-3μm
Dust mass density (ρ)	2600 kg/m^3
Dust Mass (m_d)	$\approx 1.7\times10^{-13} Kg$
Dust Density (n_d)	$\approx 1\times10^{9} m^{-3}$
Dust Temperature (T_d)	1-1.2 eV
Dust charge Number (Z_d)	$\approx 4.5\times10^4$
Theoretical acoustic velocity ($v_{ph_{cal}}$)	$\approx$ 2.4 cm/sec.
Experimental acoustic velocity ($v_{ph_{Exp}}$)	$\approx$ 2.5 cm/sec.

If the source is held stationary (as in the present experiment) then the fluid (plasma) moves in the opposite direction with speed v_d. The coefficient A (Eq.5.13) accounts for the change in the low frequency dynamics of the system as compared to the ion acoustic case [43] due to the involvement of the dust motion. A simple way to recover the form of the forced KdV for the ion acoustic case is to take the limit $\delta = \sigma_i = 0$ and replace n_{d1} by n_{i1}. The estimated value of coefficient A for our experimental parameter as given in Table 5.1 is 6.2. In deriving Eq. 5.12, we have neglected dust neutral collisional damping rate ν_{dn} of the solitonic solutions which can be calculated by using the standard formula, $\nu_{dn} = \frac{4}{3}\gamma_{Eps}\pi r_d^2 m_n n_n V_{Tn}/m_d$ [51]. For Ar gas of pressure $P = 0.090$ mbar, $m_n \sim 6.66\times10^{-26}$ kg, $n_n \sim 1.87\times10^{21}$m^{-3} and average neutral velocity $V_{Tn} \sim 428$ m/sec (assuming the gas temperature is 0.03eV). The Epstein coefficient (γ_{Eps}) is measured in our device as

$\gamma_{Eps} \sim 1.2$ [117]. Using all these parameters ν_{dn} comes out to be $\approx 9s^{-1}$. In the presence of damping the soliton energy decays as $e^{-\nu_{dn}t}$ while its amplitude and width scale as $e^{-2\nu_{dn}t/3}$ and $e^{\nu_{dn}t/3}$ respectively [83, 165]. For a soliton speed of $v_s \sim 4.15$ cm/sec, the damping length is therefore approximately $3v_s/2\nu_{dn} \sim 7$ mm which is about nine times larger than the width ($\Delta \sim 0.8$ mm) of the soliton. Hence to a first approximation one can neglect dissipative contributions [83] to Eq. 5.12. In our experiment we observe the development of a soliton to take place over an average distance of about 5 mm and its average propagation length without significant decay is about 9.5 mm as can be seen in Fig. 5.5 where the scale measure of 10 mm is clearly marked. Our model equation is therefore physically justified for describing soliton propagation over these distances. Over a longer time scale the calculated dissipation would lead to an exponential decay of the soliton amplitude and a broadening of its width. Fig. 5.7 shows typical time evolution

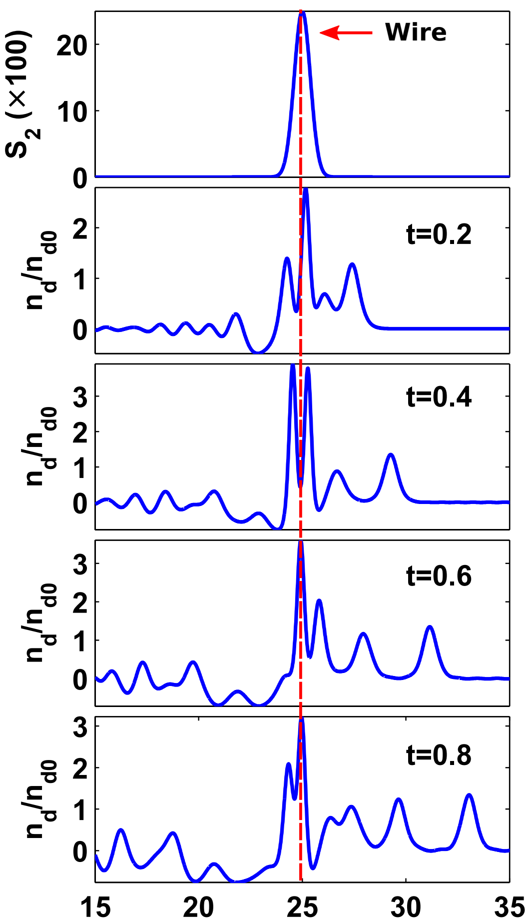

Figure 5.7: Time evolution of precursor solitons and wakes obtained from a numerical solution of the fKdV equation (5.12).

plots of n_{d1} for $v_d > 1$ from a numerical solution of Eq.(5.12) with a Gaussian source term S_2 to model the wire generated potential hill. To compare with the experimental observations the solutions have been plotted in the frame of the moving source which is now stationary at the point marked by the dashed line. As can be seen the source periodically excites solitons ahead of its path that travel away at a faster speed. Weaker excitations consisting of wakes are seen to emerge in the downstream direction. Thus the fKdV model provides a consistent description of our experimental observations. To further confirm the

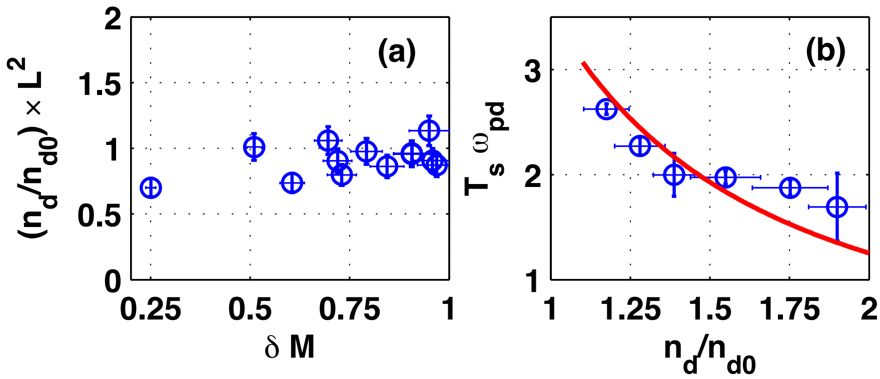

Figure 5.8: Variation of (a) soliton parameter (amplitude $\times$ width^2) with excess Mach number $\delta M = M - 1$ where the Mach number M is normalized to the dust acoustic wave speed and (b) time interval between the generation of two fully developed solitons with the amplitude. The solid line in Fig. 5.8(b) is a plot of the curve $T_s\omega_{pd} = \alpha/(n_d/n_{d0})^{3/2}$, where $\alpha = 3.54$.

consistency of our experimental findings with the model description we have carried out two more tests. A well known property of a KdV soliton is that the product of its amplitude with the square of its width is a constant quantity[2] [166]. This property also holds in the weakly dissipative limit where the decrease in the amplitude and broadening of the width due to dissipation are such as to still keep the product constant. In Fig. 5.8(a) we have plotted the measured value of this quantity for the solitonic structures of different sizes observed in our experiments. As can be seen this quantity is nearly a constant (of value close to unity) thereby confirming the KdV like solitonic nature of these excitations. The fKdV model also predicts a scaling law for the inter-solitonic intervals, namely, T_s[3] $\propto \phi_m^{-3/2}$ where T_s is the interval between generation of the solitons and A is the amplitude of the

[2]The amplitude and width of the soliton is related to the Mach number (M) as: $\phi_m = 3\delta M/A$ and $\Delta_s = \sqrt{4B/\delta M}$. Where, A and B are soliton constants and $\delta = n_{i0}/n_{e0}$. Hence $\phi_m \times \Delta_s^2$ is constant and does not varies with Mach number.

[3]$T_s \propto \Delta_s/M \Rightarrow 1/\sqrt{\phi_m}/\phi_m \Rightarrow 1/\phi_m^{3/2}$

soliton [39]. In Fig. 5.8(b) we have plotted the experimentally observed time intervals (normalized to the dust plasma frequency) against the soliton amplitudes (n_{d1}/n_{d0}) and the time intervals are seen to decrease monotonically with increasing amplitudes of the solitons. The solid curve is an analytic plot of the function $T_s\omega_{pd} = \alpha/(n_d/n_{d0})^{3/2}$ with $\omega_{pd} \approx 30Hz$, $\alpha = 3.54$ and serves as a visual aid to discern the trend in the data points.

5.7 Conclusion

In conclusion, we have experimentally demonstrated, for the first time, the existence of precursor soliton excitations in a plasma medium caused by a supersonic flow of the plasma over an electrostatic potential hill. The mechanism underlying the excitation of such solitons can be understood in terms of the following physical picture. When an object moves through a fluid at a subcritical (subsonic) velocity the build-up of the density perturbation in front of it is able to move away as linear waves traveling at the phase speed of the linear excitations of the medium. This leads to the formation of wake fields. However when the object speed is supercritical (supersonic) such a reduction of the density perturbation is not possible and as it starts to build up nonlinear effects begin to become important. It is this process that eventually leads to the formation of solitons i.e. when nonlinear effects are balanced by dispersion, and these structures now travel ahead of the moving body. We would like to emphasize that these solitonic excitations arising due to the interaction of a flowing plasma with a barrier are fundamentally different from past observations of standard dust acoustic solitons that are created by impulsive excitations of the plasma [83, 84, 160–162]. They also go beyond the usual wake field excitations seen behind a moving charged object in a plasma and are a distinctly *forewake* phenomenon analogous to that observed in hydrodynamic experiments and are associated with transcritical flows. Transcritical (supersonic) flows of plasmas can occur in many natural situations such as in astrophysical jets, solar winds etc. The encounter of such flows with a stationary charged object can recreate the situation discussed in our experiment. Likewise, instances of charged objects moving at supersonic speeds in a plasma are those of satellites (which naturally acquire surface charges) orbiting the earth in the ionospheric region, high energy ion beams impinging on targets in inertial fusion schemes etc. It would be interesting to look for precursor solitons in such situations since their presence can have significant practical implications. For example, in particle beam fusion applications they could impact the heating and or compression dynamics of the target pellet. In the satellite orbital regions above the earth, the detection of such solitonic excitations from charged debris objects could help provide an early warning scheme for satellites to avoid collisions with such objects [43]. The study of such precursor soliton excitations, which surprisingly has not received any attention so far in the plasma physics community, can open up new areas of experimental and theoretical research in the field and our present experimental investigations are a first step in that direction.

Chapter 6

Flow Induced Excitation of Shock waves

*S. Jaiswal, P. Bandyopadhyay and A. Sen, Phys. Plasmas, **23**, 083701 (2016)*

6.1 Introduction

An important and active area of research in flowing dusty plasmas pertains to the study of various nonlinear phenomena and their impact on the collective dynamics of the medium. A very important nonlinear phenomenon of precursor soliton formation in flowing dusty plasma has already been discussed in previous chapter (Chap. 5). Shock waves constitute an another very special class of nonlinear waves in the form of propagating discontinuous disturbances that are characterized by sharp jumps in velocity, pressure, temperature and density across a narrow front. They occur in a variety of neutral media such as in gases [167], fluids [168] and solids [169]. They have also observed in space during the early stages of strar fomation and the interaction of the magnetic fields of Earth and the solar wind. In plasma medium, the shock waves can be excited when a large amplitude mode propagates in the presence of strong dissipation such as due to collisions with neutrals, viscosity or Landau damping [170, 171]. The dynamics of shock waves have also been studied in complex (dusty) plasmas both theoretically as well as experimentally. In a weakly coupled dusty plasma kinematic viscosity [172] arising from dust-ion collisions and the presence of dust charge fluctuations [173] have been identified as two important dissipation sources contributing to the formation of shock waves. In a strongly coupled dusty plasma, on the other hand, the shear and bulk viscosities play an important role in the formation of monotonic and oscillatory dust acoustic shock waves [62, 174]. Usually, when an object moves through a stationary fluid with highly supersonic speed then shock waves get excited [164]. They can also be excited when a supersonically flowing fluid encounters a charged stationary object. While a rich literature available on the experimental study of shock waves formation by applying an external pulse, only a few experiments have been reported on the shock wave excitation in a flowing complex plasma for different experimental situation. In particular, there has not been any detailed experimental observation of flow induced excitation of dust acoustic shock waves and variation of their propagation characteristic as a function of different perturbation strength in terms of flow velocity and hill height. In this chapter, we report on neutral flow driven excitation and propagation characteristics of shock waves in a DC glow discharge dusty plasma.

The chapter is organized as follows. To lend some perspective to the present work, we review some of the relevant earlier works in the next section (Sec. 6.2). In Sec. 6.3 we describe the experimental arrangement used in this experiments and plasma generation. Sec. 6.4 is concerned with the excitation of shock waves and their propagation characteristic. The theoretical and experimental results are compared in Sec. 6.5. Finally, we conclude the whole chapter in Sec. 6.6.

6.2 An Overview of Previous Works

Shock waves in complex (dusty) plasmas were described theoretically as well as experimentally by different authors. Samsonov*et al.* [81] were the first to report an experimental observation of shock formation in a rf produced 3D complex plasma under microgravity conditions in the PKE-Nefedov device. In that experiment, a sudden gas pulse from an electromagnetic valve was used as travelling perturbation to excite the shock waves. Soon after, Fortov *et al.* [175] reported the propagation of compressional shock waves in a dusty plasma in which an impulse of axial magnetic field was used to excite the perturbation. Later in 2009, Heinrich*et al.* [109] observed the repeated occurrence of self-excited dust acoustic shock waves (DASWs) in a DC glow discharge dusty plasma by using high speed video imaging. The shocks were generated when the dust cloud was passed through two slits with a vertical separation of 1 cm. They observed the steepening of dust acoustic wave into a saw-tooth wave with sharp gradient in dust density while propagating away from the slits. Nakamura *et al.* [176] experimentally investigated the ion acoustic shock waves in dusty plasma. In that experiment, the shock waves were excited by applying a positive ramp voltage and they found that initially it became solitons when plasma contained no dust grains whereas became shock wave when dust was mixed with the plasma. They also observed that above a critical value of dust density it become a monotonic shock wave. Nakamura *et al.* [112] reported the experimental observation of two-dimensional bow shocks formation in a large area two-dimensional complex plasma system with a super-sonic flow of charged microparticles interacting with a stationary object. A thin conducting needle was used to make a potential barrier as an obstacle for the particle flow and flow was generated by changing the tilt angle of the device under gravitational force. The bow shocks was formed when the flow became super-sonic. Very recentally, Usachev *et al.* [177] experimentally investigated the formation and dissipation of an externally excited planer dust acoustic shock wave in a three-dimensional uniform dust cloud under the microgravity condition.

In all the above experiments, the shock wave had been excited by different method including electrical pulse, and magnetic field fluctuation. None of the above were included a flowing dusty plasma which is very close to the existing phenomenon occurred in nature such as shock formation during the early stages of star formation and in other various media. Nakamura *et al.* [112] and Heinrich *et al.* [109] were successfully conducted experiments where the the shock wave had been excited in flowing dust fluid but they did not have precise control over the flow and perturbation strength in their experiments. Additionally, they did not include a detailed characterization of such type of structure with the change of flow velocity of fluid and other plasma and dusty plasma parameters.

This chapter represents the first experiment on controlled observation of shock waves and its propagation characteristics with the change of flow speed and perturbation strength in terms of the potential hill height.

6.3 Experimental Set-up and Plasma generation

The similar experimental arrangement (as described in Chap. 5) is used to perform the experiment on flow induced excitation of dust acoustic shock waves. A copper wire of 1 mm diameter, insulated to the cathode by ceramic beads, is mounted in between the strips at a height of 1 cm from the cathode. Normally the wire is kept at floating potential but there is a provision to make the wire acquire a ground potential. In fact, we can adjust the potential of the wire to different potential levels by connecting variable resistors (arranged in a resistor bank) ranging from 10 kΩ to 10 MΩ in between the wire and ground (as shown in Fig. 6.1). To create the dusty plasma, micron sized kaolin particles (with a size dispersion ranging from 2 to 6 μm) acting as a dust are sprinkled on the cathode tray before closing the experimental device.

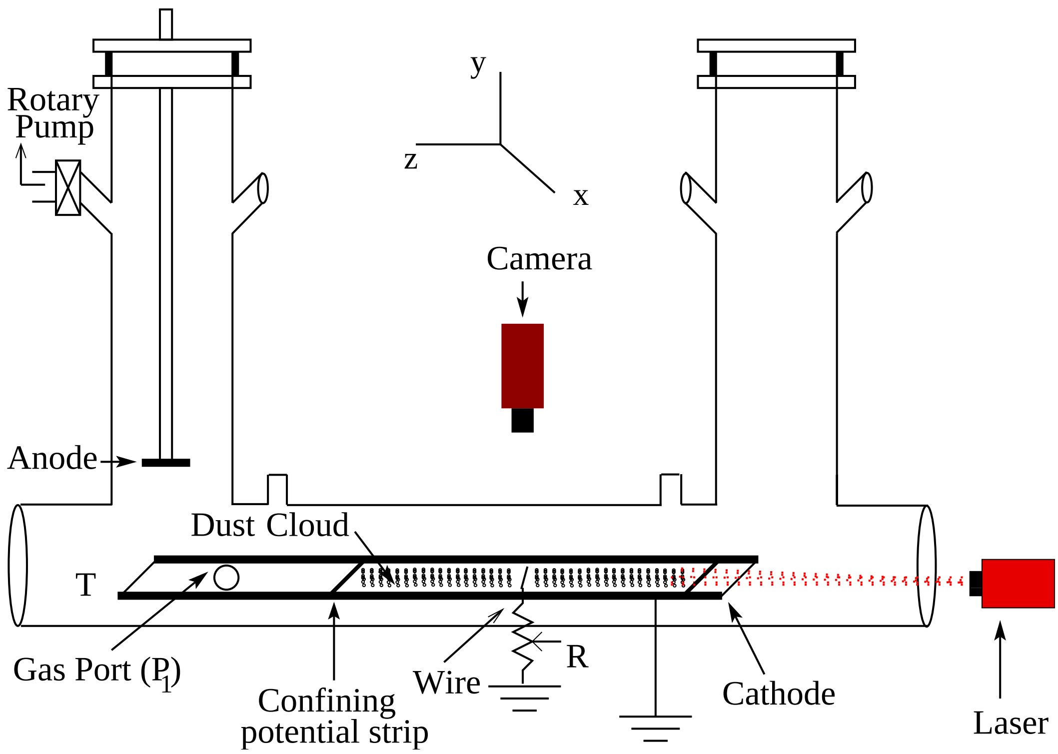

Figure 6.1: A schematic of the Dusty Plasma Experimental (DPEx) Device. T: grounded cathode tray, R: variable resistance to change the height of the potential hill.

The system is operated in a similar manner as described in previous chapters. The working pressure for this experiment is set to a pressure of $P = 0.110 - 0.120$ mbar by adjusting the pumping speed and the gas flow rate. In this condition, the gate valve

Table 6.1: Discharge and plasma parameters

Parameters	Values
Pressure (P)	0.10–0.120 mbar
Discharge Voltage (V_d)	360–370 Volt
Discharge current (I_d)	4 mA
Electron Temperature (T_e)	4-5 eV
Ion Temperature (T_i)	0.03 eV
Plasma Density (n_e)	$(1-3)\times 10^{15} m^{-3}$

(connected on the mouth of the pump) is approximately opened to 20% and the mass flow controller is opened to 10% (corresponding to flow rate of 27.5 ml$_s$/min) to maintain a constant pressure. A DC glow discharge plasma is then produced in between the anode and the grounded cathode by applying a voltage, $V_d = 400$ V. The applied voltage is reduced to $360-370$ V at a discharge current of $I_d \sim 4$ mA so that a stable dense dust cloud forms over the cathode at the cathode sheath boundary. A red diode laser along with the line generator is used to shine the levitated dust particles in X-Z plane. The dust dynamics are captured by a CCD camera (130 fps) with 1000 pixels $\times$ 225 pixel resolution. The single Langmuir probe and emissive probes are used to measure the plasma parameters in the absence of dust particles as discussed in Chap 2 and Chap. 3. For the present discharge condition, the discharge and plasma parameters are tabulated in the table 6.1.

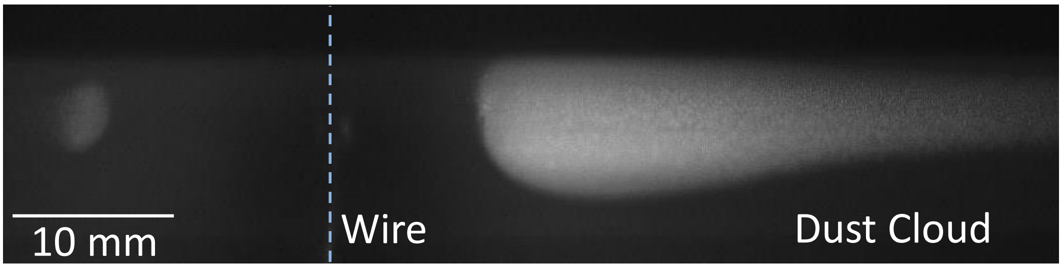

Figure 6.2: A stable dust cloud confined at right side of the wire. The discharge parameters are 370 Volt and 4 mA. The background pressure is P=0.11 mbar

For the given discharge voltage of 370 V, a dense stable dust cloud is found to levitate near the cathode sheath boundary (shown in Fig. 6.2) confined in between the wire and the potential strip placed on the right edge of the cathode. It is clearly seen from the Fig. 6.2 that there is no background oscillation exists in the cloud. The details of the criteria of existence of spontaneous oscillation is discussed in Chap.3. By using the techniques of density and temperature calculation of dust particles as discussed in Chap. 3, the dust density (n_{d0}) and temperature (T_d) are estimated to be $n_d \approx 10^{11} m^{-3}$ and $0.6 - 1.5$ eV. The average dust mass is $m_d \approx 10^{-14} - 10^{-13}\ kg$ and the average charge on a dust particle (inferred from the plasma parameters and the particle size) is approximately $Q_d \approx 10^4 e$. The electron density is obtained from the quasi-neutrality condition by taking account of the dust contribution. Based on these values the typical magnitude of the linear phase velocity of a dust acoustic wave (DAW) for our experimental conditions turns out to be $v_{ph} \sim 4 - 5$ cm/sec.

6.4 Excitation of Shock waves and their Propagation characteristics

For the flow generation we start with adjusting the pumping speed and the gas flow rate in a precise manner to achieve a stationary dust cloud in the region to the right of the wire mounted over the cathode. This equilibrium state is achieved at $\sim$ 10% opening of the mass flow controller and $\sim$ 20% opening of the gate valve. Now when we change the gas flow rate near the gas feeding port (P_1) as shown in Fig. 6.1, the particles are found to move either towards the direction of the pump (in case of decreasing flow rate) or away from the pump (in case of increasing flow rate). A detailed study on the flow generation techniques has been discussed in Chap.4. In the present set of experiments, the flow of the dust fluid over the wire is generated by reducing the gas flow rate in steps of 1% which corresponds to 2.75 ml_s/min.

The trapped stationary dust cloud is allowed to flow from right to left by reducing the neutral gas flow rate suddenly from its equilibrium condition for a time duration less than a second. When this change of background gas flow rate is relatively smaller (e.g. when the opening of mass flow controller changes from 10% to 5% or less), it is found that the dust fluid simply flows over the potential hill created by the floating wire with the grounded wire merely creating a hindrance in the path of the particle flow. A detailed discussion on the change of hill height with grounded and floating wire is given in Sec. 4.4.3 of Chap. 4. Fig. 6.3 depicts the flow of dust fluid over the floating wire in X-Z plane when

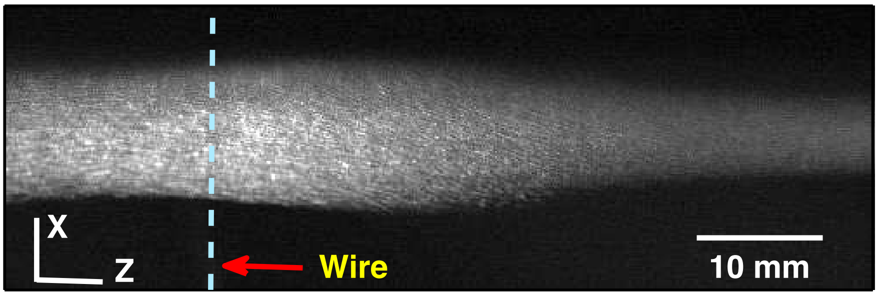

Figure 6.3: Dust fluid flow over the floating wire when the flow rate difference is 8%. Dashed line represents the location of the wire.

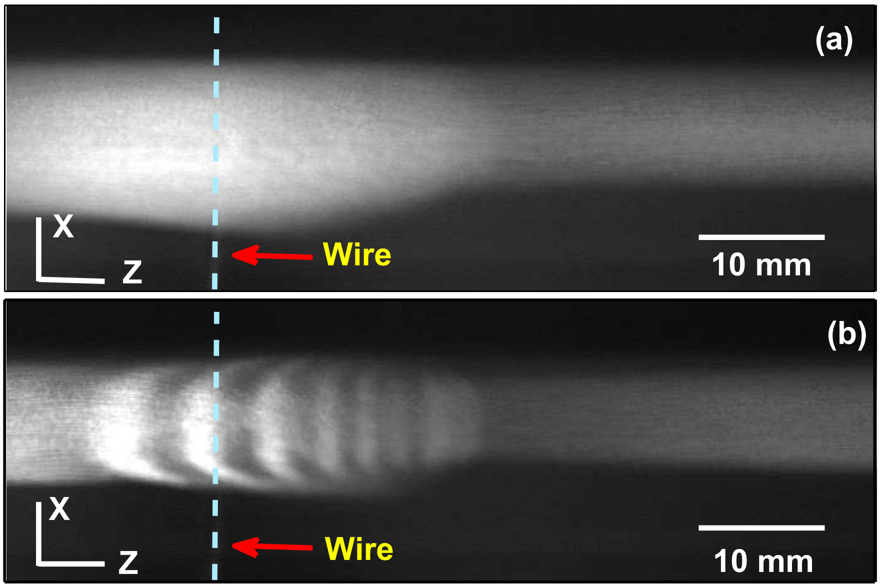

Figure 6.4: Typical image of (a) Transition stage and (b) Oscillatory shock wave fronts.

the background gas flow rate is changed from 10% to 2% (27.5 ml$_s$/min to 5.50 ml$_s$/min) in a time less than a second. The dashed line represents the location of the wire. Since the wire is at the floating potential, which is approximately equal to the surface potential of the dust, the dust fluid does not feel the presence of the wire and hence it simply exhibits streamline flow over the wire in the entire range of flow rate change.

To excite the dust acoustic shock waves [178, 179], the wire is kept at the ground potential. The sheath around the wire acts as a potential barrier (or hill) to the flowing dust fluid. The dust fluid is then forced to flow over the potential hill by reducing the gas flow rate suddenly from 10% (27.75 ml$_s$/min) to below 5% (13.75 ml$_s$/min) at point P_1. Due to the sudden decrease of neutral density at point P_1, the neutrals rush towards this point from all directions to attain a homogeneous equilibrium neutral density. As a result, the dust particles (carried by the neutrals) are also found to flow towards the pump with a supersonic velocity [117]. The potential hill created by the wire opposes the free motion of the particles, resulting in a compression of the dust cloud near its base. Consequently it leads to a sudden density jump near the wire which subsequently expands and form a shock that is found to propagate in the direction of the fluid flow. The transient stage of density accumulation is shown in fig. 6.4(a). Afterwords with the evolution of time, this transition is transformed into a dispersive dust acoustic shock waves (DASW) by the creation of compression and rarefaction in the dust density near the wire. Fig. 6.4(b) displays a typical image of the curved dispersive shock fronts. It is noted that along with the discharge voltage, the flow velocity of the fluid is also very important parameter for the generation of the structure. There exists a threshold (13.75 ml_s/min.) in the difference of gas flow rate below which the DASWs do not get triggered, because in that case, the fluid flow remains subsonic. The structure can be generated only when the flow become supersonic.

Fig. 6.5 shows the time evolution of a dispersive DASW. Fig 6.5(a) shows the real picture of the structure and corresponding intensity plot is shown in Fig 6.5(b). The dashed line in Fig 6.5(a) and ('0') position in Fig 6.5(b) represents the location of the wire. As discussed above, it can be seen from the figure that due to sudden jump of dust density near the wire (as seen from the first three curves of Fig. 6.5), a shock wave is generated and later (after $\sim$ 70 ms, although in the figure the time evolution is shown after 160 ms when the small fluctuations in the dust density fully converts into the shock fronts) a small oscillation develops near the base of the potential hill which grows with time and evolves into an oscillatory shock front. As a result, the pulse grows in amplitude as it propagates towards the wire and after crossing the wire the amplitude of the pulse decreases whereas the width increases. Depending upon the discharge condition and the change of gas flow rate the dispersive dust acoustic shock propagate with a velocity in the range of $10 - 20$ cm/sec.

In addition to the threshold in the flow rate, there is also a threshold in the height of the potential hill above which shock waves get triggered. Fig. 6.6 shows the flow of the dust fluid over the wire for different heights of the potential hill. A resistance bank of variable

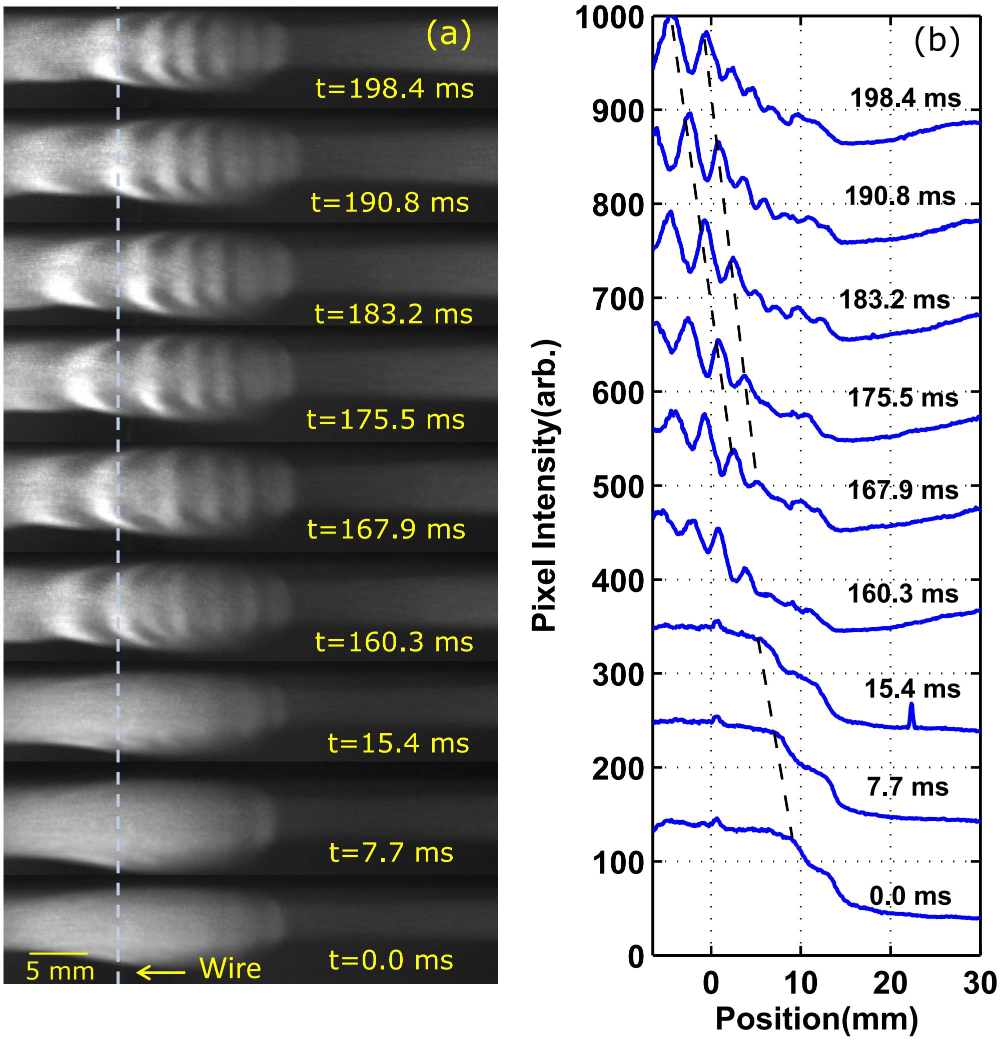

Figure 6.5: Time evolution of oscillatory dust acoustic shock fronts. a) the real picture, b) Corresponding intensity plot. The dashed ('0') position in the picture (plot) corresponds to the position of the wire connected to the ground.

resistance from 10 kΩ to 10 MΩ, connected between the wire and the ground, is used to change the height of the potential hill. By drawing current through different combinations of resistances one can change the height of the potential hill (V_{wg}). As is well known, dust particles at equilibrium do not draw a net current ($I_e = I_i$), which implies that they have nearly the same potential as that of the floating wire. Therefore, when the dust fluid flows over the floating ($V_f = V_{wp} \sim 250$ V) wire it barely feels the presence of a potential hill whereas it experiences the maximum obstruction from the potential hill when it flows over the grounded wire ($V_{wp} = 0$ V). Fig. 6.6(a) shows the excitation of shock waves when the potential of the wire is 3 V which is approximately the value of the ground potential. If the wire potential with respect to ground keeps on increasing towards the floating potential the

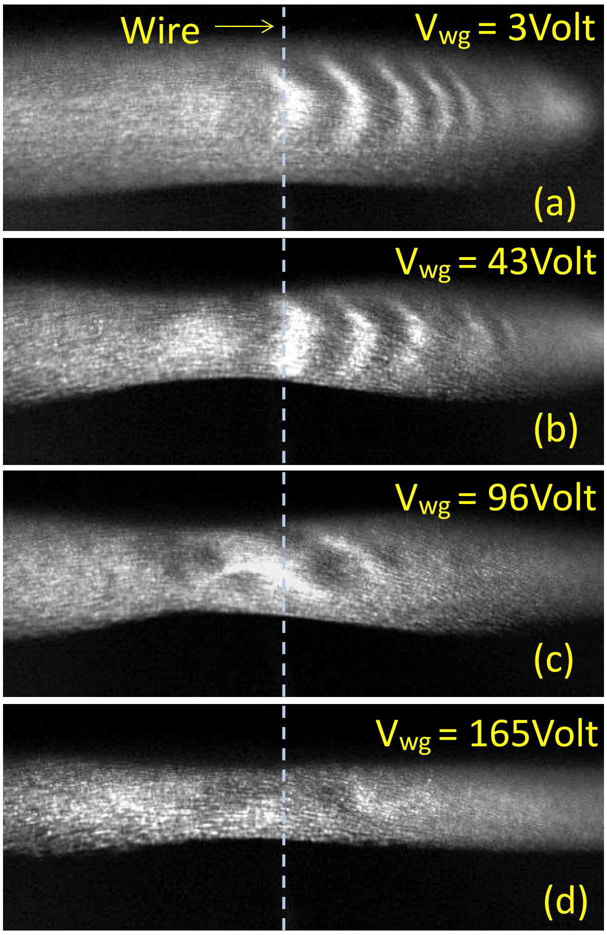

Figure 6.6: Images of shock waves for different values of potential hill for a) 3 Volt, b) 43 Volt, c) 96 Volt, d) 165 Volt. V_{wg} is the potential of the wire with respect to the grounded cathode. The dashed line is representing the position of the wire which acts as potential hill for the flow of dust fluid.

dust fluid faces a smaller and smaller hindrance in its path of flow. Fig. 6.6(b) shows that the number of shock fronts decreases (from five to three) with the decrease of the height of the potential hill. If we increase the wire potential further with respect to ground (hence decrease the height of the potential hill), we find a threshold value beyond which we could not excite DASWs. In our experiments the threshold value is found to be ~ 50 V. If the wire potential is increased further (see Fig. 6.6(c)), the structures becomes unstable and break up into turbulence. In Fig. 6.6(d), the potential of the wire is 165 V, which is quite far from the floating potential but sufficiently large such that potential hill over the wire is very small and therefore incapable of exciting shock waves. Consequently we observe an almost streamline motion of the dust particles over the wire. We have characterize the experimentally observed shock waves by measuring their amplitudes ($\Delta n_d/n_{d0}$) as well as the thicknesses (δ_w) of the leading pulses of dispersive shock fronts when the small fluctuations in the dust density are completely transformed into oscillatory shock fronts. These shock parameters are obtained by following the technique used by Heinrich *et al.* [109] and Annibaldi *et al.* [180]. The amplitude which is also proportional to $\Delta I/I_{avg}$ is calculated from the measured pixel intensities I, where ΔI $(= I_{max} - I_{avg})$ is the difference between the maximum intensity (I_{max}) of the leading shock front from its average value (I_{avg}). The shock thickness (δ_w) is defined as the difference between the steep edge point and the peak point of a crest. Fig. 6.7 shows the variation of amplitude (indicated by '$*$') and shock thickness (indicated by 'o') of oscillatory DASWs with position. The '0' level in the figure corresponds to the position of the wire which is taken as reference point for the propagation of dispersive dust acoustic shock waves (DASW). It can be seen in the figure that the shock amplitude follows approximately a linear decay whereas the thickness increases as the shock front propagates away from the wire. The amplitude fall off is a possible evidence of dissipation within the shock which is similar to that observed in the gas dynamic shocks and can be attributed to the effects of viscosity [81, 109].

6.5 Theoretical Model

To understand our experimental result, we have compared the evolution of experimentally observed large amplitude dust acoustic shock waves (DASWs) to an analytical solutions of a model Korteweg-de Vries-Burgers (K-dV-Burgers) type equation that is derived by

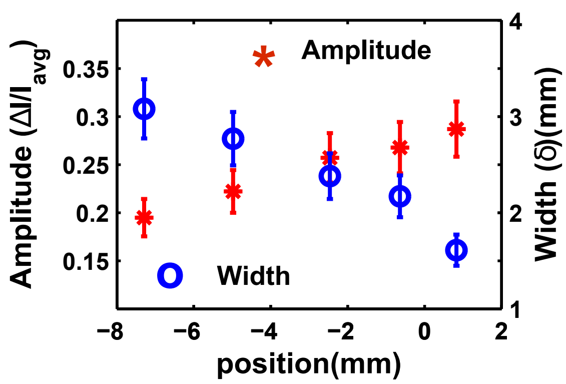

Figure 6.7: Variation of amplitude ($*$) and shock thickness (o) of a leading oscillatory shock front with position. In this set of experiments the change of flow rate is 19.25 ml/min.

Shukla and Mamun [62]. The equation is derived by using well known GH equation [181], which is valid for strongly coupled fluid state ($1 \ll \Gamma \ll \Gamma_c$) and provides a simple physical picture of strong correlation effect through the introduction of viscoelastic coefficients. For a weakly coupled plasma, the viscoelastic coefficient leads to viscous damping of the collective mode and for a strongly coupled plasma, the restoring force comes from elasticity. By using these equation, Shukla and Mamun showed that the nonlinear propagation of the dust-acoustic waves in a strongly coupled dusty plasma is governed by Korteweg-de Vries-Burgers (K-dV-Burgers) equation. The possible solutions of the K-dV- Burgers equation can be presented in terms of monotonic/oscillatory shock profile.

To derive such an equation, they consider an unmagnetized strongly coupled dusty plasma whose constituents are electrons, ions, and negatively charged massive dust grains. The charge neutrality condition at equilibrium for such a system is given by $n_{i0} = Z_d n_{d0} + n_{e0}$, where n_{i0}, n_{d0} and n_{e0} are the unperturbed ion, dust, and electron number densities, respectively, and Z_d is the number of charges residing on the dust grain surface. The lighter ion and electron species can be described by Boltzmann distributions at temperatures T_i and T_e respectively and are coupled weakly to each other due to their higher temperatures and smaller electric charges. The dust grains of mass m_d, on the other hand, are strongly coupled to each other because of their lower temperature (T_d) and larger electric charge ($Q_d = Z_d e$). In a weakly collisional dusty plasma ($\nu_{dn}\tau_m \to 0$), the generalized hydrodynamic (GH) equations for the dynamics of the nonlinear DAWs in such a strongly coupled dusty plasma are given by,

$$\frac{\partial n_d}{\partial t} + \frac{\partial}{\partial x}(n_d u_d) = 0, \tag{6.1}$$

$$D_t u_d + \nu_{dn} u_d - \frac{\partial \phi}{\partial x} = \frac{\eta_l}{n_d}\frac{\partial^2 u_d}{\partial x^2}, \tag{6.2}$$

$$\frac{\partial^2 \phi}{\partial x^2} = n_d + \alpha_e e^{\sigma\phi} - \alpha_i e^{-\phi}. \tag{6.3}$$

where n_d is the instantaneous dust density normalized by its equilibrium value n_{d0}, u_d is the dust fluid velocity normalized by the dust acoustic speed $C_d = (Z_d T_i/m_d)^{1/2}$, ϕ is the electrostatic wave potential normalized by T_i/e. The constants quantities are defined as, $\alpha_e = n_{e0}/Z_d n_{d0}$, $\alpha_i = n_{i0}/Z_d n_{d0}$ and $\sigma = T_i/T_e$. The time and space variables

Table 6.2: Dusty plasma parameters

Parameters	Values
Dust particle radius (r_d)	1-3 μm
Dust mass density (ρ)	2600 kg/m^3
Dust mass (m_d)	$(1-30)\times 10^{-14}$ Kg
Inter particle distance (d)	$100-170$ μm
Dust density (n_d)	$(5-30)\times 10^{10} m^{-3}$
Particle temperature (T_d)	$0.6-1.5$ eV
Dust charge (Q_d)	$1-4\times 10^4 e$
Coulomb coupling parameter (Γ)	$50-110$
Ion thermal velocity (V_{Ti})	$300-500$ m/sec
Dust neutral collision frequency (ν_{dn})	$11-20$ Hz
Plasma Debye length (λ_{Di})	$40-60$ μm
Dust Debye length (λ_D)	$35-55$ μm
Theoretical acoustic velocity ($v_{ph_{cal}}$)	6 cm/sec
Experimental acoustic velocity ($v_{ph_{Exp}}$)	5.2 cm/sec

are in units of the dust plasma period $\tau_{pd} = (m_d/4\pi n_{d0} Z_d^2 e^2)^{1/2}$ and the Debye length $\lambda_D = (T_i/4\pi Z_d n_{d0} e^2)^{1/2}$, respectively and $D_t = \partial/\partial t + u_d \partial/\partial x$. Furthermore, ν_{dn} is the dust-neutral collision frequency normalized by the dust plasma frequency τ_{pd}^{-1} and τ_m is the relaxation time. The normalized longitudinal viscosity coefficient can be expressed as, $\eta_l = (\tau_{pd}/m_d n_{d0} \lambda_D^2)[\eta_t + (4/3)\zeta_t]$, [62] where η_t and ζ_t represent shear and bulk viscosities.

Using the plasma and dusty plasma parameters mentioned in tableřeftab5:tab2, the screened Coulomb coupling parameter, $\Gamma = \frac{Q_d^2}{4\pi\epsilon_0 d k_B T_d} exp(-\kappa)$ [182], is estimated as ~ 109 for a screening parameter of $\kappa = d/\lambda_{Di} \sim 3.9$, where $d \sim 168$ μm is the inter-particle distance, $T_d = 1.2$ eV and $\lambda_{Di} \sim 43$ μm is the ion Debye screening length. To derive the K-dV-Burgers equation, we have used the reductive perturbation technique with the stretched coordinates

$$\xi = \epsilon^{1/2}(x - v_{ph} t), \tag{6.4}$$

$$\tau = \epsilon^{3/2} t. \tag{6.5}$$

where ϵ is the smallness parameter measuring the weakness of the amplitude or dispersion and v_{ph} is the wave phase velocity (normalized by C_d). In the expansion of variables n_d, u_d

and ϕ, we include the equilibrium flow velocity (i.e. the terminal velocity [117]) of fluid U_t at the equilibrium condition in accordance with our experiments. Then, the variables about the unperturbed state in power series of ϵ can be expanded as

$$n_d = 1 + \epsilon n_d^{(1)} + \epsilon^2 n_d^{(2)} + ..., \tag{6.6}$$

$$u_d = U_t + \epsilon u_d^{(1)} + \epsilon^2 u_d^{(2)} + ..., \tag{6.7}$$

$$\phi = \epsilon\phi^{(1)} + \epsilon^2\phi^{(2)} + ..., \tag{6.8}$$

$$\eta_l = \epsilon^{1/2}\eta_0. \tag{6.9}$$

where η_0 is the kinematic viscosity [62].

Substituting Eq. (6.4)-(6.9) into Eq. (6.1)-(6.3), we obtain from the equation of the lowest order in ϵ,

$$u_d^{(1)} = \frac{-\phi^{(1)}}{(v_{ph} - U_t)} \tag{6.10}$$

$$n_d^{(1)} = \frac{-\phi^{(1)}}{(v_{ph} - U_t)^2} \tag{6.11}$$

$$v_0 = U_t + \frac{1}{(\sigma\alpha_e + \alpha_i)^{1/2}}. \tag{6.12}$$

From the next higher order of ϵ, we have

$$\frac{\partial n_d^{(1)}}{\partial \tau} - (v_{ph} - U_t)\frac{\partial n_d^{(2)}}{\partial \xi} + \frac{\partial u_d^{(2)}}{\partial \xi} + \frac{\partial}{\partial \xi}\left[n_d^{(1)} u_d^{(1)}\right] = 0, \tag{6.13}$$

$$\frac{\partial u_d^{(1)}}{\partial \tau} - (v_{ph} - U_t)\frac{\partial u_d^{(2)}}{\partial \xi} - \frac{\partial \phi^{(2)}}{\partial \xi} + u_d^{(1)}\frac{u_d^{(1)}}{\partial \xi} = \eta_0\frac{\partial^2 u_d^{(1)}}{\partial \xi^2}, \tag{6.14}$$

$$\frac{\partial^2 \phi^{(1)}}{\partial \xi^2} = n_d^{(2)} + (\sigma\alpha_e + \alpha_i)\phi^{(2)} + \frac{1}{2}(\sigma^2\alpha_e - \alpha_i)\left[\phi^{(1)}\right]^2. \tag{6.15}$$

Using the expressions obtained from the first order calculation in Eq. (6.13)-(6.15) and by eliminating $n_d^{(2)}$, $u_d^{(2)}$ and $\phi^{(2)}$, we readily obtain the K-dV-Burgers equation:

$$A^{-1}\frac{\partial \phi^{(1)}}{\partial \tau} + \phi^{(1)}\frac{\partial \phi^{(1)}}{\partial \xi} + \beta\frac{\partial^3 \phi^{(1)}}{\partial \xi^3} = \mu\frac{\partial^2 \phi^{(1)}}{\partial \xi^2} \tag{6.16}$$

where the constants are give by the following expressions,

$$\begin{aligned}
\delta &= -\frac{3}{(v_{ph}-U_t)^4} - \sigma^2\alpha_e + \alpha_i \\
A &= \delta(v_{ph}-U_t)^3/2 \\
\mu &= \eta_0/[\delta(v_{ph}-U_t)^3] \\
\beta &= 1/\delta
\end{aligned}$$

It is very important to be noted that for a weakly coupled or collisionless dusty plasma ($\nu_{dn}\tau_m \to 0$), $\delta < 0$, which corresponds to A< 0, $\mu < 0$, and $\beta < 0$.

To obtain a stationary solution of the K-dV Burgers equation we further transform to a frame defined by $\zeta = \xi - U_0\tau$, and $\tau = \tau$. Eqn.(6.16) can then be integrated once and converted to,

$$\beta\frac{\partial^2\phi^{(1)}}{\partial\zeta^2} - \mu\frac{\partial\phi^{(1)}}{\partial\zeta} + \frac{1}{2}[\phi^{(1)}]^2 - \frac{U_0}{A}\phi^{(1)} = 0 \tag{6.17}$$

where we have imposed the appropriate boundary conditions, ie; $\phi^{(1)} \to 0, d\phi^{(1)}/d\zeta \to 0, d^2\phi^{(1)}/d\zeta^2 \to 0$ at $\zeta \to \infty$. A monotonic shock wave is formed when the dissipation term (second term of Eqn.(6.17)) dominates over the dispersion term (first term of Eqn.(6.17)). In this case the solution of Eq. (6.17) can be expressed as :

$$\phi^{(1)} = \frac{U_0}{A}\left[1 - \tanh\left(\frac{U_0}{2A\mu}(\xi - U_0\tau)\right)\right]. \tag{6.18}$$

where, U_0, $\phi_0 = U_0/A$ and $\Delta = A\mu/U_0$ are the speed, height and thickness of the shock fronts, respectively. It is worth mentioning that for a given μ, if the amplitude of the shock front decreases the shock thickness increases and vice versa. It is also to be noted that if μ is extremely small, the shock will have an oscillatory profile in which the first few oscillation at the wave front will be close to a solitonic form [174]. There exists a critical value of dissipation coefficient μ that determines whether a monotonic or an oscillatory shock solution [62] is formed. This critical value of μ, as determined from the theoretical model, is $\mu_c = (4\beta U_0/A)^{1/2}$. The shock wave has a monotonic profile for $\mu^2 > \mu_c^2$ and an oscillatory profile for $\mu^2 < \mu_c^2$. For $\mu^2 < \mu_c^2$, the oscillatory solution is given as

$$\phi^{(1)} = \varphi + C\exp\left(\frac{Z\mu}{2\beta}\right)\cos\left(Z\sqrt{\frac{U_0}{A\beta}}\right) \tag{6.19}$$

where, $Z = \xi - U_0\tau$ and C is a constant. It should be noted here that for a weakly collisional dusty plasma ($\nu_{dn}\tau_m \rightarrow 0$), we have $\delta < 0$, which corresponds to A< 0, $\mu < 0$, and $\beta < 0$.

For the completeness of this study, we now make an attempt to compare qualitatively the results obtained in experiments with the analytical results we get by solving the the KdV-Burgers equation. For this comparison, the experimentally measured plasma and dusty plasma parameters are used to estimate the constants associated with KdV-Burgers equation. For the given values of discharge and plasma parameters in our experiments, the coefficients of KdV-Burgers equation come out to be $\delta = -1.36$, $A = -0.85$, $\beta = -0.73$ and $\mu = -0.12$. The kinematic viscosity at $\Gamma \sim 109$ is taken as $\eta_0 = 0.2$ [183] as in the experiments of Nakamura *et al.* [176]. This highly viscous dusty plasma fluid (due to the strong coupling between the particles) provides necessary dissipation in the medium to form stable shock fronts. As the magnitude of fluid velocity determines the strength of the perturbation in the dust medium, hence this flow also plays an important role to determine the shape and size of the shock structure. The analytical solutions (Eq. 6.19) of KdV-Burgers equation for $U_t = 8$ cm/sec at $\eta_0 = 0.2$ is plotted in Fig. 6.8(a). It shows the oscillatory shock fronts appear when there is a sudden jump of perturbed dust density. Similar trend of shock fronts have also been observed in our experiments (as shown in Fig. 6.8(b)) when the background intensity is subtracted from raw data. In addition, it is also found that when the fluid flow is increased further (not shown in the figure), the velocity as well as the amplitude of the shock waves increase whereas the width decreases which essentially shows a clear signature of nonlinearity in the structure. This amplitude-width relationship is also revealed from experimental observation which is shown in the Fig. 6.7.

The above agreement in the nature of the experimental observations and the theoretical results suggests that the Generalized-Hydrodynamic model [181] is able to capture the

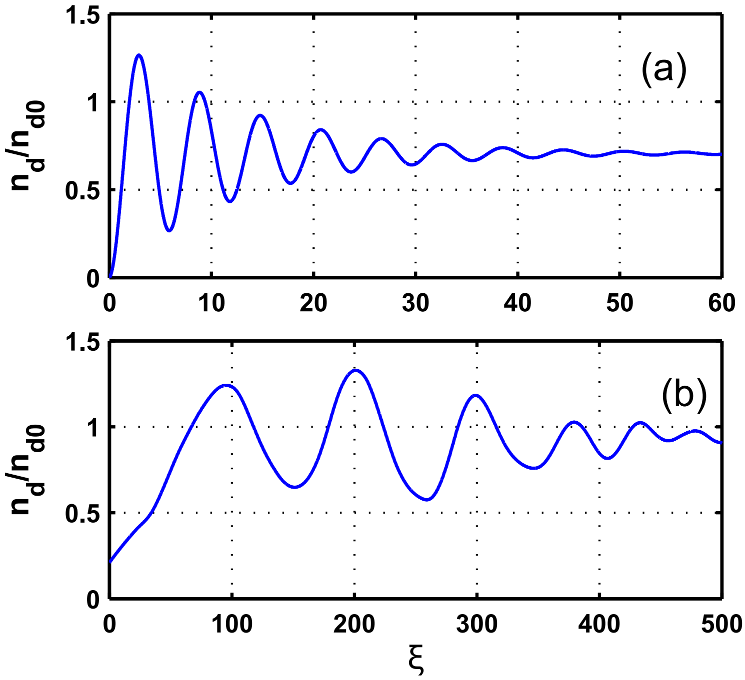

Figure 6.8: Nature of shock waves find a) theoretically and b) experimentally. The analytical results are plotted for fluid velocity 8 cm/sec and $\eta = 0.2$.

essential underlying dynamics governing the formation of these shock structures both in terms of the existence and observed trend in the variation of the amplitude and thicknesses of the shock structures. The model however falls short of providing an accurate quantitative measure of the shock thickness - the experimental values are about 5 to 10 times higher than the theoretical values. This mismatch indicates that some additional dissipation processes other than the dissipation due to strong correlation between the particles could be playing a role in the experimental situation and needs to be incorporated in the model. Since in our experiments we excite the shock waves by introducing a strong neutral gas flow, this additional dissipation could come from dust-neutral collisions which have been neglected in the model. The shock thickness in such a case can be approximately equal to the dust-neutral collision mean free path [81, 109] and can be defined as $\delta_w = \lambda_{dn} = U_t/\nu_{dn}$. The dust-neutral collision frequency (ν_{dn}) can be obtained from the standard relation for the Epstein [51] drag. For a pressure of 0.12 mbar and dust radius $r_d = 2\ \mu m$, ν_{dn} turns out for for our experimental conditions to be $\sim 18 s^{-1}$. The typical shock thicknesses, based on the above parameters, are then found to be $\delta_w \sim 3.6$ mm for $U_t = 6.5$ cm/sec which is quite close to the experimental values shown in Fig. 6.5 and Fig.

6.7.

6.6 Conclusion

In this chapter, we have experimentally demonstrated the formation of dispersive shock waves in DPEx device by generating a flow of dust fluid over a grounded wire. The flow of dust fluid is initiated by sudden reduction of mass flow rate of neutral gas. This instantaneous change of flow rate creates a dust density jump near the potential hill, created by the grounded wire. Eventually this jump of density propagates in the form of oscillatory shock fronts. The propagation characteristics of these oscillatory shock structures have been characterized thoroughly by varying the strength of the potential hill and the gas flow rate at a constant discharge parameters. It is found that the amplitude of the shock fronts decays whereas the shock thickness increases when it propagates away from the wire. The nature of shock waves become turbulent through a intermediate state when the height of the potential hill reduces to a small value (i.e., when the potential of the wire changes from being grounded to being floating). It is also observed that there exists a threshold of the height of the potential hill below which the shock waves could not be excited.

A Generalized Hydrodynamic equation has been used to model the experimental observation of shock formation by accounting for the effect of dust-dust interaction in the form of viscosity and to derive a KdV-Burgers equation including the effect of flow velocity. This model explains qualitatively the formation of shock waves and the changes in its nature with the change of flow velocity. Moreover, the model also validates the variation of experimentally obtained amplitude and width of shock fronts. An effect of dust-neutral collision is also introduced to delineate the exact dissipation mechanism. Our experimental observation of shock formation in a flowing dusty plasma besides providing insights into the nonlinear dynamics of complex plasmas, can also be of potential value in understanding shock phenomena in space plasmas such as during solar wind interactions with the earth as well as in astrophysical scenarios where shock waves are a common occurrence in galactic dust clouds during the early stages of star formation.

Chapter 7

Summary and Future Scope

7.1 Summary

The primary focus of this thesis has been on the experimental studies of flow induced excitation of nonlinear waves and structures in dusty plasmas. In particular the investigation is concentrated on the excitation of precursor soliton and shock waves by a plasma flow supersonically over a charged stationary obstacle. Surprisingly this topic has not received much attention in plasma physics community and problem of precursor excitations in a flowing plasma has remained an open and relatively unexplored area of research although various investigations has been done in the hydrodynamics. We have investigated these open problems and experimentally explored the possibility of observing such phenomena in a controlled laboratory situation. The nature and conditions governing the existence of such nonlinear structure in plasmas, besides being of fundamental scientific importance, can also help provide insights into nonlinear events happening in many real life situations.

The experiments have been carried out in a newly built table top Dusty Plasma Experimental (DPEx) device [117]. The device has been commissioned and is operational at the Institute for Plasma Research. The unique feature of the device is its ability to induce a flow in the dust component in a controlled manner by adjusting the vacuum pumping speed and the gas flow rate of the device. The device consist of Π-shaped glass tube of 65 cm length, 30 cm height and 8 cm diameter. The glass tube facilitates the easy viewing and optical measurement of the dust dynamics from any side of the experimental chamber. For various experimental convenience, it is divided into two parts namely experimental part and service part. The experiments are performed into the experimental part which is the horizontal portion of the Π-tube whereas two vertical sections which constitute the service part are intended for pumping, gas inlet, anode connection and for venting the system. A rotary pump is used for the evacuation of the vacuum vessel and mass flow controller is used to introduced the gas into the vessel in a precisely controlled manner and to manipulate the dust particles by changing the gas flow rate. A stainless steel (SS) disc covered with ceramic from back side is used as anode and a SS long tray placed inside the experimental part of the vessel is used as a cathode. Various stainless steel strips of different dimensions placed over the cathode provides the radial and axial confinement to the dust particles. In some of the experiments at single particle level, a mono-dispersive Melamine Formaldehyde (MF) particle of different sizes are used as dust particles which are introduced into the plasma by using a dust dispenser mounted over the experimental part of the chamber. In rest of the experiments at fluid level, micron sized poly-dispersive kaolin (hydrated aluminum silicate) powder are used as dust particles which simply sprinkled over the cathode before closing the device.

A DC glow discharge plasma is produced between the disc shaped anode and grounded cathode by applying a high voltage DC in the background of Ar gas. Couple of electrostatic probes namely, Langmuir probes and emissive probes are used to measure the plasma parameters *viz.*, the plasma density, the electron temperature, the floating potential, the plasma potential and the electron energy distribution function in the absence of dust particles. The plasma density is found to be of the order of 10^{15} m^{-3}, whereas the electron temperature is varied from 2 eV to 5 eV for a range of discharge voltages between 250 to 350 V and working pressure between 0.1 and 0.2 mbar. The plasma density increases and temperature decreases with the increase of neutral gas pressure and discharge voltage. This suggests that the sheath thickness over the cathode decreases with the increase of discharge voltage and background pressure. The plasma and floating potential increases with the increase of the discharge voltage and decreases with the increase of neutral gas pressure although the change is not significant.

A dusty plasma is formed by introducing the micron sized dust particles that get charged by collecting ions and electrons and levitated in cathode sheath boundary. The vertical component of the cathode sheath electric field provides the necessary electrostatic force to the particles to levitate against the gravitational force field. The radial and axial sheath electric fields due to bent edges of the cathode and the strips are responsible for the radial and axial confinement of the dust particles against their mutual Coulomb repulsive force. The equilibrium dust cloud is formed by adjusting the pumping speed and gas flow rate. A set of optical instruments such as combination of red or green diode laser and line generator are used to illuminate axial length of the experimental chamber to view the complete dust cloud, and couple of CCD cameras of high (low) speed and of low (high) resolution are used for imaging the dust dynamics of the dust cloud as well as the single dust particles from top and side of the experimental part. Parameters like dust density, inter-grain spacing, dust temperature and Coulomb coupling parameters are estimated over a wide range of discharge parameters from the consecutive frames of the images. Analysis of the images are made using IDL based super Particle Identification and Tracking (sPIT) code, MATLAB based open source Particle Image Velocimetry (PIV) and ImageJ software. The dusty plasma is characterized over a wide range of discharge parameters. It is observed that, the pair correlation function changes its nature with the change of background pressure and several peaks are observed for 0.14 mbar whereas a single peak followed by 2^{nd} and 3^{rd} peak are observed in the case of 0.11 mbar. It shows that the dusty plasma are in fluid regime at lower pressure. The inter-particle distance, calculated from the first peak of the pair-correlation function, comes in the range of $500 - 160$ μm whereas dust density varies from $(0.5 - 6) \times 10^{10}/m^3$ for the range of discharge voltage and background pressure. The highly charged dust particles are influenced by a small sheath electric field and as a result the dust particles acquires a finite temperature in both axial and radial direction. Dust temperature is estimated from the mean velocity of the particles from consecutive frames. It is found that the dust thermal velocity and temperature decreases with the increase of background gas pressure due to enhancement of the dust neutral collisions. The Coulomb coupling parameter (Γ) calculated over the range of discharge parameters is in the range of $80 - 220$ for a range of background pressure of 0.1-0.15 mbar. It suggests that we have a dusty plasma in a strongly coupled fluid regime upto pressure 0.12 mbar whereas it arranged in ordered structure on and above to 0.14 mbar.

Different techniques of flow generation and tools to measure the flow velocity in DPEx have been explored and establish for flow induced excitations experiments [184]. The initial steady state equilibrium dust cloud is formed in a confining potential well by adjusting the pumping speed and the gas flow rate. The equilibrium dust cloud are made to flow by reducing or inducing neutrals from single gas injection or dual gas injection ports. In both of the techniques neutrals streaming plays an important role to initiate the flow of the dust cloud. In an alternate way, the equilibrium dust cloud is formed in between the confining potential strip placed at the right edge of the cathode and a potential hill formed over a biased wire which is placed in between the two confining strips placed over the cathode. The trapped stationary dust cloud is made to flow by switching the grounded wire to the floating potential (i.e. by reducing the potential hill over the wire). In the single gas injection method the particle velocity can be raised upto 20-25 cm/sec. In this method the equilibrium state is disturbed momentarily. In the dual gas injection method the equilibrium can be maintained during the entire duration of flow of particles. In the altering potential method, one could achieve only modest values of induced flow velocities. The dust fluid velocity is measured by using a sPIT code and a PIV analysis. Another novel way is by exciting DAWs - a technique that we have successfully tried out for the first time in our experiments. Each method has its strengths and limitations which we have pointed out on the basis of our experimental findings. The dust flow in our experiment is seen to initially depend on the position, time, discharge parameters and the gas flow rate. However, the dust particles/fluid attains a terminal velocity which is independent of the spatial location and time. It is found that the terminal velocity increases linearly with the increase of the gas flow rate but decrease with the increase of neutral gas pressure due to frequent dust-neutral collisions. The neutral drag force which is responsible for the achievement of the terminal velocity and, the Epstein drag coefficient are estimated from the initial acceleration of the particles. In our experiment, the Epstein drag coefficient varies from 1 to 1.4 [51] and neutral drag force are estimated to be 1×10^{-13} N to 3×10^{-13} N. These findings are further employed to facilitate experimental explorations of linear/nonlinear wave and other phenomena associated with flowing complex plasmas.

After establishing the various means of flow generation and tools to measure the flow velocity, we have carried out experiments on the wave excitation in flowing dusty plasma medium. In the first set of experiments, we have experimentally demonstrated, for the first time, the existence of precursor soliton excitations in a plasma medium caused by a supersonic flow of the plasma over an electrostatic potential hill [185]. They also go beyond the usual wake field excitations seen behind a moving charged object in a plasma and are a distinctly *forewake* phenomenon analogous to that observed in hydrodynamic experiments and are associated with transcritical flows. The experiment has been performed at a discharge voltage of 340-350 V with the working pressure of P=0.09 mbar with kaolin particles (with a size dispersion ranging from 4 to 6 μm) as a dust component. For flow generation the third technique discussed above has been used, namely, a potential hill created by a wire mounted on the cathode has been used to induce dust flow by a sudden change in the hill height [184]. The flow velocity has been controlled by changing the hill height. It is found that whenever the mass flow over the electrostatic potential hill is supersonic nonlinear solitary dust acoustic waves (DAWs) are excited. In the frame where the fluid is stationary and the hill is moving the solitons are found to propagate ahead of it in the upstream direction as precursors while wake structures consisting of linear DAWs are seen to propagate in the downstream region. The solitary structures are seen only for supersonic flows and up to an upper limit of flow. For flows that are slow compared to the DAW phase speed and hence subsonic, only wakes are excited in the downstream direction. We have also made a detailed characterization of these nonlinear structures by plotting the variation of the parameter consisting of the product of the soliton amplitude and the square of its width with the Mach number and found it to be nearly constant - a property characteristic of KdV solitons. It is also found that the the time interval between generation of two such solitons (T_s) varies inversely with the 3/2 power of the amplitude i.e. $T_s \propto A^{-3/2}$ - which is in agreement with theoretical results obtained from a solution of a forced KdV equation for precursor solitons [39, 43].

In the next set of experiments, we have experimentally investigated the formation of flow induced dispersive dust acoustic shock waves (DASW) and its propagation characteristic by generating a dust fluid flow over a stationary biased object with very high velocity (high Mach number of M>2) [186]. In this experiment, a potential hill created by the copper wire placed over the cathode acts an obstruction for the dust fluids. The potential hill height can be varied by connecting it to a variable resistor ranging from 10 kΩ to 10 MΩ. The equilibrium dust cloud has been formed in a DC glow discharge plasma at a discharge voltage of $V_d = 360 - 370$ V and neutral pressure of P=0.11-0.12 mbar at a discharge current of $I_d \sim 4$ mA. A sudden reduction of mass flow rate of the neutral gas has initiated the flow of dust fluid. This instantaneous change of the flow rate creates a sudden density jump near the base of the potential hill and hence trigger the onset of high velocity dust acoustic shocks whose dynamics has been captured by fast video pictures of the evolving structures. The physical characteristics of these shocks have been delineated through a parametric scan of their dynamical properties over a range of flow speeds and potential hill heights. It has been found that a threshold in the difference of gas flow rate exists below which the DASWs do not get triggered. Similarly, there is also a threshold in the height of the potential hill above which shock waves get triggered. Also the shocks are not excited whenever the wire is kept on a floating potential as the particles then did not feel the presence of the wire (the surface potential of the dust is always close to the floating potential). The observed evolution of the shock waves and their propagation characteristics are found to compare well with model numerical results based on a modified Korteweg-de-Vries-Burgers type equation [62]. The effect of dust-neutral collision has also been considered in accounting for the underlying dissipation mechanism [109]. These finding besides providing insights into nonlinear phenomenon in complex plasma, can also be of potential value in understanding the shock formation in various astrophysical situation.

7.2 Future Scope

The experimental studies of the present thesis can form the basis for further in-depth investigations of flow induced nonlinear wave patterns and structures in dusty plasmas and can motivate new theoretical, experimental or simulation studies. Below we discuss a few possible future directions of research in this area:

- A study of the flow past an obstacle with different sized obstacle and their influence on the flow of fluid is another interesting extension of our work that can be usefully carried out. The Renold's number varies with the variation of flow velocity and obstacle size which is the important parameter for the investigation of laminar flow and its transition to turbulent regime. Thus a precise experiment with the variation in fluid velocity and obstacle size is need to be carried out.

- We have experimentally investigated the phenomenon on precursor soliton excitation in weakly coupled dusty plasma. One can extend this work by performing a controlled experiment with variation of coupling parameter Γ and their effect on the formation of such nonlinear structures. A controlled variation of Γ is of course a challenging experimental task particularly close to the phase transition region.

- Our experimental results for the excitation of precursor soliton do not agree very well with fK-dV soliton solutions quantitatively particularly the amplitude and width variation. It would be useful to attempt theoretical extensions of the fK-dV model with higher nonlinearities and other effect such as charge fluctuation and examine the possibility of understanding the deviations on the basis of such a theory.

- One can extend the flow experiments with smaller inter-particle gap between the particles and look on the impact of neutral gas or ion flow perturbation or wakes on the motion of nearby particles.

- In our experiments we did not calculate the neutral drag force for different particle size and different gases. The particle material and neutral gas species affect the Epstein coefficient and the neutral drag on the dust particles.

Appendix A

Physical mechanism of scaling law for inter-solitonic generation time and amplitde

From am arbitrary Gaussian shaped density lump of amplitude ϕ_m, different solitons emerge by steepening, getting the effect of dispersion and separation of the soliton from the rest of the density lump and so on till one soliton emerges and a second one is forming by fresh steepening. The typical time taken for the emergence of the soliton is

$$T_s = \frac{\Delta_s}{v} \tag{A.1}$$

where, Δ_s and v is the width and velocity of solitary pulse respectively. From the KdV equation, the multiplication of amplitude and width can be written in terms of the Mach number $\phi_m = 3\delta M/A$, $\Delta_s = \sqrt{4B/\delta M}$. Thus,

$$\phi_m \times \Delta_s^2 = \frac{3\delta M/A}{4B/\delta M} = 3/4AB \tag{A.2}$$

Since A and B are a constant quantity thus multiplication of the amplitude and square of the width is a constant. Thus, $\Delta_s \propto 1/\sqrt{\phi_m}$. From equation A.1 we get

$$T_s \propto \frac{\frac{1}{\sqrt{\phi_m}}}{\phi_m} \qquad \Rightarrow T_s \propto 1/\phi_m^{3/2} \tag{A.3}$$

Appendix B

Dust-acoustic waves

Dusty plasma has ability to support new low frequency waves mode. One of the simplest wave is Dust Acoustic Wave (DAW). To solve the dispersion relation for DAW, we consider a plasma which consists of electrons, ions, dust and neutrals. T_i , T_e and T_d are temperature of ions, electrons and dust particles. We also consider that the neutrals are cold so their thermal velocity are very small with compare with the others species. As dust are massive particles with compare with the electrons and ions. So we can consider that the electrons and ions are follows Maxwell-Boltzman's distribution

$$n_e = n_{e0} \exp\left(\frac{e\phi}{kT_e}\right) \tag{B.1}$$

$$n_i = n_{i0} \exp\left(\frac{-e\phi}{kT_i}\right) \tag{B.2}$$

Where n_{e0} and n_{i0} are the electron and ion density far away from the charged particles.

To derive the dispersion relation we used the fluid and Maxwells equations.If we consider that the thermal energy of the electrons and ions are very high than the interaction potential energy then from the Maxwell-Boltzman relation we will get as

$$n_{e1} = n_{e0} \frac{e\phi}{kT_e} \tag{B.3}$$

$$n_{i1} = -n_{i0} \frac{e\phi}{kT_i} \tag{B.4}$$

And Fluid equations for dust particle with the condition that $T_d = 0$ is

$$\frac{\partial n_{d1}}{\partial t} + n_{d0}\nabla \cdot \vec{u_d} = 0 \tag{B.5}$$

$$\frac{m_d \partial \vec{u}}{\partial t} + (\vec{u} \cdot \nabla)\vec{u} = q_{d0}\vec{E} \tag{B.6}$$

If we consider the linearized form of the above equation then we may neglect the second term of the left hand side of the momentum equation. After neglecting the second term of the above equation we will get

$$\frac{\partial \vec{u}}{\partial t} = \frac{q_{d0}}{m_{d0}}\vec{E} \tag{B.7}$$

Finally we have Poisson's equation. And the form of the Poisson's equ is

$$\nabla \cdot \vec{E} = \frac{(en_{e1} - q_{d0}n_{d1} - en_{i1})}{\epsilon_0} \tag{B.8}$$

Let us consider simple wave solution that means small amplitude sinusoidal. So, the perturbed quantity ϕ , v_d n_d all are varies as exponential like $e^{i(kx-\omega t)}$. So we can express all the equation in terms of algebraic form by fourier trick like $\frac{\partial}{\partial t} = -i\omega$ and $\nabla = ik$. Thus from continuity equation

$$-i\omega n_{d1} + n_{d0}ikv_{d1} = 0$$

$$\Rightarrow \omega n_{d1} = n_{d0}kv_{d1}$$

$$n_{d1} = \frac{n_{d0}kv_{d1}}{\omega} \tag{B.9}$$

and from poission's equation using that electrons and ions follows Boltzma's distribution we will get

$$-k^2\phi_1 = \frac{en_{e0}e\phi_1}{\epsilon_0 kT_e} - \frac{q_{d0}n_{d1}}{\epsilon_0} + \frac{en_{i0}e\phi_1}{\epsilon_0 kT_i} \tag{B.10}$$

using equation B.9 in above equation

$$-k^2\phi_1 = \frac{e^2 n_{e0}\phi_1}{\epsilon_0 k T_e} - \frac{q_{d0} n_{d0} k v_{d1}}{\epsilon_0 \omega} - \frac{e^2 n_{i0}\phi_1}{\epsilon_0 k T_i} \tag{B.11}$$

$$-k^2\phi_1 = \frac{\phi_1}{{\lambda_e}^2} + \frac{\phi_1}{{\lambda_i}^2} - \frac{q_{d0} n_{d0} k v_{d1}}{\epsilon_0 \omega} \tag{B.12}$$

$$(-k^2 - \frac{1}{{\lambda_e}^2} - \frac{1}{{\lambda_i}^2})\phi_1 = -\frac{q_{d0} n_{d0} k v_{d1}}{\epsilon_0 \omega} \tag{B.13}$$

$$(k^2 + \frac{1}{{\lambda_D}^2})\phi_1 = \frac{q_{d0} n_{d0} k v_{d1}}{\epsilon_0 \omega} \tag{B.14}$$

where λ_D is the debye length of dust acoustic wave

$$\frac{1}{\lambda_D^2} = \frac{1}{\lambda_e^2} + \frac{1}{\lambda_i^2} \tag{B.15}$$

$$(\frac{k^2{\lambda_D}^2 + 1}{{\lambda_D}^2})\phi_1 = \frac{q_{d0} n_{d0} k v_{d1}}{\epsilon_0 \omega} \tag{B.16}$$

$$\phi_1 = \frac{q_{d0} n_{d0} k v_{d1}}{\epsilon_0 \omega} \frac{{\lambda_D}^2}{k^2{\lambda_D}^2 + 1} \tag{B.17}$$

now from momentum equation

$$-i\omega m_d v_{d1} = -i q_{d0} k \phi_1 \tag{B.18}$$

using equation B.17 in above equation,we get

$$-i\omega m_d v_{d1} = -i q_{d0} k \frac{q_{d0} n_{d0} k v_{d1}}{\epsilon_0 \omega} \frac{{\lambda_D}^2}{k^2{\lambda_D}^2 + 1} \tag{B.19}$$

$$-i\omega^2 m_d = -i \frac{q_{d0}^2 k^2 n_{d0}}{\epsilon_0} \frac{{\lambda_D}^2}{k^2{\lambda_D}^2 + 1} \tag{B.20}$$

$$\omega^2 = -\frac{q_{d0}^2 k^2 n_{d0}}{\epsilon_0 m_d} \frac{{\lambda_D}^2}{k^2{\lambda_D}^2 + 1} \tag{B.21}$$

$$\omega^2 = {\omega_{pd}}^2 \frac{k^2{\lambda_D}^2}{k^2{\lambda_D}^2 + 1} \tag{B.22}$$

$$\omega^2 = {\omega_{pd}}^2 \frac{k^2{\lambda_D}^2}{k^2{\lambda_D}^2 + 1} \tag{B.23}$$

$$\omega^2 = {\omega_{pd}}^2 \frac{k^2{\lambda_D}^2}{k^2{\lambda_D}^2 + 1} \tag{B.24}$$

$$\frac{1}{\omega^2} = \frac{k^2{\lambda_D}^2 + 1}{{\omega_{pd}}^2 k^2{\lambda_D}^2} \tag{B.25}$$

$$\frac{{\omega_{pd}}^2}{\omega^2} = 1 + \frac{1}{k^2{\lambda_D}^2} \tag{B.26}$$

$$\omega^2 = \frac{{\omega_{pd}}^2 k^2{\lambda_D}^2}{1 + k^2{\lambda_D}^2} \tag{B.27}$$

$$\omega = \frac{v_{DAW}k}{\sqrt{1 + k^2{\lambda_D}^2}} \tag{B.28}$$

This is the required dispersion relation. For long wavelength ($k^2{\lambda_D}^2 \ll 1$), this equation reduces to $\omega \approx c_{DAW}k$.

Bibliography

[1] Lewi Tonks and Irving Langmuir. Oscillations in ionized gases. *Phys. Rev.*, 33:195–210, Feb 1929.

[2] Irving Langmuir. Oscillations in ionized gases. *Proc. Nat. Acad. Sci.*, 14:627, 1928.

[3] Francis F. Chen. *Introduction to Plasma Physics and Controlled Fusion.* Physics, Engineering, Astronomy. Plenum Press, New York., 1994.

[4] N. F. Ness. Observed Properties of the Interplanetary Plasma. *Ann. Rev. Astron. Astrophys.*, 6:79–114, 1968.

[5] P.K. Shukla and A.A. Mamun. *Introduction to Dusty Plasma Physics.* Series in Plasma Physics. CRC Press, 2001.

[6] P K Ed. by Shukla, D. A. Mendis, and T. Desai. Advances in dusty plasmas. *(Singapore: World Scientific)*, pages 3–19, 1997.

[7] S. M. Collins, J. F. O' Hanlon, and R. N. Carlile. Effects of particle clouds in a plasma etch system on silicon dioxide wafer contamination. *Journal of Vacuum Science and Technology A*, 12(4), 1994.

[8] Pere Roca i Cabarrocas, Patrick Gay, and Aomar Hadjadj. Experimental evidence for nanoparticle deposition in continuous argon-silane plasmas: Effects of silicon nanoparticles on film properties. *Journal of Vacuum Science and Technology A*, 14(2), 1996.

[9] B. T. draine. Scattering by interstellar dust grains. I. Optical and ultraviolet. *The Astrophysical Journal*, 598:1017–1025, December 2003.

[10] G. E. Morfill and H. M. Thomas. Spoke formation under moving plasma clouds-The Goertz Morfill model revisited. *icarus*, 179:539–542, December 2005.

[11] Z. Sekanina. Anisotropic emission from comets: Fans versus jets. 1: Concept and modeling. In E. J. Rolfe and B. Battrick, editors, *Diversity and Similarity of Comets*, volume 278 of *ESA Special Publication*, September 1987.

[12] B. J. Bok. Gas and dust in interstellar clouds. *aj*, 60:146, June 1955.

[13] William T. Reach, Bryan A. Franz, and Janet L. Weiland. The three-dimensional structure of the zodiacal dust bands. *Icarus*, 127(2):461 – 484, 1997.

[14] F. Li and O. Havnes. Low frequency dust wave modes in planetary rings. *Planetary and Space Science*, 48(2-3):117 – 125, 2000.

[15] T. W. Hartquist, O. Havnes, and G. E. Morfill. Charged rings: The effects of charged dust on Saturn's rings. *Astronomy and Geophysics*, 44(5):5.26–5.30, October 2003.

[16] Norman F. Ness, Clell S. Scearce, and Joseph B. Seek. Initial results of the imp 1 magnetic field experiment. *J. Geophys. Res.*, 69(17):2156–2202, 1964.

[17] Gary S. Selwyn, John E. Heidenreich, and Kurt L. Haller. Rastered laser light scattering studies during plasma processing: Particle contamination trapping phenomena. *Journal of Vacuum Science and Technology A*, 9(5), 1991.

[18] Y. Oda, T. Nakata, T. Yamamoto, Y. Seki, I. Aoki, S. Ueda, and R. Kurihara. Development of dust removal system for fusion reactor. *Journal of Fusion Energy*, 16(3):231–236, 1997.

[19] J Winter. Dust in fusion devices - experimental evidence, possible sources and consequences. *Plasma Physics and Controlled Fusion*, 40(6):1201, 1998.

[20] Y. Nakamura. *New Developments in Nuclear Fusion Research.* Nova Science Publishers, 2006.

[21] Noel A. Clark, Alan J. Hurd, and Bruce J. Ackerson. Single colloidal crystals. *Nature*, 281(5726):57–60, 1979.

[22] A. Melzer, T. Trottenberg, and A. Piel. Experimental determination of the charge on dust particles forming coulomb lattices. *Physics Letters A*, 191(3):301 – 308, 1994.

[23] S. A. Khrapak, S. V. Ratynskaia, A. V. Zobnin, A. D. Usachev, V. V. Yaroshenko, M. H. Thoma, M. Kretschmer, H. Höfner, G. E. Morfill, O. F. Petrov, and V. E. Fortov. Particle charge in the bulk of gas discharges. *Phys. Rev. E*, 72:016406, Jul 2005.

[24] J. H. Chu and Lin I. Direct observation of coulomb crystals and liquids in strongly coupled rf dusty plasmas. *Phys. Rev. Lett.*, 72:4009–4012, Jun 1994.

[25] H. Thomas, G. E. Morfill, V. Demmel, J. Goree, B. Feuerbacher, and D. Möhlmann. Plasma crystal: Coulomb crystallization in a dusty plasma. *Phys. Rev. Lett.*, 73:652–655, Aug 1994.

[26] Gregor E. Morfill and Alexei V. Ivlev. Complex plasmas: An interdisciplinary research field. *Rev. Mod. Phys.*, 81:1353–1404, Oct 2009.

[27] G. E. Morfill, H. M. Thomas, U. Konopka, H. Rothermel, M. Zuzic, A. Ivlev, and J. Goree. Condensed plasmas under microgravity. *Phys. Rev. Lett.*, 83:1598–1601, Aug 1999.

[28] H. Ikezi. Coulomb solid of small particles in plasmas. *Physics of Fluids*, 29(6), 1986.

[29] Gregor E. Morfill, Milenko Rubin-Zuzic, Hermann Rothermel, Alexei V. Ivlev, Boris A. Klumov, Hubertus M. Thomas, Uwe Konopka, and Victor Steinberg. Highly resolved fluid flows: "liquid plasmas" at the kinetic level. *Phys. Rev. Lett.*, 92:175004, Apr 2004.

[30] V. Nosenko and J. Goree. Shear flows and shear viscosity in a two-dimensional yukawa system (dusty plasma). *Phys. Rev. Lett.*, 93:155004, Oct 2004.

[31] P. G. Drazin and W. H. Reid. *Hydrodynamic Stability.* Cambridge University Press, second edition, 2004. Cambridge Books Online.

[32] A.V. Gurevich and N.T. Paschenko. Non-linear behaviour effect on mach cone behind the body moving in rarefied ionosphere. *Acta Astronautica*, 7(1):67 – 71, 1980.

[33] O. Havnes, F. Li, F. Melandsø, T. Aslaksen, T. W. Hartquist, G. E. Morfill, T. Nitter, and V. Tsytovich. Diagnostic of dusty plasma conditions by the observation of mach cones caused by dust acoustic waves. *Journal of Vacuum Science & Technology A*, 14(2), 1996.

[34] A. Brattli, O. Havnes, and F. Melandsø. Wake patterns behind boulders in the rings of saturn. *Physics of Plasmas*, 9(3), 2002.

[35] E. Engwall, A. I. Eriksson, and J. Forest. Wake formation behind positively charged spacecraft in flowing tenuous plasmas. *Physics of Plasmas*, 13(6), 2006.

[36] A. Melzer, S. Nunomura, D. Samsonov, Z. W. Ma, and J. Goree. Laser-excited mach cones in a dusty plasma crystal. *Phys. Rev. E*, 62:4162–4176, Sep 2000.

[37] D. Samsonov, J. Goree, H. M. Thomas, and G. E. Morfill. Mach cone shocks in a two-dimensional yukawa solid using a complex plasma. *Phys. Rev. E*, 61:5557–5572, May 2000.

[38] V. Nosenko, J. Goree, Z. W. Ma, and A. Piel. Observation of shear-wave mach cones in a 2d dusty-plasma crystal. *Phys. Rev. Lett.*, 88:135001, Mar 2002.

[39] T. Yao-Tsu Wu. Generation of upstream advancing solitons by moving disturbances. *Journal of Fluid Mechanics*, 184:75–99, 1987.

[40] T. R. Akylas. On the excitation of long nonlinear water waves by a moving pressure distribution. *J. Fluid Mech.*, 141(1):455, 1984.

[41] W. C. Webster R. C. Ertekin and J. V. Wehausen. Waves caused by a moving disturbance in a shallow channel of finite width. *J. Fluid Mech.*, 169(1):275, 1986.

[42] N. F. Smyth. Formation of one-dimensional waves for resonant flow in a channel. *Pure Appl. Geophys. PAGEOPH*, 133(4):619âĂŞ633, 1990.

[43] S. Mishra A. Sen, S. Tiwari and P. Kaw. Nonlinear wave excitations by orbiting charged space debris objects. *Adv. Sp. Res*, 56(3):429–435, 2015.

[44] G. B. Murphy, D. L. Reasoner, A. Tribble, N. D'Angelo, J. S. Pickett, and W. S. Kurth. The plasma wake of the shuttle orbiter. *Journal of Geophysical Research: Space Physics*, 94(A6):6866–6872, 1989.

[45] R. L. Merlino and N. D'Angelo. The interaction of a conducting object with a supersonic plasma flow: ion deflection near a negatively charged obstacle. *Journal of Plasma Physics*, 37:185–198, 4 1987.

[46] V. E. Fortov, A. G. Khrapak, S. A. Khrapak, V. I. Molotkov, and O. F. Petrov. Dusty plasmas. *Phys. Usp.*, 47(5):447–492, 2004.

[47] A. Barkan, N. D'Angelo, and R. L. Merlino. Charging of dust grains in a plasma. *Phys. Rev. Lett.*, 73:3093–3096, Dec 1994.

[48] Themis Matsoukas and Marc Russell. Particle charging in lowâĂŘpressure plasmas. *Journal of Applied Physics*, 77(9), 1995.

[49] T Nitter. Levitation of dust in rf and dc glow discharges. *Plasma Sources Science and Technology*, 5(1):93, 1996.

[50] Michael S. Barnes, John H. Keller, John C. Forster, James A. O'Neill, and D. Keith Coultas. Transport of dust particles in glow-discharge plasmas. *Phys. Rev. Lett.*, 68:313–316, Jan 1992.

[51] Paul S. Epstein. On the resistance experienced by spheres in their motion through gases. *Phys. Rev.*, 23:710–733, Jun 1924.

[52] N.N. Rao, P.K. Shukla, and M.Y. Yu. Dust-acoustic waves in dusty plasmas. *Planetary and Space Science*, 38(4):543 – 546, 1990.

[53] P K Shukla and V P Silin. Dust ion-acoustic wave. *Physica Scripta*, 45(5):508, 1992.

[54] Frank Melandsø. Lattice waves in dust plasma crystals. *Physics of Plasmas*, 3(11), 1996.

[55] N. N. Rao. Dust coulomb waves in dense dusty plasmas. *Physics of Plasmas*, 6(12), 1999.

[56] Frank Verheest. Waves and instabilities in dusty space plasmas. *Space Science Reviews*, 77(3):267–302, 1996.

[57] A A Mamun and P K Shukla. Electrostatic solitary and shock structures in dusty plasmas. *Physica Scripta*, 2002(T98):107, 2002.

[58] I. Kourakis and P. K. Shukla. Nonlinear theory of solitary waves associated with longitudinal particle motion in lattices. *The European Physical Journal D - Atomic, Molecular, Optical and Plasma Physics*, 29(2):247–263, 2004.

[59] P.K. Shukla and S.G. Tagare. Ion-acoustic shock waves in multi-electron temperature collisional plasma. *Physics Letters A*, 59(1):38 – 40, 1976.

[60] P. K. Shukla. Dust ion-acoustic shocks and holes. *Physics of Plasmas*, 7(3), 2000.

[61] S. I. Popel, A. A. Gisko, A. P. Golub', T. V. Losseva, R. Bingham, and P. K. Shukla. Shock waves in charge-varying dusty plasmas and the effect of electromagnetic radiation. *Physics of Plasmas*, 7(6), 2000.

[62] P. K. Shukla and A. A. Mamun. Dust-acoustic shocks in a strongly coupled dusty plasma. *IEEE Transactions on Plasma Science*, 29(2):221–225, Apr 2001.

[63] B. Eliasson and P. K. Shukla. Dust acoustic shock waves. *Phys. Rev. E*, 69:067401, Jun 2004.

[64] N N Rao. Dust-acoustic kdv solitons in weakly non-ideal dusty plasmas. *Physica Scripta*, 1998(T75):179, 1998.

[65] A. A. Mamun, R. A. Cairns, and P. K. Shukla. Solitary potentials in dusty plasmas. *Physics of Plasmas*, 3(2), 1996.

[66] A A Mamun. Solitary waves in a three-component dusty plasma with trapped ions. *Physica Scripta*, 57(2):258, 1998.

[67] A.A Mamun and P.K Shukla. Spherical and cylindrical dust acoustic solitary waves. *Physics Letters A*, 290(34):173–175, 2001.

[68] Ju-Kui Xue. Head-on collision of dust-acoustic solitary waves. *Phys. Rev. E*, 69:016403, Jan 2004.

[69] S.K. El-Labany, E.F. El-Shamy, W.F. El-Taibany, and P.K. Shukla. Head-on collision of quantum ion-acoustic solitary waves in a dense electron-positron-ion plasma. *Physics Letters A*, 374(7):960 – 964, 2010.

[70] E.F. El-Shamy, W.M. Moslem, and P.K. Shukla. Head-on collision of ion-acoustic solitary waves in a thomas-fermi plasma containing degenerate electrons and positrons. *Physics Letters A*, 374(2):290 – 293, 2009.

[71] A. Barkan, R. L. Merlino, and N. D'Angelo. Laboratory observation of the dust-acoustic wave mode. *Physics of Plasmas*, 2(10), 1995.

[72] J. B. Pieper and J. Goree. Dispersion of plasma dust acoustic waves in the strong-coupling regime. *Phys. Rev. Lett.*, 77:3137–3140, Oct 1996.

[73] P. Bandyopadhyay, G. Prasad, A. Sen, and P.K. Kaw. Experimental observation of strong coupling effects on the dispersion of dust acoustic waves in a plasma. *Physics Letters A*, 368(6):491 – 494, 2007.

[74] H. R. Prabhakara and V. L. Tanna. Trapping of dust and dust acoustic waves in laboratory plasmas. *Physics of Plasmas*, 3(8), 1996.

[75] J. Pramanik, B.M. Veeresha, G. Prasad, A. Sen, and P.K. Kaw. Experimental observation of dust-acoustic wave turbulence. *Physics Letters A*, 312(1-2):84–90, 2003.

[76] S. Nunomura, D. Samsonov, and J. Goree. Transverse waves in a two-dimensional screened-coulomb crystal (dusty plasma). *Phys. Rev. Lett.*, 84:5141–5144, May 2000.

[77] J. Pramanik, G. Prasad, A. Sen, and P. K. Kaw. Experimental observations of transverse shear waves in strongly coupled dusty plasmas. *Phys. Rev. Lett.*, 88:175001, Apr 2002.

[78] P. K. Kaw and A. Sen. Low frequency modes in strongly coupled dusty plasmas. *Physics of Plasmas*, 5(10), 1998.

[79] Y. Nakamura and A. Sarma. Observation of ion-acoustic solitary waves in a dusty plasma. *Physics of Plasmas*, 8(9), 2001.

[80] Y. Nakamura, H. Bailung, and P. K. Shukla. Observation of ion-acoustic shocks in a dusty plasma. *Phys. Rev. Lett.*, 83:1602–1605, Aug 1999.

[81] D. Samsonov, G. Morfill, H. Thomas, T. Hagl, H. Rothermel, V. Fortov, A. Lipaev, V. Molotkov, A. Nefedov, O. Petrov, A. Ivanov, and S. Krikalev. Kinetic measurements of shock wave propagation in a three-dimensional complex (dusty) plasma. *Phys. Rev. E*, 67:036404, Mar 2003.

[82] D. Samsonov, S. K. Zhdanov, R. A. Quinn, S. I. Popel, and G. E. Morfill. Shock melting of a two-dimensional complex (dusty) plasma. *Phys. Rev. Lett.*, 92:255004, Jun 2004.

[83] D. Samsonov, A. V. Ivlev, R. A. Quinn, G. Morfill, and S. Zhdanov. Dissipative longitudinal solitons in a two-dimensional strongly coupled complex (dusty) plasma. *Phys. Rev. Lett.*, 88:095004, Feb 2002.

[84] P. Bandyopadhyay, G. Prasad, A. Sen, and P. K. Kaw. Experimental study of non-linear dust acoustic solitary waves in a dusty plasma. *Phys. Rev. Lett.*, 101:065006, Aug 2008.

[85] H. Rothermel, T. Hagl, G. E. Morfill, M. H. Thoma, and H. M. Thomas. Gravity compensation in complex plasmas by application of a temperature gradient. *Phys. Rev. Lett.*, 89:175001, Oct 2002.

[86] Bin Liu, J. Goree, V. Nosenko, and L. Boufendi. Radiation pressure and gas drag forces on a melamine-formaldehyde microsphere in a dusty plasma. *Physics of Plasmas*, 10(1), 2003.

[87] S. A. Khrapak, A. V. Ivlev, G. E. Morfill, and H. M. Thomas. Ion drag force in complex plasmas. *Phys. Rev. E*, 66:046414, Oct 2002.

[88] A V Ivlev, S K Zhdanov, S A Khrapak, and G E Morfill. Ion drag force in dusty plasmas. *Plasma Physics and Controlled Fusion*, 46(12B):B267, 2004.

[89] Bin Liu, J. Goree, V. Nosenko, and L. Boufendi. Radiation pressure and gas drag forces on a melamine-formaldehyde microsphere in a dusty plasma. *Physics of Plasmas*, 10(1), 2003.

[90] Edward Thomas and Jeremiah Williams. Experimental measurements of velocity dissipation and neutral-drag effects during the formation of a dusty plasma. *Phys. Rev. Lett.*, 95:055001, Jul 2005.

[91] Y. Nakamura and O. Ishihara. A complex plasma device of large surface area. *Review of Scientific Instruments*, 79(3), 2008.

[92] P. K. Shukla. A survey of dusty plasma physics. *Physics of Plasmas*, 8(5), 2001.

[93] P. K. Shukla and B. Eliasson. *Colloquium* : Fundamentals of dust-plasma interactions. *Rev. Mod. Phys.*, 81:25–44, Jan 2009.

[94] R. Heidemann, S. Zhdanov, K. R. Sütterlin, H. M. Thomas, and G. E. Morfill. Shear flow instability at the interface among two streams of a highly dissipative complex plasma. *EPL (Europhysics Letters)*, 96(1):15001, 2011.

[95] V. Nosenko, K. Avinash, J. Goree, and B. Liu. Nonlinear interaction of compressional waves in a 2d dusty plasma crystal. *Phys. Rev. Lett.*, 92:085001, Feb 2004.

[96] S. Ratynskaia, K. Rypdal, C. Knapek, S. Khrapak, A. V. Milovanov, A. Ivlev, J. J. Rasmussen, and G. E. Morfill. Superdiffusion and viscoelastic vortex flows in a two-dimensional complex plasma. *Phys. Rev. Lett.*, 96:105010, Mar 2006.

[97] V. Steinberg, A. V. Ivlev, R. Kompaneets, and G. E. Morfill. Shear instability in fluids with a density-dependent viscosity. *Phys. Rev. Lett.*, 100:254502, Jun 2008.

[98] Ashwin J. and R. Ganesh. Kelvin helmholtz instability in strongly coupled yukawa liquids. *Phys. Rev. Lett.*, 104:215003, May 2010.

[99] Ashwin J. and R. Ganesh. Parallel shear flow instabilities in strongly coupled yukawa liquids: A comparison of generalized hydrodynamic model and molecular dynamics results. *Physics of Plasmas*, 17(10), 2010.

[100] Sanat Kumar Tiwari, Amita Das, Dilip Angom, Bhavesh G. Patel, and Predhiman Kaw. Kelvin-helmholtz instability in a strongly coupled dusty plasma medium. *Physics of Plasmas*, 19(7), 2012.

[101] D. Banerjee, M. S. Janaki, N. Chakrabarti, and M. Chaudhuri. Nonlinear shear wave in a non newtonian visco-elastic medium. *Physics of Plasmas*, 19(6), 2012.

[102] K. Avinash and A. Sen. Rayleigh-taylor instability in dusty plasma experiment. *Physics of Plasmas*, 22(8), 2015.

[103] S. Sen, A. Fukuyama, and F. Honary. Rayleigh taylor instability in a dusty plasma. *Journal of Atmospheric and Solar-Terrestrial Physics*, 72(13):938 – 942, 2010.

[104] S. Garai, D. Banerjee, M. S. Janaki, and N. Chakrabarti. Stabilization of rayleigh-taylor instability in a non-newtonian incompressible complex plasma. *Physics of Plasmas*, 22(3), 2015.

[105] K. A. Pacha, J. R. Heinrich, S.-H. Kim, and R. L. Merlino. Observation of the taylor instability in a dusty plasma. *Physics of Plasmas*, 19(1), 2012.

[106] S. Mitic, R. Sütterlin, A. V. Ivlev H. Höfner, M. H. Thoma, S. Zhdanov, and G. E. Morfill. Convective dust clouds driven by thermal creep in a complex plasma. *Phys. Rev. Lett.*, 101:235001, Dec 2008.

[107] M. Kroll, J. Schablinski, D. Block, and A. Piel. On the influence of wakefields on three-dimensional particle arrangements. *Physics of Plasmas*, 17(1), 2010.

[108] H. Kählert, J. Carstensen, M. Bonitz, H. Löwen, F. Greiner, and A. Piel. Magnetizing a complex plasma without a magnetic field. *Phys. Rev. Lett.*, 109:155003, Oct 2012.

[109] J. Heinrich, S.-H. Kim, and R. L. Merlino. Laboratory observations of self-excited dust acoustic shocks. *Phys. Rev. Lett.*, 103:115002, Sep 2009.

[110] B. Eliasson and P. K. Shukla. Dust acoustic shock waves. *Phys. Rev. E*, 69:067401, Jun 2004.

[111] J. R. Heinrich, S.-H. Kim, and R. L. Merlino. Dust jets produced by a dust-discharge instability. *Physics of Plasmas*, 17(8), 2010.

[112] Y. Saitou, Y. Nakamura, T. Kamimura, and O. Ishihara. Bow shock formation in a complex plasma. *Phys. Rev. Lett.*, 108:065004, Feb 2012.

[113] M. A. Fink, S. K. Zhdanov, M. H. Thoma, H. Höfner, and G. E. Morfill. Pearl-necklace-like structures of microparticle strings observed in a dc complex plasma. *Phys. Rev. E*, 86:065401, Dec 2012.

[114] M. A. Fink, S. K. Zhdanov, M. Schwabe, M. H. Thoma, H. Höfner, H. M. Thomas, and G. E. Morfill. Autowaves in a dc complex plasma confined behind a de laval nozzle. *EPL (Europhysics Letters)*, 102(4):45001, 2013.

[115] John K. Meyer and Robert L. Merlino. Transient bow shock around a cylinder in a supersonic dusty plasma. *Physics of Plasmas*, 20(7), 2013.

[116] J. K. MEYER, J. R. HEINRICH, S.-H. KIM, and R. L. MERLINO. Interaction of a biased cylinder with a flowing dusty plasma. *Journal of Plasma Physics*, 79:677–682, 10 2013.

[117] S. Jaiswal, P. Bandyopadhyay, and A. Sen. Dusty plasma experimental (dpex) device for complex plasma experiments with flow. *Review of Scientific Instruments*, 86(11), 2015.

[118] M. H. Thoma, H. Höfner, M. Kretschmer, S. Ratynskaia, G. E. Morfill, A. Usachev, A. Zobnin, O. Petrov, and V. Fortov. Parabolic flight experiments with pk-4. *Microgravity - Science and Technology*, 18(3):47, 2006.

[119] A. Usachev, A. Zobnin, O. Petrov, V. Fortov, and M. *et al.* Thoma. The project "plasmakristall - 4" (pk-4) is a dusty plasma experiment in a combined dc/rf(i) discharge plasma under microgravity conditions. *Czech. Journal of Physics*, 54, 2004.

[120] F. F. Chen. *Electric Probes, in "Plasma Diagnostic Techniques", ed. by R. H. Huddlestone and S. L. Leonard A, Chap. 4.* cademic Press, New York, 1965.

[121] L. Schott. *Electric Probes, in "Plasma Diagnostics", ed. by W. LochteHoltgreven, Chap. 11.* John Wiley, New York, 1968.

[122] N. Hershkowitz. *How Langmuir Probes Work, in "Plasma Diagnostics", ed. by O. Auciello and D.L. Flamm, Chap. 3.* Academic Press, Boston, 1989.

[123] Ramakant A. Gayakwad. *Op-Amps and Linear Integrated Circuits.* Prentice Hall, New Delhi, 1983.

[124] Hill Horowitz, Paul Winfield. *The art of electronics* . Cambridge University Press, 1989.

[125] Yuri P Raizer. *Gas Discharge Physics.* Springer-Verlag Berlin Heidelberg., 1991.

[126] M. A. Lieberman and A. J. Lichtenberg. *Princeples of Plasma Dicharges and Materials Processing.* Physics, Engineering, Astronomy. Wiley, New York., 1994.

[127] C Torres, P G Reyes, F Castillo, and H Martinez. Paschen law for argon glow discharge. *Journal of physics: Conference Series*, 370:012067, 2012.

[128] J P Sheehan and N Hershkowitz. Emissive probes. *Plasma Sources Science and Technology*, 20(6):063001, 2011.

[129] T. E. Sheridan and J. Goree. Collisional plasma sheath model. *Physics of Fluids B*, 3(10), 1991.

[130] M. J. Druyvesteyn. Der niedervoltbogen. *Zeitschrift für Physik*, 64(11):781–798, 1930.

[131] E. I. Toader, A. Fredriksen, and A. Aanesland. Characterization of a high-density electron-cyclotron resonance plasma source operating in nitrogen. *Review of Scientific Instruments*, 74(7), 2003.

[132] Mierk Schwabe. Dynamical effects in fluid complex plasmas. November 2009.

[133] Y. Feng, J. Goree, and Bin Liu. Accurate particle position measurement from images. *Review of Scientific Instruments*, 78(5), 2007.

[134] A. Melzer, A. Homann, and A. Piel. Experimental investigation of the melting transition of the plasma crystal. *Phys. Rev. E*, 53:2757–2766, Mar 1996.

[135] A. V. Ivlev, V. Steinberg, R. Kompaneets, H. Höfner, I. Sidorenko, and G. E. Morfill. Non-newtonian viscosity of complex-plasma fluids. *Phys. Rev. Lett.*, 98:145003, Apr 2007.

[136] M.H. Thoma, H. Hoefner, S. A. Khrapak, M. Kretschmer, R.A. Quinn, S. Ratynskaia, G.E. Morfill, A. Usachev, A. Zobnin, O. Petrov, and V. Fortov. Measurement of the ion drag force in a complex dc-plasma using the pk-4 experiment. *Ukr. J. Phys.*, 50, 2005.

[137] Y. Nakamura and O. Ishihara. A complex plasma device of large surface area. *Review of Scientific Instruments*, 79(3), 2008.

[138] Yan Feng, J. Goree, and Bin Liu. Observation of temperature peaks due to strong viscous heating in a dusty plasma flow. *Phys. Rev. Lett.*, 109:185002, Oct 2012.

[139] William. Thielicke and Eize J. Stamhuis. Pivlab-towards user-friendly, affordable and accurate digital particle image velocimetry in matlab. *Journal of open research software*, 2, 2014.

[140] R L Merlino, J R Heinrich, S-H Kim, and J K Meyer. Dusty plasmas: experiments on nonlinear dust acoustic waves, shocks and structures. *Plasma Physics and Controlled Fusion*, 54(12):124014, 2012.

[141] J. J. Stoker. *Water Waves*. John Wiley & Sons, Inc, 1992.

[142] Leo H. Holthuijsen. *Waves in Oceanic and Coastal Waters*. Cambridge University Press, 2007.

[143] Hu Huang. *Dynamics of Surface Waves in Coastal Waters*. Springer, 2009.

[144] A. J. Hermans. *Water Waves and Ship Hydrodynamics*. Springer, 2 edition, 2011.

[145] TR Akylas. On the excitation of long nonlinear water waves by a moving pressure distribution. *Journal of Fluid Mechanics*, 141:455–466, 1984.

[146] RC Ertekin, WC Webster, and JV Wehausen. Waves caused by a moving disturbance in a shallow channel of finite width. *Journal of Fluid . . .*, 169:275–292, 1986.

[147] N.F. Smythe. Formation of One-dimensional Waves for Resonant Flow in a Channel. *Pure and Applied Geophysics*, 133(4):619–633, 1990.

[148] DAO-HUA ZHANG and ALLEN T. CHWANG. Generation of solitary waves by forward- and backward-step bottom forcing. *J. Fluid Mech.*, 432(1):341–350, 2001.

[149] N J Zabusky and C J Galvin. Shallow-water waves, the Korteweg-deVries equation and solitons. *Journal of Fluid Mechanics*, 47(4):811–824, 1971.

[150] Seung-Joon Lee, George T. Yates, and T. Yaotsu Wu. Experiments and analyses of upstream-advancing solitary waves generated by moving disturbances. *Journal of Fluid Mechanics*, 199:569–593, 02 1989.

[151] Kenneth L Jones and Yunkai Chen. EXISTENCE OF PERIODIC TRAVELING WAVE SOLUTIONS TO THE GENERALIZED FORCED BOUSSINESQ EQUATION. *International Journal of Mathematics and Mathematical Sciences*, 22(3):643–648, 1999.

[152] Benjamin J. Binder, Mark G. Blyth, and Sanjeeva Balasuriya. Non-uniqueness of steady free-surface flow at critical Froude number. *EPL (Europhysics Letters)*, 105(4):44003, 2014.

[153] A V Gurevich and N T Paschenko. Non-linear behaviour effect on Mach cone behind the body moving in rarefied ionosphere. *Acta Astronautica*, 7:67–71, 1980.

[154] O. Havnes. Diagnostic of dusty plasma conditions by the observation of Mach cones caused by dust acoustic waves. *Journal of Vacuum Science & Technology A: Vacuum, Surfaces, and Films*, 14(2):525, March 1996.

[155] a. Brattli, O. Havnes, and F. Melandsø. Wake patterns behind boulders in the rings of Saturn. *Physics of Plasmas*, 9(3):958, 2002.

[156] E. Engwall, A I. Eriksson, and J. Forest. Wake formation behind positively charged spacecraft in flowing tenuous plasmas. *Physics of Plasmas*, 13(6):062904, 2006.

[157] Francois Sylla. *Ion acceleration from laser-plasma interaction in underdense to near-critical regime: wakefield effects and associated plasma structures*. PhD thesis, Ecole Polytechnique - CNRS, 2011.

[158] I. H. Hutchinson. Nonlinear collisionless plasma wakes of small particles. *Physics of Plasmas*, 18(3):032111, 2011.

[159] Dietmar Block, Jan Carstensen, Patrick Ludwig, Wojciech J Miloch, Franko Greiner, Alexander Piel, Michael Bonitz, and Andre Melzer. Wake formation and wake field effects in complex plasmas. *Contributions to Plasma Physics to Plasma Physics*, 52(10):804–812, 2012.

[160] V. Nosenko, S. Nunomura, and J. Goree. Nonlinear compressional pulses in a 2d crystallized dusty plasma. *Phys. Rev. Lett.*, 88:215002, May 2002.

[161] R. Heidemann, S. Zhdanov, R. Sütterlin, H. M. Thomas, and G. E. Morfill. Dissipative dark soliton in a complex plasma. *Phys. Rev. Lett.*, 102:135002, Mar 2009.

[162] S. Zhdanov, R. Heidemann, M. H. Thoma, R. Sütterlin, H. M. Thomas, H. Höfner, K. Tarantik, G. E. Morfill, A. D. Usachev, O. F. Petrov, and V. E. Fortov. Dissipative dark solitons in a dc complex plasma. *EPL (Europhysics Letters)*, 89(2):25001, 2010.

[163] Christian Bernt Haakonsen and Ian H. Hutchinson. The electron forewake: Shadowing and drift-energization as flowing magnetized plasma encounters an obstacle. *Physics of Plasmas*, 22(10), 2015.

[164] Sanat Kumar Tiwari and Abhijit Sen. Fore-wake excitations from moving charged objects in a complex plasma. *Physics of Plasmas*, 23(10), 2016.

[165] S. K. Zhdanov, D. Samsonov, and G. E. Morfill. Anisotropic plasma crystal solitons. *Phys. Rev. E*, 66:026411, Aug 2002.

[166] Robert M. Miura. The korteweg-devries equation: A survey of results. *SIAM Review*, 18(3):412–459, 1976.

[167] j. bond, K. Watson, and J. Welch. *Atomic Theory of Gas Dynamics*. MA. Addison-Wesley, 1965.

[168] S. Hørlück and P. Dimon. Statistics of shock waves in a two-dimensional granular flow. *Phys. Rev. E*, 60:671–686, Jul 1999.

[169] Robert A. Graham. *Solids Under High-Pressure Shock Compression*. Springer New York, 1993.

[170] R. Z. Sagdeev. Cooperative Phenomena and Shock Waves in Collisionless Plasmas. *Reviews of Plasma Physics*, 4:23, 1966.

[171] H. K. Andersen, N. D Angelo, P. Michelsen, and P. Nielsen. Experiments on shock formation in a q-device. *Physics of Fluids*, 11(3), 1968.

[172] P. K. Shukla. Dust ion-acoustic shocks and holes. *Physics of Plasmas*, 7(3), 2000.

[173] S. I. Popel, A. A. Gisko, A. P. Golub', T. V. Losseva, R. Bingham, and P. K. Shukla. Shock waves in charge-varying dusty plasmas and the effect of electromagnetic radiation. *Physics of Plasmas*, 7(6), 2000.

[174] Hamid Reza Pakzad and Kurosh Javidan. Dust acoustic solitary and shock waves in strongly coupled dusty plasmas with nonthermal ions. *Pramana*, 73(5):913–926, 2009.

[175] V. E. Fortov, O. F. Petrov, V. I. Molotkov, M. Y. Poustylnik, V. M. Torchinsky, V. N. Naumkin, and A. G. Khrapak. Shock wave formation in a dc glow discharge dusty plasma. *Phys. Rev. E*, 71:036413, Mar 2005.

[176] Y. Nakamura. Experiments on ion-acoustic shock waves in a dusty plasma. *Physics of Plasmas*, 9(2), 2002.

[177] A Usachev, A Zobnin, O Petrov, V Fortov, M H Thoma, H Höfner, M Fink, A Ivlev, and G Morfill. Externally excited planar dust acoustic shock waves in a strongly coupled dusty plasma under microgravity conditions. *New Journal of Physics*, 16(5):053028, 2014.

[178] Q.-Z. Luo, N. D'Angelo, and R. L. Merlino. Experimental study of shock formation in a dusty plasma. *Physics of Plasmas*, 6(9), 1999.

[179] H. R. Pakzad. Dust acoustic shock waves in coupled dusty plasmas with nonthermal ions. *Shock Waves*, 21(4):357–365, 2011.

[180] S V Annibaldi, A V Ivlev, U Konopka, S Ratynskaia, H M Thomas, G E Morfill, A M Lipaev, V I Molotkov, O F Petrov, and V E Fortov. Dust-acoustic dispersion relation in three-dimensional complex plasmas under microgravity. *New Journal of Physics*, 9(9):327, 2007.

[181] P. K. Kaw and A. Sen. Low frequency modes in strongly coupled dusty plasmas. *Physics of Plasmas*, 5(10), 1998.

[182] J. Pramanik, G. Prasad, A. Sen, and P. K. Kaw. Experimental observations of transverse shear waves in strongly coupled dusty plasmas. *Phys. Rev. Lett.*, 88:175001, Apr 2002.

[183] Setsuo Ichimaru, Hiroshi Iyetomi, and Shigenori Tanaka. Statistical physics of dense plasmas: Thermodynamics, transport coefficients and dynamic correlations. *Physics Reports*, 149(2):91 – 205, 1987.

[184] S Jaiswal, P Bandyopadhyay, and A Sen. Flowing dusty plasma experiments: generation of flow and measurement techniques. *Plasma Sources Science and Technology*, 25(6):065021, 2016.

[185] Surabhi Jaiswal, P. Bandyopadhyay, and A. Sen. Experimental observation of precursor solitons in a flowing complex plasma. *Phys. Rev. E*, 93:041201, Apr 2016.

[186] S. Jaiswal, P. Bandyopadhyay, and A. Sen. Experimental investigation of flow induced dust acoustic shock waves in a complex plasma. *Physics of Plasmas*, 23(8):083701, 2016.